UNIVERSITÀ DEGLI STUDI DI BRESCIA

DIPARTIMENTO DI MEDICINA MOLECOLARE E TRASLAZIONALE

UNIVERSITÀ
DEGLI STUDI
DI BRESCIA

DOTTORATO DI RICERCA IN

GENETICA MOLECOLARE, BIOTECNOLOGIE E MEDICINA SPERIMENTALE

XXXVII CICLO

Settore Scientifico Disciplinare: BIOS-10/A, BIOLOGIA CELLULARE E APPLICATA

miR-23b-3p, miR-126-3p and GAS5 delivered by extracellular vesicles inhibit breast cancer xenografts in zebrafish

Supervisore:

Prof. Alessandro Salvi

Co-Supervisore:

Prof. Giuseppina De Petro

Dottoranda:

Dott.ssa Iulia - Andreea Pelisenco

Anno Accademico 2023/2024

Table of contents

Abstract

Le vescicole extracellulari (EV) sono strutture membranose secrete dalle cellule, in grado di trasportare molecole biologiche per la comunicazione intercellulare. Svolgono ruoli importanti in diversi processi fisiologici e patologici. Dato il loro contenuto, le EV possono essere utilizzate per trasportare acidi nucleici, proteine e metaboliti verso cellule bersaglio. Le EV offrono una serie di vantaggi rispetto ai vettori tradizionali, aprendo così la strada a nuove strategie innovative per la somministrazione di farmaci.

Lo scopo di questo studio è stato quello di valutare l'efficacia delle EV come nanovettori efficienti per modulare i livelli di espressione di determinati *non-coding RNA* (ncRNA) nelle cellule tumorali bersaglio e ridurre le proprietà aggressive del carcinoma mammario *in vitro* e *in vivo*. Abbiamo verificato che trattando line cellular umane di carcinoma mammario con un inibitore multichinasico, il sorafenib, si sono osservati livelli aumentati di miR-23b-3p, miR-126-3p e GAS5 nelle EV secrete. Le EV arricchite di ncRNA, utilizzate come veicoli nelle cellule tumorali, hanno determinato un aumento dei livelli di espressione dei 3 ncRNA e hanno causato un'inibizione della proliferazione cellulare. Per stabilire ulteriormente il ruolo delle EV come vettori di ncRNA *in vivo*, abbiamo iniettato le cellule umane di carcinoma mammario in embrioni di zebrafish e abbiamo trattato gli xenotrapianti con le EV arricchite. Quindi abbiamo osservato una diminuzione della massa tumorale negli xenotrapianti, una considerevole riduzione del numero di micrometastasi nella coda di zebrafish ed una significativa inibizione dell'angiogenesi.

Pertanto i risultati ottenuti indicano una nuova modalità per arricchire le EV con specifici ncRNA oncosoppressori trattando le cellule con un farmaco antitumorale; il ruolo delle EV come veicoli di ncRNA; e l'effetto combinato di miR-23b-3p, miR-126-3p e GAS5 nel limitare le proprietà aggressive del carcinoma mammario *in vitro* e *in vivo*. Tali dati potrebbero essere di utilità per sviluppare nuove possibili strategie terapeutiche molecolari contro questo tipo di tumore.

1. Introduction

1.1.Breast cancer

Cancer is now widely recognized as a global problem that unfortunately fails to have a global solution [1]. Cancer is defined as a genetic disorder that results from either epigenetic or genetic alterations that can occur in the somatic cells. Malignant transformation is a multistep process, in which mutations required for the malignancy can be acquired gradually during one's lifetime, or inherited, ultimately leading to tumorigenic transformation [2]. The lack of treatment specificity and effectiveness makes cancer one of the most major burdens that humans are confronting all over the world [3].

1.1.1. Epidemiology and etiology

Breast cancer (BC) is the second most commonly diagnosed cancer and the leading cause of cancer-related death among women, with an incidence of 2.29 million new cases in 2022, according to GLOBOCAN [4]. The major risk factors in breast cancer development include increasing age, breast molecular characteristics, hormone use, alcohol, tobacco, diet, and ethnic group (Fig. 1) [5].

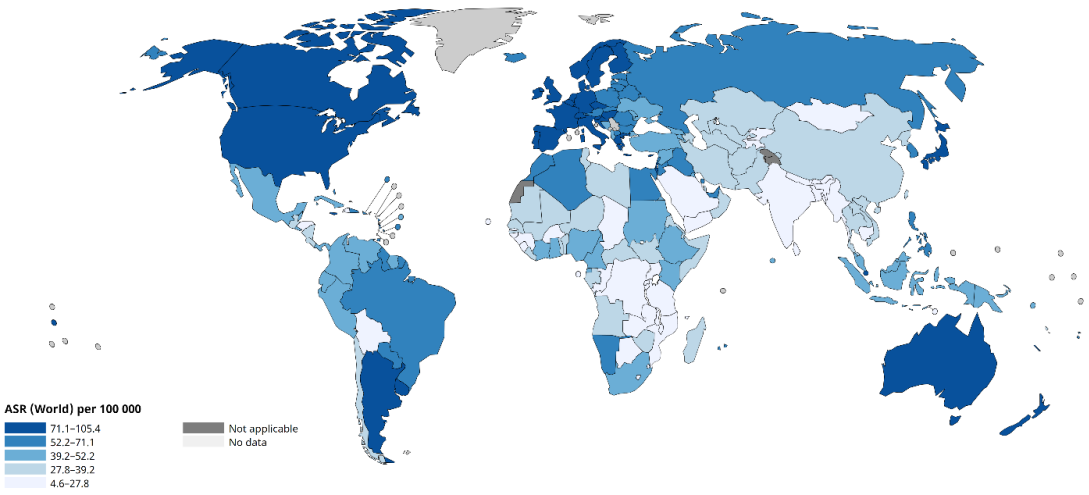

Fig. 1. Estimated ranked age-standardized incident rate (ASR) of BC worldwide. BC incidence varies based on the geographic regions. This disease affects more people in North America, Argentina, and some countries in West Europe such as France and Germany, as well as some Mediterranean countries (Italy, Spain, Portugal). In addition, the average age is higher in these countries than in the others. Eastern Asia and Southern Africa have a relatively low incidence rate of BC. Graphical representation from GloboCan (Global Cancer Observatory) [4].

1.1.2. Molecular classification

BC is defined as a heterogeneous neoplasm that requires an efficient, cost-effective, and noninvasive method of classification. Based on these premises, immunohistochemical analysis of BC based on estrogen receptor, (ER), progesterone receptor (PR), and human epidermal growth factor 2 receptor (HER2) is used in clinical practice to categorize BC into four subtypes [6].

The first and less aggressive subtype, with a lower incidence of relapse and a higher survival rate, is luminal A, characterized by the presence of ER and/or PR, the absence of HER2, and by a low expression of the cell proliferation marker Ki-67, with a percentage less than 20 % (Fig. 2) [7]. Due to the presence of these receptors, patients suffering from the luminal A subtype of BC have a better response rate to hormone therapy.

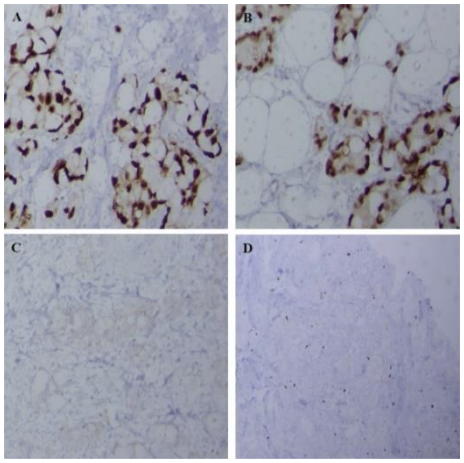

Fig 2. Immunohistochemistry aspects of Luminal A breast cancer. nuclear staining of **(A)** ER-positive, **(B)** PR positive, **(C)** HER-2 negative membrane staining, **(D)** nuclear staining of Ki-67 positive 3% [7].

The luminal B subtype is known as a more aggressive form of ER-positive BC, being characterized by the presence of ER and/or PR and the presence or absence of HER2, according to different studies, approximately 20% of luminal B breast cancers were HER2-positive [8]. Moreover, the luminal B subtype has a high expression of the proliferation marker Ki-67 (greater than 20%) (Fig. 3).

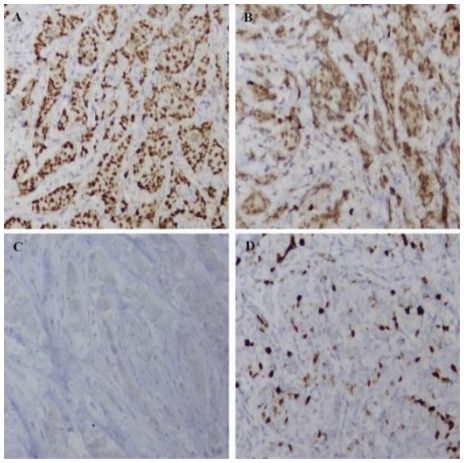

Fig 3. Immunohistochemistry aspects of Luminal B breast cancer. nuclear staining of **(A)** ER-positive, **(B)** PR positive, **(C)** HER-2 negative membrane staining, **(D)** nuclear staining of Ki-67 positive 30% [7].

HER2-positive is found in approximately 20% of BC and is often associated with poor prognosis and short overall survival [9]. This subtype is characterized by high HER2 expression with the absence of ER and PR (Fig. 4). The HER2-positive subtype can be further divided into two other subgroups: luminal HER2 (E+, PR+, HER2+, and Ki-67:15–30%) and HER2-enriched (E-, PR-, HER2+, Ki-67>30%) [7].

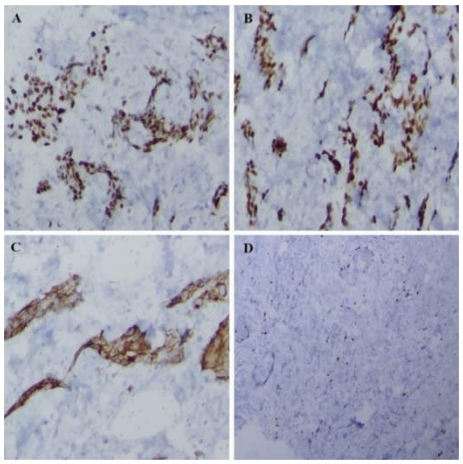

Fig 4. Immunohistochemistry aspects of HER2-positive breast cancer. nuclear staining of **(A)** ER-positive, **(B)** PR positive, **(C)** HER-2 positive membrane staining, **(D)** nuclear staining of Ki-67 positive 5% [7].

Triple-negative BC is characterized by a loss of ER, PR, and the absence of HER2 overexpression (Fig. 5). They constitute about 10.6-29.5% of all BC [10]. Lehmann *et al*. classified TNBC into 6 subgroups [11]: basal-like 1 (BL1), basal-like 2 (BL2), mesenchymal (M), mesenchymal stem-like (MSL), immunomodulatory (IM), and luminal androgen receptor (LAR). Younger women tend to be diagnosed with TNBC, which has a mortality rate of approximately 40% in advanced stages. In addition, 45% of TNBC-diagnosed patients will develop distant metastases to the brain and/or visceral organs [12].

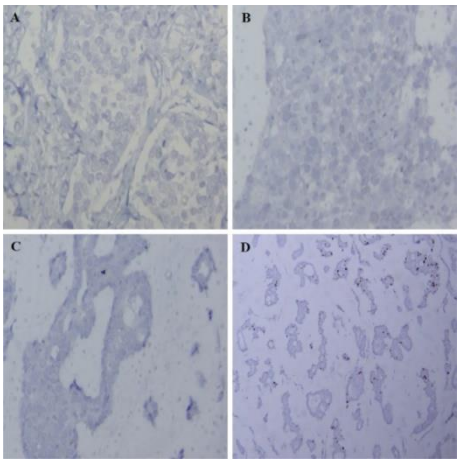

Fig 5. Immunohistochemistry aspects of triple-negative breast cancer. (A) ER-negative, **(B)** PR negative, **(C)** HER-2 negative membrane staining, **(D)** nuclear staining of Ki-67 positive 10% [7].

1.1.3. Detection, diagnosis and staging

BC is the leading cause of death among women, yet based on recent reports, the death rate has dropped from 48 deaths per 100,000 women in 1975 to 27 deaths per 100,000 women in 2019, in the United States. This is largely due to the treatment advancing and early detection. These results highlight the importance of early detection and screening for a better therapeutic outcome [13].

Early detection is the key when referring to BC, and in this context, there are two main scenarios: (i) identification of the disease in asymptomatic patients by screening test; (ii) early detection following patient complaints or following physical examination [14]. Still, in low- and middle-income countries, screening mammography may not be feasible due to resource-limited health care systems, and thus most frequently, BC patients present late-stage diagnosis. Recent studies

have shown that in high-income countries, 70% of BC patients present with stage I-II disease due to the screening programs [15].

The main techniques used in diagnosing breast cancer are mammography, ultrasound, biopsy, the core biopsy, lymph node biopsy, and fine needle aspiration (Fig. 6) [16].

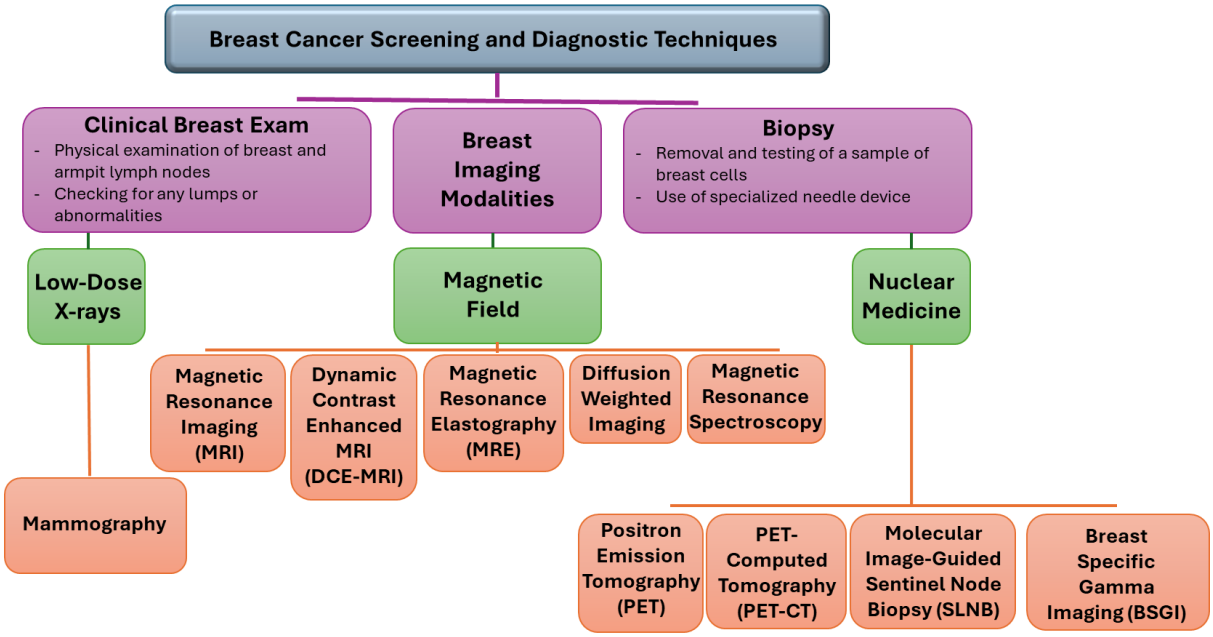

Fig 6. Various imaging techniques used in breast cancer diagnosis. Schematic representation of different breast cancer screening and diagnostic techniques [17].

The standardization of the Tumor–Node–Metastasis (TNM)-based staging of BC by the new, 8th editions of the relevant Union for International Cancer Control (UICC) and American Joint Committee on Cancer (AJCC) has allowed BC patients to be evaluated using a standard language, facilitating effective communication regarding appropriate treatment planning [18]. Accordingly, there are two staging categories: the anatomic and the prognostic one. The anatomic category is based on the primary tumor size (T), the nodal status (N), and distant metastasis (M), while the prognostic stage takes into consideration aspects such as tumor grade, biomarker status (ER, PR, HER2), and genomic panels [19].

1.1.4. Treatment

When deciding the treatment approach in BC patients, it is taking into account the grade, stage and BC molecular subtype (Fig. 7).

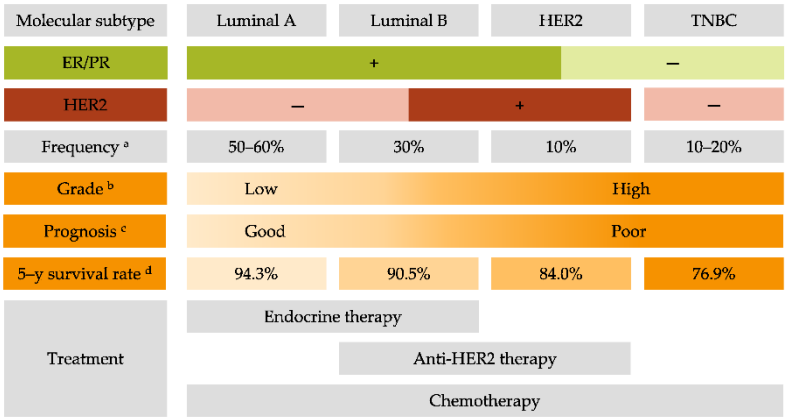

Fig 7. Breast cancer molecular subtype. Estrogen receptor (ER); Progesterone receptor (PR); Human epidermal growth factor receptor 2 (HER2); Triple-negative breast cancer (TNBC) [20].

The treatment approach is divided into three categories: (i) early BC, (ii) locally advanced BC and (iii) metastatic BC.

i. Early BC: Patients are clinically negative for lymph nodes and the tumor size is <5 cm. Treatment strategies are usually based on surgical treatment, except for some patients of this category, for example those diagnosed with triple-negative and HER-2-positive tumors equal to or greater than 2 cm in size in which case neoadjuvant systemic therapy is recommended. Chemotherapy, radiation therapy, hormone therapy, immunotherapy and PARP inhibitor therapy are also suggested [21].

ii. Locally advanced BC: Patients are clinically positive for lymph nodes and the tumor size is >5 cm. Treatment strategies include surgical treatment aiming to achieve clear histologic margins [22]; radiation therapy, given that this type of tumor is with high radiosensitivity; systemic treatment should be considered if both surgery and radiation fail to achieve disease control [23].

iii. Metastatic BC: Systemic treatment with either endocrine therapy or cytotoxic chemotherapy has become the cornerstone in managing metastatic breast cancer [24]. To control brain, bone and lung metastasis, palliative radiation may be used [25]

There are still many challenges when it comes to BC, arising from patient's resistance to treatment and recurrence, as it has been demonstrated that 30% of the early-stage BC present recurrent disease [20]. Early diagnosis and appropriate, timely treatment of breast cancer should be our focus.

1.1.5. Drug resistance

Drug resistance is a great challenge as it is a major obstacle to successful treatment, being responsible for up to 90% of deaths. Drug resistance is a process that can be acquired or innate, in both cases a variety of mechanisms are employed. These mechanisms mainly include drug efflux and inactivation, enhanced DNA repair, induction of epithelial-mesenchymal transition (EMT), epigenetic modifications and tumor microenvironment (TME) (Fig 8) [26].

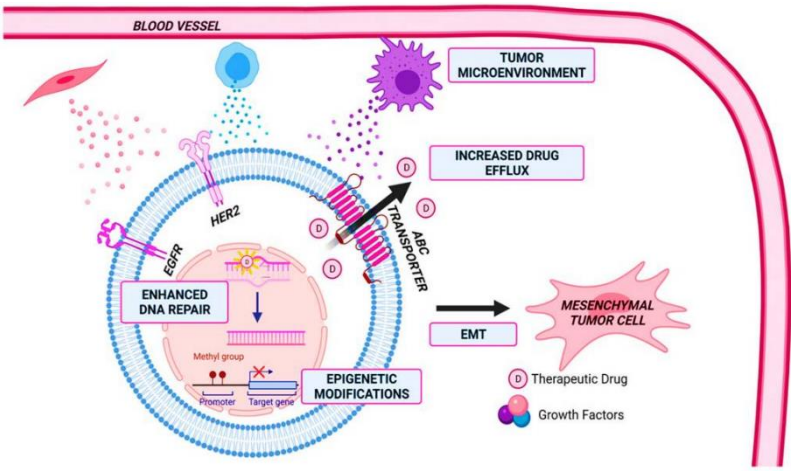

Fig 8. Mechanisms involved in drug resistance. The mechanisms mainly involved in the development of drug resistance are tumor microenvironment, drug efflux, epigenetic modification, epithelial-mesenchymal transition (EMT) [27].

New delivery systems seem to offer a good prospective, for instance extracellular vesicles as nano-carriers of a wide range of molecules such as nucleic acids, proteins, lipids, metabolites, and anti-tumor agents to target cancer cells, deliver and release their cargo in a controlled manner. Furthermore, they can enhance the efficacy of the existing anticancer drugs [28].

1.2. Sorafenib in breast cancer

1.2.1. Sorafenib targets and cellular effects

Sorafenib is a small molecule, orally administrated, that acts as a potential inhibitor of various tyrosine kinase receptors, such as BRAF, C-RAF, vascular endothelial growth factor receptor (VEGFR) and platelet-derived growth factor receptor (PDGFR), RET, c-KIT and FMS-like tyrosine kinase-3 [29]. Aberrant activation of certain signaling pathways such as the RAS-RAF-MEK-ERK signaling pathway, is commonly observed in cancer cells, leading to increased proliferative ability and cancer cell growth, but also preventing apoptosis and promoting tumor invasion. Thus, administration of drugs capable of inducing cell apoptosis and that are targeting receptors such as VEGF, may prevent invasion and metastasis caused by the ability of cancer cells to induce angiogenesis (Fig. 9).

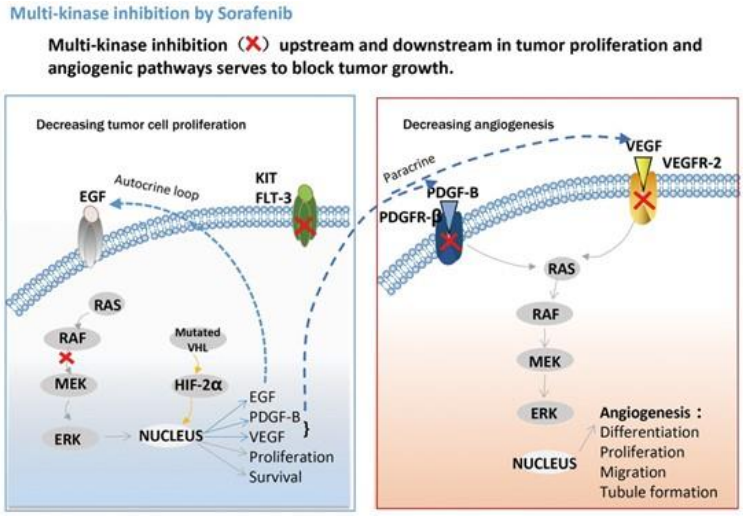

Fig 9. Sorafenib cellular targets. Sorafenib blocks the activity of certain tyrosine kinase receptors and inhibits the RAS-RAF-MEK-ERK signaling pathway, preventing tumor growth [30].

It has been well demonstrated that sorafenib was able to inhibit proliferation ability of several cancer cells, including breast cancer cells (MCF-7 and HCC 1937), in a dose-dependent manner. Moreover, BC cells treated with sorafenib expressed increased levels of GAS5 (Growth Arrest Specific 5), which acts as a tumor suppressor gene, compared to non-treated cells, suggesting that this drug can restore the expression levels of different tumor suppressor ncRNAs that are down-

modulated during cancer [31]. In a different study, MCF-7 and MDA-MB-231 were treated with 10μM sorafenib and its effect on proliferation, migration and invasion was assessed. They revealed that at this dose, the treatment was not only able to reduce the proliferative ability of these BC cells, but also to inhibit migration in a remarkable manner. 3D spheroid invasion assay allowed them to conclude that sorafenib has the power to negatively affect the ability of BC cells to invade, highlighting that the invasion ability of both MCF-7 and metastatic MDA-MB-231 cells was drastically reduced on collagen matrix in the presence of sorafenib [32]. Based on these results, we concluded that sorafenib is an effective drug able to suppress the proliferation, invasion and migration capability of BC cells, but also to restore the expression levels of downregulated tumor suppressor genes.

1.2.2. Status of sorafenib in breast cancer treatment

Sorafenib is an orally administrated drug, characterized by low solubility and high permeability, being rapidly absorbed with peak plasma levels reached in 3 hours [33]. To our knowledge, sorafenib is not typically used as a standard treatment for BC patients; however, several studies have reported its effects in this context.

The tolerability and efficacy of sorafenib have been evaluated in various cohorts of BC patients and in different combinations. For example, in HER-2 negative metastatic BC patients the efficiency of sorafenib was evaluated as monotherapy, and in combination with cytotoxic drugs (docetaxel, paclitaxel, ixabepilone), targeted agents (bevacizumab), endocrine therapy (tamoxifen, fulvestrant), and radiation therapy. Currently, in patients presenting stages I-III BC, sorafenib has been added to standard adjuvant chemotherapy [33]. Combinations of sorafenib with other agents in metastatic BC have shown fewer promising results. It has been studied that sorafenib administered in combination with vinorelbine in patients with metastatic BC presented manageable toxicity but also low efficacy; sorafenib administered together with bevacizumab gave substantial toxicity and minimal efficacy. The effect of sorafenib administered in combination with endocrine therapy has been reported. The results suggest that sorafenib may be able to enhance hormone therapy by restoring the sensitivity to it [29].

1.3.Non-coding RNA (ncRNA)

According to the Encyclopedia of DNA Elements (ENCODE) transcriptome project, only about 1.2% of the human genome is transcribed into protein-coding mRNAs, whereas approximately 80% is transcribed into a wide range of non-coding RNAs, some of which have been characterized while others are under investigation [34]. The main types of ncRNA that have been found to play an important role in cancer are: microRNA (miRNA), long ncRNA (lncRNA), circular RNA (circRNA) and PIWI interacting RNA (piRNA). All of these ncRNA can act as oncogenes or tumor suppressor genes, thus playing a crucial role in human malignancy [35].

1.3.1. MicroRNAs

MicroRNA (miRNA) is the most abundant class of ncRNAs, which was first observed in *Caenorhabditis elegans* larvae. The human genome has the largest number of miRNA genes, with approximately 2000 annotated miRNAs [36]. The first discovered miRNA, *lin-4*, was made in 1993 by the two Nobel laureates, Victor Ambros and Gary Ruvkun, who received the prize in 2024. Both groups investigated mutant *C. elegans* nematodes with developmental defects caused by alterations at the *lin-4* and *lin-14* genetic loci. By cloning the *lin-4* gene, Ambro's group made the great discovery that it did not code for a protein, but it encoded a short 22-nucleotide ncRNA. Meanwhile, Ruvkun's group discovered that *lin-4* regulates *lin-14* via multiple elements, together defining partial sequence complementarity between the short non-coding *lin-4* RNA and the 3'UTR elements of *lin-14* [37,38]. Seven years later, in 2000, the second miRNA discovered was *let7,* which was also found to be conserved across species [39].

1.3.1.1.Biogenesis

Canonical miRNA biogenesis starts in the nucleus where genomic DNA is transcribed into long primary RNA (pri-miRNA). The pri-miRNA is then cleaved by the Drosha enzyme to form a precursor miRNA (pre-miRNA) of about 70 nucleotides (nt) and a hairpin structure. The pre-miRNA is then exported to the cytoplasmic compartment of the cell, where it is cleaved by the Dicer enzyme to form mature miRNA, with a length of about 19-23 nt. Mature miRNA will form the RNA-induced silencing complex (RISC), which will block the translation of certain mRNAs by binding to their 3'-UTR end, one miRNA can target multiple mRNAs (Fig. 10) [40].

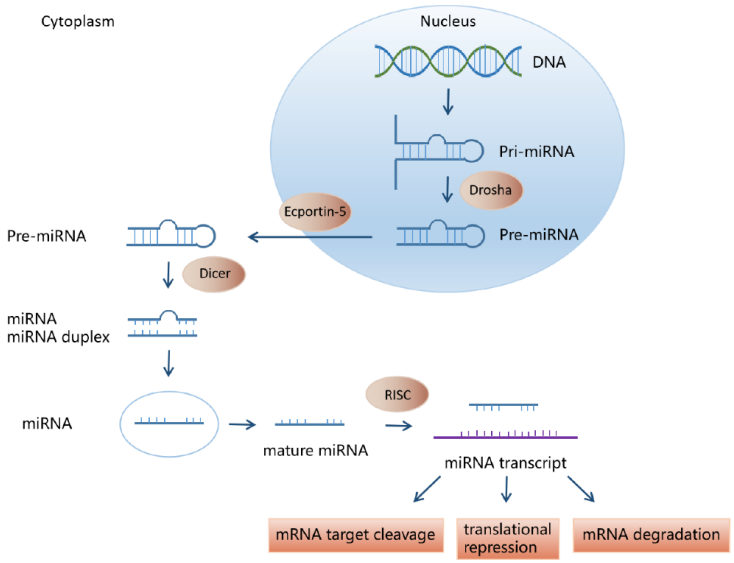

Fig 10. miRNA canonical biogenesis process. miRNAs biogenesis begins with pri-miRNA synthesis cleaved by Drosha enzyme and exported into the cytoplasm. At this level, newly form pre-miRNA will be further cleaved by Dicer enzyme and mature miRNA will form RISC for further establish its function [40].

There are also non-canonical pathways for miRNA biogenesis, which can be divided into Drosha/DGCR8-independent and Dicer-independent pathways[39]. An example of Drosha/DGCR8-independent pre-miRNA are the miRtrons, which are generated from the intronic sequence of the mRNA during splicing. After the splicing, miRtrons are exported to the cytoplasm where they are processed by Dicer to form a mature miRNA [41]. Another example of this category is the biogenesis of 7-methylguanosine (m^7G)-capped pre-miRNA, such as pre-miR-320, which is immediately exported to the cytoplasm without the need for Drosha cleavage [42]. The miRNAs generated in a Dicer-independent manner are processed by Drosha from endogenous short hairpin RNA (shRNA) transcripts [39]. An example is pre-miR-451, which is processed at the beginning by Drosha to release the pre-miRNA. Having a short stem-loop sequence that does not allow its recognition by Dicer, Ago2 appears to be sufficient for RISC loading and proper guide strand selection [41].

1.3.1.2.Functions

Animal knockout models are one way to dissect the biological function of miRNA. However, it has been shown that knocking out one miRNA may not be sufficient to determine a phenotype, therefore inactivating multiple members of a miRNA family is a way to detect a phenotypic outcome [43]. miRNAs fulfill the function of downmodulating the expression of mRNA by directing

miRISC and they can do so by two post-transcriptional mechanisms: (i) translational repression and (ii) mRNA cleavage [44].

i. All eukaryotic mRNAs are characterized by the presence of a 5'-cap structure, the 5′ terminal cap is recognized by eukaryotic translation initiation factor 4E (eIF4E) to initiate the translation process. The exact mechanism involved in the translational repression of the target mRNA through miRISC is not fully understood, but it has been demonstrated that mRNAs lacking the 5' cap but possessing an Internal RibosomeEntry Site (IRES) are refractory to miRNA-induced silencing [45]. Based on these observations, it may be due to the interaction between miRNA and the 5' cap that causes the interruption of IF4F-mediated cap-dependent translation initiation [45].
ii. Previous studies revealed that when miRNA exhibits high complementarity with the target mRNA then, its degradation is facilitated by the Argonaute (Ago) proteins, which are found in almost all eukaryotes, bacteria and archaea [44,46]. Xu K. *et al.* demonstrated in their paper that targeted gene silencing mediated by a miRNA family called let-7 could be initiated by Ago2-catalyzed cleavage at base-paired miRNA:mRNA target sites [47]. Recent studies brought to light that not only Ago is responsible for mRNA degradation, but also other mechanisms, such as deadenylation, decapping, and exonucleolytic digestion of mRNA [44].

Therefore, defining the exact mechanism involved in the modulation of mRNA expression by miRNA could provide great opportunities for the development of targeted therapies.

1.3.1.3.MicroRNAs in cancer

In cancer, miRNAs can exert oncogenic or tumor suppressor function, therefore they are named oncogenic miRNAs (onco-miRNAs) or tumor suppressor miRNAs (TS-miRNAs) [48]. Many miRNAs are highly expressed in cancer cells and in the tumor microenvironment (TEM) and have been shown to promote tumor progression. For instance, miR-17-5p it is highly expressed in a series of cancer, BC being one of them, and its over-expression negatively regulates the activity of certain tumor suppressor proteins such as AT Atypical Cadherin 4 (FAT4) and cyclin-dependent kinase 12 (CDK12), leading to the observation that suppressing multiple tumor suppressor genes simultaneously, increase the proliferative capacity of the cancer cells [49]. There are also miRNAs that have been reported to act as TS-miRNAs, such as let-7 and miR-34a. Their expression levels were found to be down-modulated in a number of cancers such as BC, colon cancer, hepatocellular

carcinoma [50]. Let-7 manifests its tumor suppressor function by negatively modulating various oncogenes resulting in a decreased stemness. Levels of let-7 are inversely correlated with the number of cancer stem cells (CSC) in BC [51]. Several studies have demonstrated that low levels of miR-34a inhibit asymmetric cell division, thereby enhancing colon cancer progression and it is being associated with a poor prognosis [50]. All these findings suggest that targeting miRNAs is a promising approach for modulating the cancer aggressiveness.

1.3.2. miR-23b-3p

1.3.2.1.Biogenesis and Functions

miR-23b-3p, formerly known as miR-23b, belongs to miR-23b/27b/24 cluster (9q22.32) (Fig. 11) [52]. miR-23b biogenesis is similar to other miRNAs, the double strand formation is catalyzed by Dicer enzyme-containing protein complex. The one strand determined to be the passenger one will be degraded, while the other will become miR-23b [53]. miR-23b was found to be involved in regulating normal physiological functions including, cell differentiation, proliferation, development and cell immunity, and is highly expressed in the brains of humans and rodents [54]. Therefore, when levels of miR-23b are dysregulated, the normal physiological functions are altered, and disease may occur.

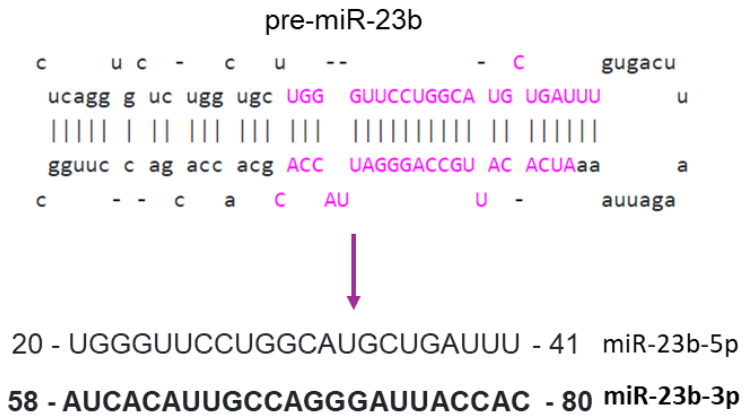

Fig. 11. Sequence of pre-miR-23b, mature miR-23b-5p and mature miR-23b-3p (miRbase).

1.3.2.2.miR-23b-3p in cancer

Multiple studies support that in a variety of cancers, low levels of miR-23b-3p led to cancer progression, suggesting that it may act as tumor suppressor ncRNA [54]. For instance, the circulating

levels of miR-23b-3p are significantly lower in patients suffering from hepatocellular carcinoma than healthy controls, and this may have potential clinical value [55]. In BC, miR-23b-3p reduces cell motility and ability to invade, on the opposite, inhibition of its expression led to increased cell migration and metastasis *in vivo* BC model. Moreover, when investigating its effect on angiogenesis, it has been observed that miR-23b over-expression decreased the expression of important pro-angiogenetic target genes such as uPA/PLAU, AMOTL1, while reducing tube-formation by endothelial cells [56]. In patients suffering from cervical cancer (CC), the expression of miR-23b-3p was reduced, moreover the overexpression of this miRNA was found to significantly reduce proliferation, migration, and invasion of CC lines by reducing c-Met expression [57]. In other types of cancer, such as endometrial cancer, when using mimic miR-23b to determine its upregulation it caused suppression of the proliferative ability of the cancer cells [58]. The same outcome was present when performing analysis on bladder cancer cells, moreover miR-23b triggers G0/G1 arrest in miR-23b transfected cells according to Majid A., *et al* [59]. All these studies suggest that miR-23b-3p mainly acts as tumor suppressor ncRNA in a variety of human cancers and could represent a predictive biomarker and therapeutic target.

1.3.3. miR-126-3p

1.3.3.1.Biogenesis and Functions

miR-126 is a member of a family of miRNA encoded by intron 7 of epidermal growth factor-like domain-containing gene 7 *(EGFL7)* located on human chromosome 9q34.3 (Fig. 12). Isoforms A, B and C of the EGFL7 have the same open reading frame but each one of them is transcribed from a separate promoter [60]. EGFL7 is a highly expressed gene in endothelial cells and vascularized tissues, controlling the vasculogenesis, this leads to a high level of miR-126 in vascularized tissues such as liver, lung, heart, and human umbilical vein endothelial cells [61,62]. Previous studies demonstrated that miR-126 target genes such as mTOR, PIK3R2, PI3K and AKT silencing them, playing an important role in anti-metastasis and anti-angiogenesis *in vitro* [62,63]. Its involvement in cell proliferation, migration, angiogenesis, vascular integrity, and inflammation has also been reported [55].

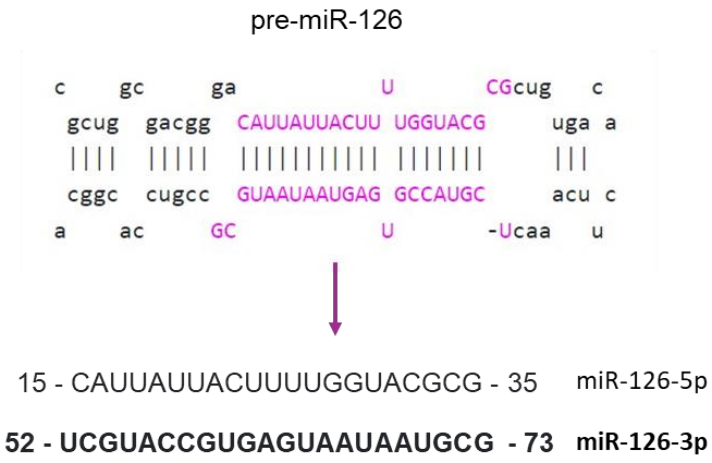

Fig. 12. Sequence of pre-miR-126, mature miR-126-5p and mature miR-126-3p (miRbase).

1.3.3.2.miR-126-3p in cancer

Patients suffering from colon cancer presented lower interval of time from surgery to the time of colon cancer death, when miR-126 was lower expressed, compared to patients presenting high levels of miR-126 [64]. Multiple studies demonstrated that miR-126-3p is down-modulated in a variety of cancers such as ovarian cancer, glioblastoma, hepatocellular cancer, clear cell renal carcinoma, and that increased levels of its expression can be correlated with prolonged survival period [65–67]. In Non-small-cell lung cancer (NSCLC), miR-126-3p was the most down-regulated miRNAs among those analyzed, when compared to normal tissue, also its upregulation was proved to be effective on inhibiting the growth, migration, invasion and metastasis of NSCLC cell [67]. In BC, miR-126 targets VEGF/PI3K/AKT signaling pathway, thereby reducing tumor growth and proliferation, vascularization, and angiogenesis of BC cells [68]. Endothelial recruitment capacity is an important factor during BC metastasis, and it has been demonstrated that miR-126 knockdown significantly increased endothelial recruitment, *vice versa* endothelial recruitment was strongly reduced by the increased expression of miR-126 [69]. All these findings suggest that miR-126 acts as a TS miRNA in a series of human cancers.

1.3.4. Long non-coding RNA

Long non-coding RNAs (lncRNAs) are defined as transcripts with a length of more than 200 nucleotides, and no protein-coding ability, although some of them may have short open reading frames (ORFs) [70]. This definition defines approximatively 270,000 types of lncRNAs in humans,

even though only several thousand have been annotated [71]. Most of these annotated lnRNAs are polymerase II (Pol II) transcribed, leading to their so-called "mRNAs-like", but there are still other lncRNAs that are not spliced and polyadenylated, being expressed from Pol I or Pol III, or from precursors [72,73]. While there is still a lack of information regarding the functions of the majority of lncRNAs, we are beginning to understand that the small number of characterized lncRNAs work at different levels and may be involved in important biological processes such as epigenetic, transcriptional, post-transcriptional, translational and post-translational regulation [72,74].

1.3.4.1.Biogenesis

Most of the lncRNAs are transcribed by RNA Pol II, and may present a poly(A) tail or 7-methylguanosine cap, reason why mRNA and lncRNA are similar in terms of biogenesis [75]. LncRNAs can be classified based on many aspects, for instance, they can be divided into five groups: sense, antisense, bidirectional, intronic and intergenic, based on their genomic origin (Fig. 13) [76].

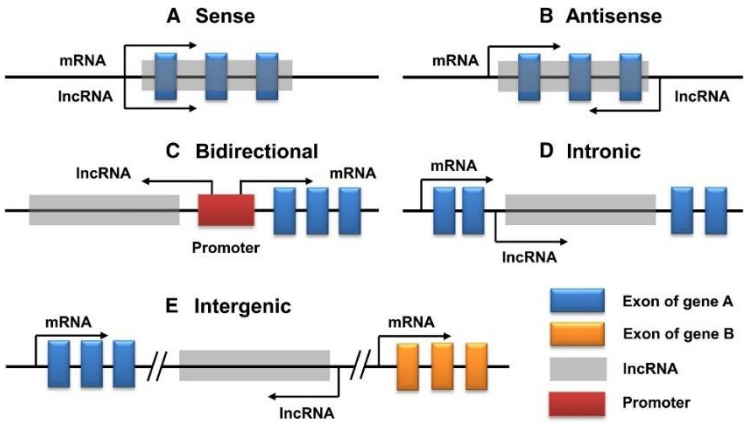

Fig. 13. Genomic origin-based classification. A Sense and **B** Antisense lncRNAs are transcribed from the sense or antisense strand of a protein-coding gene. **C** Bidirectional lncRNAs are located close to the promoter of the associated protein-coding gene. **D** Intronic lncRNAs are transcribed from inside of an intron. **E** Intergenic lncRNAs are transcribed from between two distinct genes [76].

LncRNAs can be categorized based on their functions as molecular signals, decoys, guides, and scaffolds (Fig. 14). Those transcribed in response to specific stimuli are described as molecular signals and can modulate the transcription of downstream genes, either independently or in

conjunction with transcription factors. Other lncRNAs function as decoys by directly binding to transcriptional regulators, thereby impairing their functions. Additionally, some lncRNAs influence epigenetic modifications by guiding chromatin-remodeling complexes to specific chromatin loci, while others act as scaffolds by coordinating the recruitment of repressive histone-modifying complexes to target loci [77,78].

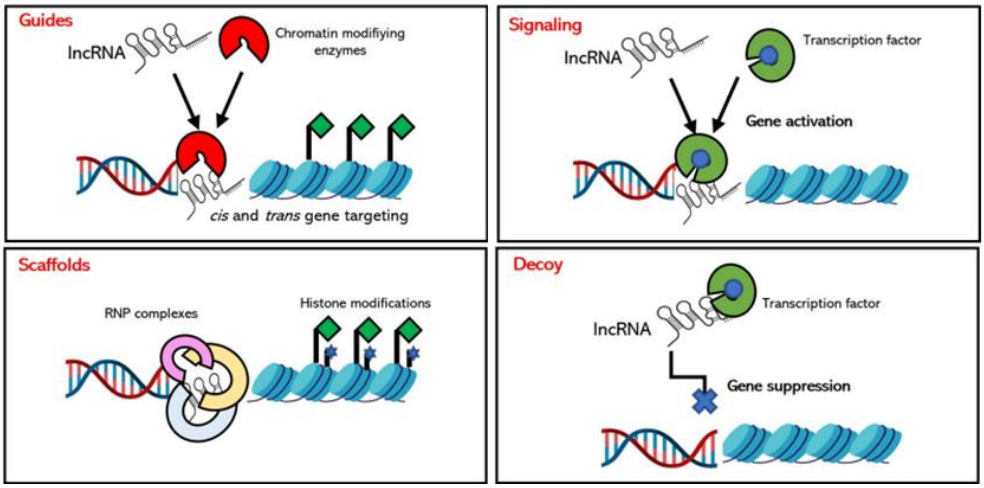

Fig. 14. LncRNA mode of action. lncRNAs act as molecular guides, scaffolds, signals, and decoys in cell [78].

1.3.4.2.Functions

LncRNA can exert both oncogenic and tumor suppressor functions, regulating gene expression in a variety of ways at epigenetic, chromatin remodeling, transcriptional, and translational levels. [79]. Due to their involvement in various biological processes such as cell differentiation and development, organogenesis and tissue homeostasis, lncRNAs have been associated with different diseases such as cancer, diabetes, rheumatoid arthritis, and neurodegenerative disorders over the years [80]. One important example is lncRNA X-inactive specific transcript (lncRNA Xist) which is involved in cell growth and development regulation. LncRNA Xist is well known for its role in X-chromosome dosage compensation, but it is also a key player in the development of tumors and other human diseases by functioning as a competing endogenous RNA (ceRNA) [81]. Nevertheless, lncRNAs involvement in physiological processes has not been overlooked, for example their role in p53-mediated tumor response to DNA damage is well known, as well as their role in

inflammation and neuropathic pain, V(D)J recombination and class switch recombination in immune cells, cholesterol biosynthesis and homeostasis [79].

1.3.4.3.LncRNA in cancer

The transformation of normal cells into cancer cells is a time-dependent, multi-step process. During this process, lncRNAs were found to be directly involved and closely related to the transformation of healthy cells into cancer cells. Moreover, lncRNAs expression in cancer was correlated with the overall survival, metastasis, tumor grade, thus having a good potential as cancer biomarkers [82]. For instance, studies have shown that the lncRNA HOTAIR promotes the metastasis of BC cells by silencing important genes within the HOXD cluster [83]. Another lncRNA that has been found to play an important role in tumor progression is MALAT1. In patients suffering from hepatocellular carcinoma, high levels of MALAT1 were correlated with cancer progression and worse prognosis [84]. HOTAIR is another lncRNA known to be involved in the progression of various cancers such as BC, liver and pancreatic cancer. Transforming growth factor β (TGF-β) stimulates the expression of HOTAIR which will further enhances epithelial-mesenchymal transition, and thus promotes cancer metastasis [85]. On the contrary, a newly characterized lncRNA, named LENGA, was found to manifest tumor suppressor effect in gastric cancer, as its knockdown caused increased migration and invasion ability of cancer cells, while cell proliferation and colony formation ability were negatively affected when LENGA was overexpressed [86]. MEG3 is another lncRNA found to have tumor suppressor functions, as its overexpression was shown to suppress both proliferation and cell cycle progression while promoting cell apoptosis in tongue squamous cell carcinoma cells [87]. All these findings support the idea that lncRNA can play a dual role, acting as either an oncogene or a tumor suppressor [88].

1.3.5. Growth arrest-specific 5 (GAS5)

1.3.5.1.Biogenesis and Functions

Growth arrest-specific is a family of lncRNA hosting 6 members (1 through 6), GAS5 is one of them, some of these isoforms are localized in the nucleus, playing a key role in various processes [89,90]. GAS5 is located on chromosome 1q25.1, with ~630 nucleotides, and consists of 12 exons that form a short open reading frame that does not code for protein (Fig.15) [91]. This lncRNA is one of the most highly expressed lncRNA in the human genome, thus being transcribed in all types of tissues. It is a 5′-terminal oligopyrimidine RNA and although GAS5 does not have protein coding

ability, it encodes for small nucleolar RNAs (snoRNAs) involved in ribosome biogenesis, 10 box C/D snoRNAs are encoded within the introns of this gene [92,93]. GAS5 has anti-tumoral functions, being involved in growth arrest and apoptosis *in vitro,* and has been found to be down-modulated in a variety of human cancers [94].

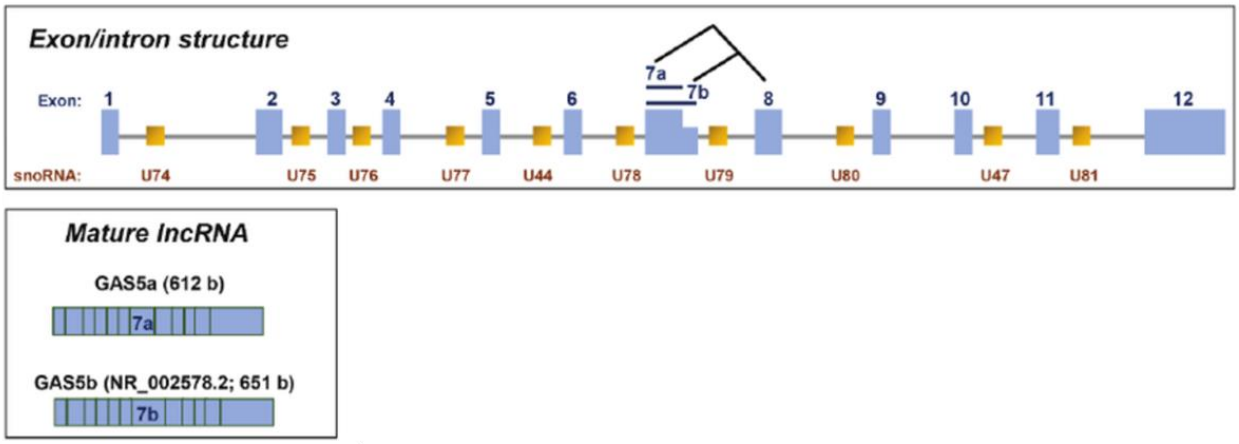

Fig. 15. Human Growth Arrest Specific 5 gene structure. The structure of the exosomes and introns and the resulting mature lncRNAs, GAS5b and GAS5a [95].

It has been well demonstrated over the years that GAS5 has a low level of expression in numerous malignant tumors, suggesting that this lncRNA may play an anticancer role. In fact, its high expression has been observed to inhibit tumor cell invasion [96]. Levels of GAS5 were considerably decreased compared to non-cancerous tissue. Moreover, high levels of mTOR were found to be responsible for BC recurrence in ER-positive BC patients and for reducing GAS5 levels leading to increased proliferation of the cancer cells [89]. Low levels of GAS5 were found to be strongly correlated with advanced stage and grade of BC, poor overall survival and disease-free survival [97]. In colorectal cancer, high levels of GAS5 were found to promote apoptosis and reduce the proliferative ability of cancer cells, on the contrary, lower levels were correlated with advanced stages and metastasis in colorectal cancer patients [96]. In lung cancer, malignant melanoma, bladder cancer and liver cancer, GAS5 manifested the same trend of expression, and its lower levels reflected an advanced tumor stage and a poor survival rate [98].

1.4. Extracellular vesicles

1.4.1. Definition and classification

Extracellular vesicles (EVs) are defined as nano-size membranous structures, ranging from 50 to 1000 nm in diameter, released by all types of cells into the extracellular space [99]. EVs have great potential as carriers as they are loaded with nucleic acids, proteins, lipids, and metabolites and can target neighboring cells *via* autocrine or paracrine signaling. EVs were first observed in 1945 by Chargaff, who described them as "membrane debris"; later on, in 1974, Nunez *et al.* also identified these "small vesicles", now known as multivesicular bodies (MVB), and characterized them as cellular products, opening the way for further research [100,101]. Between 1980 and 1990, major research was conducted and EVs were better described as biological entities, with enzymatic and functional potential, capable of intercellular communication [102].

EVs can be divided based on their size, content, function and most important, based on their biogenesis and release pathway in 3 categories: (i) ectosomes (or microvesicles); (ii) exosomes; (iii) apoptotic bodies (Fig 16) [103].

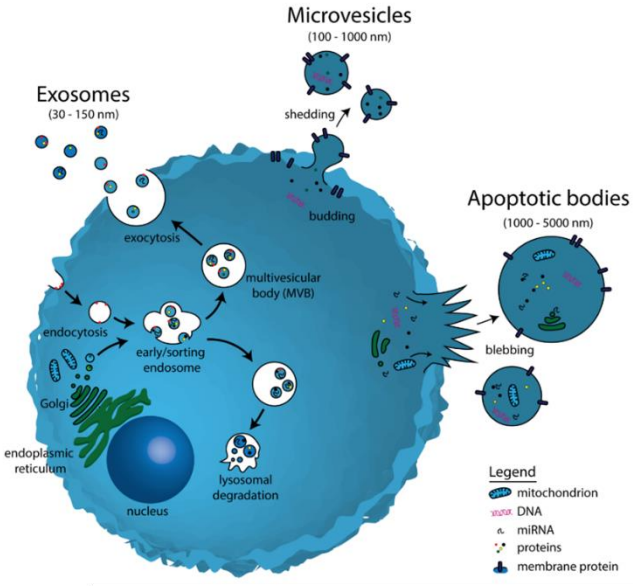

Fig.16. Classification of various EVs and representative transmission electron images. (i) Exosomes released due MVB fusion the plasma membrane; (ii) Microvesicles released *via* membrane budding; (iii) Apoptotic bodies released by the apoptotic cells [104].

1.4.2. Characterization and Biogenesis

EVs are delimitated by a membrane rich in lipids, with cholesterol being the most abundant, which prevents the degradation of the encapsulated material (nucleic acids, proteins, and metabolites). EVs are released by all cell types and can reflect their physiological or pathological status, making them useful as biomarkers for various diseases, and as biological carriers for ncRNA and drug delivery [105].

The biogenesis of EVs is different among the 3 groups and therefore ISEV encourages the use of the general term of "EVs" instead of a specific term such as "exosomes" and "endosomes" which requires knowledge of the exact biogenesis pathway [106].

i. Ectosomes (or microvesicles) are EVs derived from the direct budding and pinching of the plasma membrane, releasing newly formed microvesicles into the extracellular space [107]. Microvesicles range in size from 100-500 nm, and although the size may overlap with that of the exosomes, the distinction is made based on their biogenesis. Membrane blebbing is determined by the translocation of phosphatidylserine to the outer membrane, and it is completed by the contraction of the cytoskeleton [108,109].
ii. Exosomes (or intraluminal vesicles) have an endosomal origin. The membrane of early endosomes undergoes inward budding to mature into multivesicular bodies (MVBs). MVBs are either degraded by taking the lysosomal pathway or will fuse with the plasma membrane, resulting in the release of 30-150 nm exosomes into the extracellular space [108,110].
iii. Apoptotic bodies are released from cells undergoing programmed cell death [111]. Apoptosis is a multi-step process involving chromatin condensation, nuclear fission, membrane blebbing, and the release of membrane-enclosed vesicles, called apoptotic bodies, caused by the cleavage of cellular content [112]. Among all 3 groups of EVs, apoptotic bodies have the largest dimensions, ranging from 50 nm up to 5μm, close to the size of the platelets [111].

1.4.3. Isolation methods

Nowadays, there are many techniques that allow the isolation of EVs from different biological materials, such as: ultracentrifugation, size exclusion, precipitation, immunoaffinity capture, density gradient, each of which gives a certain yield in terms of recovery and specificity (Fig. 17) [113].

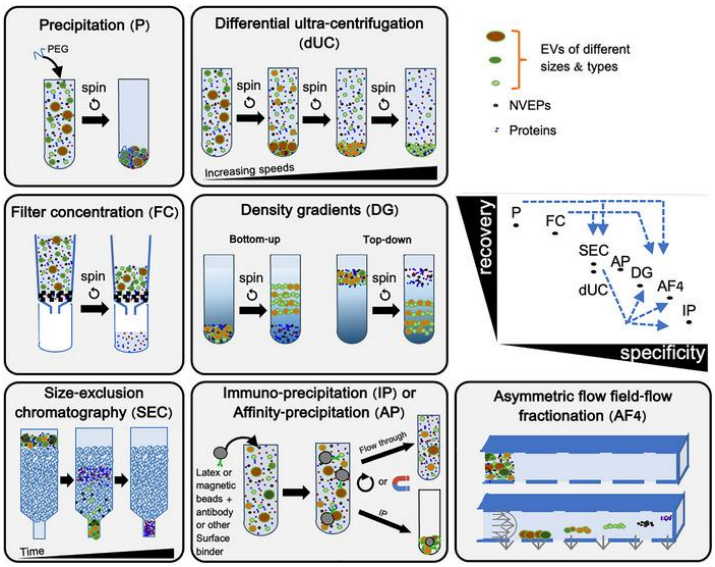

Fig 17. Schematic representation of EVs isolation methods. Precipitation (P), Filter concentration (FC) are ensuring a maximum recovery with a low specificity; immunoprecipitation (IP) is more specific but with a low recover rate [113].

Ultracentrifugation is the most commonly used method for obtaining EVs, it requires little technical expertise and is the most affordable one. During the differential centrifugation steps at speeds up to >100,000 *g*, EVs are separated based on their buoyant density [114]. Precipitation and immunoprecipitation are often used to isolate EVs. Precipitation technique will cause EVs to aggregate by adding a water-excluding polymer such as polyethylene glycol (PEG), while immunoprecipitation method is based on the use of magnetic beads coated with antibodies that will manifest immunoaffinity towards the specific surface proteins and receptors on the EVs [115]. An important difference between these two methods is that while precipitation ensures a high recovery rate but with a low specificity, immuno-precipitation is known for its high specificity but low recovery rate.

1.4.4. Extracellular vesicles in cancer

Intracellular communication is essential for proper tissue patterning and development, but also many pathological pathways are activated this way, in the context of cancer to promote its progression [116]. In this context, EVs involvement in cell-to-cell communication is well known and given that these vesicles can commute cell-derived cargoes to neighboring cells, their source of release, such as tumor cells or stem cells, is a very important aspect. Based on the cell source, EVs

will have an impact over proliferation, apoptosis, growth, migration and invasion of the recipient cells [117]. Over the years it has been well demonstrated that cancer cell-released EVs will influence non-cancer cells to create a proper tumor microenvironment that will further allow tumor growth and metastasis [118]. For the metastatic process to take place, the cells of the primary tumor must undergo an epithelial-to-mesenchymal transition (EMT) that will allow them to migrate and invade the normal surrounding tissue. It has been shown that EVs released by the cancer cells promote EMT, mediating important steps in tumor invasion and migration [119].

Nonetheless, given the excellent properties of these vesicles such as good compatibility, active substance carriers, high stability, low toxicity, EVs as vehicles to transport drugs and anti-tumor molecules arise great interest in developing new strategies in the field of cancer therapy, becoming a research hotspot [120]. To support this, previous studies demonstrated that EVs containing anti-tumor drugs could induce cell apoptosis in hepatocellular carcinoma [117]. EVs can be loaded with therapeutic cargo through active or passive methods. Directly treating the cells that will further secret the EVs with selected therapeutic drug, was found to be effective in generating drug-loaded EVs [118]. Gene therapy is holding a great potential in cancer therapy as it was demonstrated that EVs loaded with different miRNAs with anti-tumor functions were able to inhibit cell migration, invasion and self-renewal in different human cancers [120]. Moreover, EVs as biomarkers in early detection of cancer seems to have a great potential in cancer research.

1.4.5. Manipulating cargo loading

Loading therapeutic cargoes into EVs can be made in a cell-dependent or cell-independent manner. The first category is an endogenous loading that implies the direct deposition of different molecules into EVs through donner cell incubation or transfection with the desired therapeutic product that will be further load into the secreted vesicles [121]. The second category is based on post-harvest manipulation such as electroporation, sonication and transfection reagents, that will allow EVs loading with hydrophobic drugs and nucleic acids. However, these methods are challenging and can cause EVs to aggregate making the purification process very difficult [122]. Many of the recent studies have focused their work on how specific proteins can modulate the ncRNAs composition of the EVs. Heterogeneous nuclear ribonucleoprotein (hnRNP) family is one of the most studied family of proteins found to be involved in ncRNAs sorting in EVs, in this context hnRNPK enhance loading of miRNAs carrying AsUGnA motifs [123,124]. Thus, a brief

analysis allowed us to find that the mature sequence of miR-126-3p in zebrafish carries an AGUGCA motif. Moreover, fragile X messenger ribonucleoprotein 1 (FMR1) is one of the RNA binding proteins found to regulate ncRNAs sorting into EVs, Wozniak A.L. *et al.* found that in EVs, AAUGC motif was extremely concentrated and therefore FMR1 is directly involved in stimulating the loading of miRNAs presenting this specific motif into the released vesicles [125]. Interestingly, the sequence of one of the ncRNAs of our interest, mature hsa-miR-126-3p, carries an AAUGC motif which may determine a preferential incorporation into the EVs. Since the field of EVs is continuing to grow, finding efficient ways of loading desired cargoes into the vesicles could represent an important step forward in using them as target-specific drug carriers.

1.5. Danio rerio (zebrafish)

Danio rerio, zebrafish, is a small, tropical, freshwater fish, inhabitant of Himalayan region rivers of South Asia, especially Ganges River. In 1970 zebrafish was used for the first time as animal model, by George Streisinger (University of Oregon), because it was easier to genetically manipulate it compared to the mouse model [126]. Zebrafish is offering numerous advantage such as external fertilization, rapid embryonic development (blastula stage lasts only 3h, while gastrula 5h, at 24h segmentation is complete and primary organs are fully formed), it offers numerous offspring (approximatively 200 eggs/week) and has a transparent body [126,127].

1.5.1. Zebrafish as animal model for studying human disease

During past years, zebrafish became very popular as animal model, and now represents a powerful model for studying acquired and genetic human disease. Using zebrafish in modelling human disease has numerous advantages given that it has a fully sequenced genome, fast embryonic development, the embryos are translucent, and it requires economical maintenance [127]. There have been identified more than 500 mutant phenotypes allowing researchers to address issues of complex disease. What differentiates zebrafish from mouse is that early development analysis is difficult in mouse since they occur *in utero,* while zebrafish allows developmental studies starting from the fertilization until developmental stage [128]. Studies focused on metabolic diseases, for example human melanoma, acute lymphoblastic leukemia, polycystic kidney disease, Parkinson's disease, Huntington's disease, Alzheimer disease, were successfully conducted in zebrafish. Aside from the genomic similarities, 70% of human genes have zebrafish orthologues, organ systems are

conserved between human and zebrafish, allowing scientist to develop much more human disease models [129,130].

For cancer research, zebrafish is a suitable animal model since many of the factors involved in tumor progression are also conserved between human and zebrafish, 82% of human disease genes had at least one orthologue in zebrafish (Fig.18) [131]. Another strong advantage that zebrafish holds is the lack of adaptative immune system within the first 30 days post fertilization, allowing xenograft transplantation without the risk of rejection [132]. Many experiments of patients-derived xenograft transplantation were successfully conducted in zebrafish and were found to display similar cancer behavior to that observed in cancer patients. All of these could lead to personalized effective treatment design that will extend the lifespan of patients suffering from aggressive forms of cancer [133].

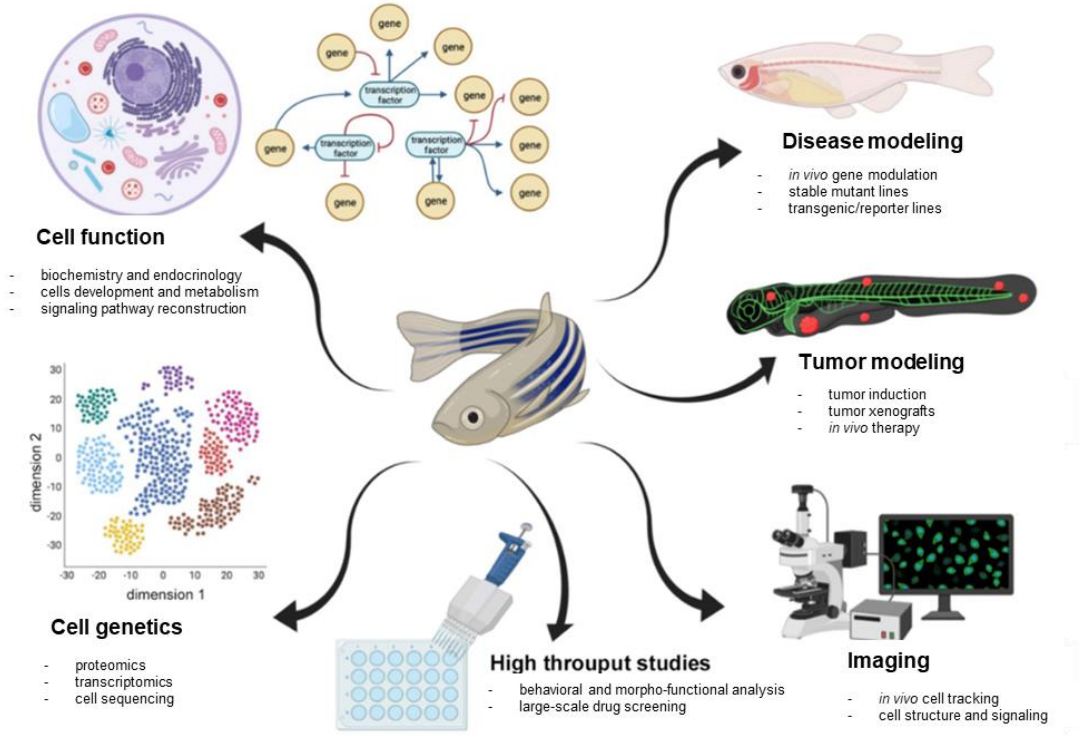

Fig. 18. Zebrafish applications. Examples of applications of the zebrafish model in cancer research [134].

2. Aim of the work

The main aim of this work was to test the capability of the EVs released by BC cells treated with a multikinase inhibitor to impair the aggressiveness of the BC *in vitro* and *in vivo*. To do this we had to:

1. Investigate the effect of sorafenib on dysregulating the levels of selected ncRNAs (miR-23b-3p, miR-126-3p and GAS5) encapsulated in EVs released by four lines of BC cells (HCC1937, MDA-MB-453, MCF-7 and MDA-MB-231).
2. Evaluate the possible correlations between the levels of these specific ncRNAs intracellularly and in EVs following treatment with sorafenib.
3. Determine whether using EVs as natural carriers could modulate the expression levels of the selected ncRNAs in target BC cells.
4. Assess if such modulation affects the aggressive properties of BC cells *in vitro*, including proliferation and apoptosis.
5. Focus on generating xenotransplantation models of BC for further treatment with EVs released by BC cells.
6. Evaluate the effects of EV-based treatment on tumor growth, metastasis formation and angiogenesis, aiming to identify innovative experimental targeted therapies.
7. Identify other miRNAs, aside from miR-23b-3p and miR-126-3p, that are dysregulated and carried by EVs released by BC cells.

3. Material and Methods

3.3. Cell culture and treatment with sorafenib

The following human breast cancer cell lines were used in this study: HCC1937 (ATCC CRL-2336), MDA-MB-453 (ATCC HTB-131), MCF-7 (ATCC HTB-22), and MDA-MB-231 (ATCC HTB-26). Cells were maintained in RPMI-1640 (Thermo Fisher Scientific); all culture media were supplemented with 20% (HCC1937 cells) and 10% (MDA-MB-453, MCF-7, and MDA-MB-231 cells) of Fetal Bovine Serum (Thermo Fisher Scientific) and 10,000 U/ml penicillin/streptomycin (ThermoFisher Scientific); cells were grown at 37 ℃ with 5% CO2.

Sorafenib, N-(3-trifluoromethyl-4-chlorophenyl)-N′-(4-(2-methylcarbamoylpyridin-4-yl) oxyphenyl) urea, was synthesized and provided by Bayer Corporation (West Haven, CT, USA). This compound was dissolved in 100% dimethyl sulfoxide (DMSO; Sigma-Aldrich) and diluted with RPMI-1640 to achieve the required concentration of 15μM. 0.1% DMSO was added to the cell cultures as a solvent-only negative control for *in vitro* studies.

3.4. Extracellular vesicles isolation

The isolation of EVs was performed *via* three methods. The first used method was Total Exosome Isolation Reagent (from cell culture media) (Thermo Fisher Scientific) as follows: cells were seeded in a 10 cm Ø dish until they rich a 90% confluence. The cell monolayer was washed 3 times with 1X PBS and 15μM sorafenib, 0.1% DMSO respectively, was added as treatment for 24h, in the absence of FBS; cell culture media represented by RPMI-1640 was harvested, centrifuged at 2,000 x g for 30 min to remove the remaining cells and debris, and the supernatant was transferred into a new tube without disturbing the pellet; afterward, the appropriate volume of Total Exosome Isolation reagent was added - for each 1 mL of cell media 500 μL of reagent were used – vortexed until obtaining a homogenous solution and incubated overnight at 4 ℃; following incubation, tubes were centrifuged at 10,000 x g for 1 h at 4 ℃, the supernatant was discarded without disturbing the pellet (not visible), where EVs were found, and resuspended in 1X PBS (for 10 mL of cell media 200 μL of 1X PBS were required). For the second used method, EVs were purified by ultracentrifugation as indicated by the International Society of Extracellular Vesicles (ISEV) [106]. Briefly, the conditioned medium was centrifuged at 300 g for 10 min at 4 °C to pellet the cells. The supernatant was collected and centrifuged at 16,500 x g for 20 min at 4 °C to eliminate apoptotic bodies and cell debris. The supernatant was then filtered through 0.22 μm filters and

ultracentrifuged at 110,000 x g for 70 min at 4 °C. Pellets were resuspended in 1X PBS and ultracentrifuged at 110,000 x g for 70 min at 4 °C. The pellet containing EVs was resuspended in 1X PBS [135]. Finally, with the third method, EVs were purified by immunoprecipitation using the Exosomes Isolation Kit Pan (Miltenyi Biotec, Germany) following the manufacturer's instructions. EVs were quantified by BCA Protein Assay Kit (Thermo Fisher Scientific).

3.5. Western blotting

EVs were lysed in Laemmli Buffer (100 mM Tris–HCl pH 6.8, 4% SDS, 20% glycerol, and 0.2% blue bromophenol) and then quantified using the BCA assay (Thermo Fisher Scientific) or by Stain-free gels (Bio-Rad, Hercules, CA, USA). Proteins were separated by SDS-PAGE and subsequently electroblotted onto polyvinylidenefluoride (PVDF) Immobilon-P membranes (Millipore, Billerica, MA, USA) as previously reported [135]. Primary antibodies were incubated overnight and anti-mouse and anti-rabbit peroxidase-conjugated secondary antibodies for 1h at room temperature. The presence of the cytosolic protein, TSG101, and three tetraspanins CD63, CD9, and CD81 (positive controls), and the absence of the non-EV component Ribosomal Protein S6 (RPS6) (negative control) were verified.

3.6. Transmission Electron Microscopy (TEM)

TEM analysis of isolated EVs was performed with a JEOL JEM-1011 transmission electron microscope at 100 kV operating voltage, equipped with a 7.1 megapixel CCD camera (Orius SC1000, Gatan, Pleasanton, CA). TEM image analysis was achieved with Gatan Digital Micrograph™ (DM) software. For sample preparation, a 5 µL drop of a concentrated vesicle suspension was dropped on a Formvar-coated copper grid and then infiltrated with a carboxymethyl dextran solution. The resulting ultrathin polysaccharide layer prevents the vesicle collapse on the dried grids. The protocol was slightly modified from the one used by Kreger B.T. *et al.* [136]. The grids were finally stained by UranyLess EM Stain (Electron Microscopy Sciences), by following the standard protocol provided by the manufacturer.

3.7. Nanoparticle tracking analysis

Nanoparticle tracking analysis (NTA) was performed using the Nanosight NS300 instrument (Malvern). A standard operating procedure was applied to acquire three independent videos of 60 seconds of each sample under a syringe pump speed 30. Samples were systematically diluted in 1X PBS to reach the recommended number of particles per frame and were recorded at Camera

level 11. Particle analysis was performed with a detection threshold of 5.0, always using NanoSight NS300 software NTA 3.4 Build 3.4.003 (Malvern).

3.8. RNA isolation and reverse transcription (RT)

3.8.1. RNA isolation and RT using extracellular vesicles

Total RNA was isolated from 200 µL of EVs resuspended in 1X PBS (Thermo Fisher Scientific) using miRNeasy Mini Kit (Qiagen), according to the manufacturer's instructions. TRIzol RNA Isolation Reagent (Thermo Fisher Scientific) was used for the total RNA isolated from cell cultures, according to the manufacturer's instructions.

For lncRNA analysis, cDNA was synthesized from 5 µL of total RNA from EVs in a 20 µL reaction volume, using M-MLV Reverse Transcriptase (Sigma-Aldrich) according to the manufacturer's instruction. The RT reaction was performed at 70 ℃ for 10 min, followed by incubation at room temperature for 10 min, a second incubation at 37 ℃ for 50 min, followed by inactivation at 94 ℃ for 10 min in a T100 Thermal Cycler (Bio-Rad Laboratories).

For miRNAs analysis, cDNA was synthesized from 5 µl of RNA from EVs in a 15 µL reaction volume, using the TaqMan microRNA Reverse Transcription Kit components (Thermo Fisher Scientific) and the stem-loop primer for miR-23b-3p (Thermo Fisher Scientific; Assay ID 000400) and miR-126-3p (Thermo Fisher Scientific; Assay ID 002228). RT reaction was performed at 16 ℃ for 30 min, 42 ℃ for another 30 min, followed by inactivation at 85 ℃ for 5 min in a T100 Thermal Cycler (Bio-Rad Laboratories).

3.8.2. RNA isolation and RT using cells

The cell-culture medium was completely removed for total RNA isolation from cells, and the cell monolayer was washed using 3 ml of phosphate buffer saline (PBS). Subsequently, PBS was discarded, and cells were disrupted by adding 1 mL TRIzol Lysis Reagent (Qiagen) to each 10 cm Ø dish. Cells were recovered using a scraper to obtain cell-lysate, which was further collected in a 1.5 mL microcentrifuge tube.

The following protocol was subsequently used:

- Add 200 µL of chloroform to every mL of added TRIzol

- Shake it vigorously for 15 sec
- Incubate at room temperature (RT) for 3 min
- Centrifuge at 12,000 x rpm for 15 min at 4 ℃. This step caused the sample's separation into 3 phases: an upper, colorless, aqueous phase containing RNA; a white interphase containing proteins; and a lower, red, organic phase containing lipids and DNA.
- The upper phase was transferred to a new collection tube. The RNA was precipitated by adding 500 µL of isopropanol, followed by incubation at RT for 10 min
- Centrifuge at 12,000 x rpm for 10 min at 4 ℃
- Discard the supernatant and wash the pellet with 1 mL of 75% ethanol
- Centrifuge at 12,000 x rpm for 15 min at 4 ℃
- Discard the ethanol and let the pellet dry at RT for up to 20 min
- Hydrate the RNA pellet with the proper amount of DEPC water.

RNA purity and concentration were assessed by NanoDropTM 1000 Spectrophotometer (ThermoFisher Scientific). NanoDrop instrument measures the UV absorbance at 230 nm, 260 nm, and 280 nm. The A260/A280 ratio of pure RNA should be between 1.8 and 2.0, while the A260/A230 ratio in the range of 2.0-2.2.

RNA integrity was assessed on 0.8% agarose gel stained with Atlas ClearSight DNA Stain (Bioatlas). The presence of two clear bands, corresponding to 28S and 18S rRNA, marks the intact RNA.

For lncRNA analysis, cDNA was synthesized from 1 µg of intracellular RNA, in a 20 µL reaction volume, using M-MLV Reverse Transcriptase (Sigma-Aldrich) according to the manufacturer's instruction. The RT reaction was performed at 70 ℃ for 10 min, followed by incubation at room temperature for 10 min, a second incubation at 37 ℃ for 50 min, followed by inactivation at 94 ℃ for 10 min in a T100 Thermal Cycler (Bio-Rad Laboratories). Intracellular cDNA was diluted 1:50.

For miRNAs analysis, cDNA was synthesized from 50 ng of cellular RNA, in a 15 µL reaction volume, using the TaqMan microRNA Reverse Transcription Kit components (Thermo Fisher Scientific) and the stem-loop primer for miR-23b-3p (Thermo Fisher Scientific; Assay ID 000400) and miR-126-3p (Thermo Fisher Scientific; Assay ID 002228). RT reaction was performed at 16 °C for 30 min, 42 °C for another 30 min, followed by inactivation at 85 °C for 5 min in a T100 Thermal Cycler (Bio-Rad Laboratories).

3.8.3. RNA isolation and RT using zebrafish embryos

Total RNA from zebrafish embryos at 72, 96, and 120 hours post fertilization (hpf) was isolated, as follows:

- Embryos were collected in 1.5 mL microcentrifuge tubes and briefly spun to pellet
- The fish water was discarded, and embryos were maintained in RNAlater (Sigma-Aldrich)
- Centrifuge at 1,500 x rpm for 5 min at 4 °C
- Discard the RNAlater and add 500 µL of TRIzol
- Start mechanically homogenizing the embryos and continue with the RNA extraction protocol reported above.

RNA purity and concentration were assessed by NanoDropTM 1000 Spectrophotometer (ThermoFisher Scientific). RNA integrity was assessed on 0.8% agarose gel stained with Atlas ClearSight DNA Stain (Bioatlas).

For lncRNA analysis, cDNA was synthesized from 1 µg of intracellular RNA, in a 20 µL reaction volume, using M-MLV Reverse Transcriptase (Sigma-Aldrich) according to the manufacturer's instruction. The RT reaction was performed at 70 °C for 10 min, followed by incubation at room temperature for 10 min, a second incubation at 37 °C for 50 min, followed by inactivation at 94 °C for 10 min in a T100 Thermal Cycler (Bio-Rad Laboratories).

For miRNAs analysis, cDNA was synthesized from 50 ng of cellular RNA, in a 15 µL reaction volume, using the TaqMan microRNA Reverse Transcription Kit components (Thermo Fisher Scientific) and the stem-loop primer for miR-23b-3p (Thermo Fisher Scientific; Assay ID 000400) and miR-126-3p (Thermo Fisher Scientific; Assay ID 002228). RT reaction was performed at 16

℃ for 30 min, 42 ℃ for another 30 min, followed by inactivation at 85 ℃ for 5 min in a T100 Thermal Cycler (Bio-Rad Laboratories).

3.9. Droplet digital PCR (ddPCR)

The synthesized cDNA was used as a template for the ddPCR experiments using the QX200 droplet digital PCR System (Bio-Rad Laboratories), and ddPCR was performed according to the ddPCR Supermix for Probes (Bio-Rad Laboratories) protocol. Briefly, 1.33 µl of the cDNA obtained using TaqMan microRNA Reverse Transcription Kit, and 3.96 µl of the cDNA obtained using M-MLV Reverse Transcriptase, were prepared for amplification in a 20 µL reaction volume containing 2X ddPCR Supermix for Probes (Bio-Rad Laboratories), 20X TaqMan assay (Thermo Fisher Scientific) specific for miR-23b-3p, miR-126-3p, and PrimeTime qPCR Assay specific for the lncRNA GAS5 (Integrated DNA Technologies) and water. Each ddPCR assay mixture (20 µL) was loaded into a disposable droplet generator cartridge (Bio-Rad) using a multichannel pipet. Then, 70 µL of droplet generation oil for probes (Bio-Rad) was loaded into the wells dedicated to oil. The cartridge was then covered with the appropriate gasket (Bio-Rad) and then placed inside the QX200 droplet generator (Bio-Rad). When droplet generation was completed, the droplets were transferred to a 96-well PCR plate using a multichannel pipette. The plate was heat-sealed with foil and placed in a T100 Thermal Cycler (Bio-Rad Laboratories). The following PCR thermal profile was used: 95 ℃ for 10 min, 94 ℃ for 30 sec (40 cycles), 60 ℃ for 1 min (40 cycles), 98 ℃ for 10 min, and 4 ℃ for 40 min. A negative control (NC) and a positive control (PC) were included. Concentration data for miR-23b-3p, miR-126-3p, and GAS5 levels were obtained using QuantaSoft Software (Bio-Rad Laboratories) as copies/µL.

TaqMan qPCR is often the first-line screening method, holding a great potential great potential in diagnostic microbiology. TaqMan chemistry is based on the presence of a short, non-extendable probe, with a specific sequence of nucleotides that will recognize and bind to the region delimitated by the primes. The 5’ end of the probe is marked by the presence of a reporter dye, while the 3’ end is tagged by a non-fluorescent quencher. Between the fluorescent dye and the quencher, a donor-acceptor FRET (fluorescence resonance energy transfer) pair is created. As the amplification takes place, the TaqMan probe will hybridize to the specific target. While the extension of one primer happens, the enzyme (Taq polymerase) will mediate the probe’s hydrolyzation which will further lead to the disruption of the FRET pair accompanied by dye release from the quenching

effect. As a result, the luminous signal is detected with a dye-specific wavelength. The emitted fluorescence signal is proportional to the accumulated amount of PCR product [137].

3.10. RNA sequencing

RNA extracted from EVs isolated by ultracentrifugation underwent RNA sequencing analysis. Briefly, the conditioned medium underwent a series of ultracentrifugation steps for obtaining a pellet containing EVs that was further resuspended in 1X PBS. Then, using miRNeasy Mini Kit (Qiagen), the RNA was extracted and quantified, its purity and concentration were assessed by NanoDropTM 1000 Spectrophotometer (ThermoFisher Scientific). One µg of fresh RNA extracted from EV_{DMSO} and $EV_{sorafenib}$ derived from HCC1937, MDA-MB-453, MCF-7 and MDA-MB-231 BC cells were used for miRNA sequencing. The RNA-sequencing was performed by Biodiversa s.r.l. (http://www.biodiversa.it/). Briefly, libraries were prepared with the SMARTer smRNA-Seq Kit for Illumina, according to the manufacturer's instruction and sequenced on Illumina NovaSeq platform. FASTQ files were trimmed accordingly to the guidelines reported in the SMARTer smRNA-Seq Kit manual using miRge3.0 software. The same software was used to align the sequences and to produce miRNA counts.

miRNA differential expression analysis (miDEA) was performed using the DESeq2 package in R, as described in Love et al., 2014. Principal Component Analysis (PCA) was performed with the PlotPCA function implemented in the DESeq2 package on the regularized log-transformed (rlog) data, using the totality of miRNA analyzed. PCA uncovered a minor batch effect due to the cell lines, therefore "cell line" was included as covariate in the model. Wald test implemented in DESeq2 was used to identify differentially expressed miRNA (miRDEGs). Pheatmap was used to generate heatmap from miRDEGs. Only miRNA expressed with at least 10 reads in at least three samples were considered for the analysis. False discovery rate BH FDR was used to control for multiple tests comparisons and genes with FDR < 0.05 were considered as DEGs. DEGs were annotated based on the Gene Ontology (GO) and the Kyoto Encyclopedia of Genes and Genome (KEGG) terms using the DAVID database. A Pareto chart was generated using Microsoft Excel to visualize and prioritize the most significant miRDEGs. The number of reads and corresponding p-values for each miRNA were plotted, and based on these two factors, the miRNAs with the highest combined significance (high read count and low p-value) were selected for further analysis. The Enrichr web tool was used to perform the enrichment analysis.

3.11. Extracellular vesicle labeling and uptake

MDA-MB-453 and MCF-7 BC cells were incubated with CellTracker™ CM-DiI Dye (Thermo Fisher Scientific) diluted 1:1,500 in RPMI (-FBS) for 24 h at 37 ℃ with 5% CO2. Cell culture media was recovered and labeled EVs were obtained using the Total Exosome Isolation Reagent (from cell culture media).

Coverslips were placed into 3 cm diameter plates and $3x10^5$ cells were seeded and incubated at 37 ℃ with 5% CO2. When indicated, labeled EVs were added to the cells in a final volume of 3 mL of RPMI (-FBS) and incubated for 24 h at 37 °C. Samples were washed with 1X PBS and fixed using methanol as follows:

- Discard cell media and wash the monolayer 3 times using 1X PBS
- Fix with 100% methanol in two successive steps: incubate cell with 1 mL for 20 min at RT; discard and add another mL for 10 min at RT
- Was the monolayer using 1X PBS
- Add DAPI (1:3,000, Merck, Inc., Darmstadt, Germany) and incubate for 15 min at RT to stain cell nuclei
- Wash with 1X PBS and mount the coverslips using Vectashield mounting medium (Vector Labs, Newark, CA, USA) and visualize using a Leitz fluorescence microscope.

3.12. Cell proliferation assay and viability assay

For cell proliferation, MTT assay was performed using CellTiter reagent (Promega) according to the manufacturer's instructions. Briefly, cells were seeded in a 96-wells plate (5 replicates for each experimental condition) having a density of 8 x 10^3 cells/well in RPMI (-FBS) and treated accordingly with 4 µL of EVs, 0.1% DMSO or 15 µM sorafenib. After 24 h viability was assessed with the addition of 10 µL/well of sterile CellTiter reagent (Promega). The plates were incubated at 37 °C for 2 h in a humidified, 5% CO2 atmosphere and the absorbance at 490 nm was recorded using the microplate reader EnSight (PerkinElmer, Waltham, MA). For assessing the viability, a 1:2 dilution of cell suspension was made in 0.4% trypan blue stain in a 0.2 ml tube (10 µl of cell suspension added to 10 µl of trypan blue). Ten microliters of the mixture were loaded into the opening of the TC20 counting slide (Bio-Rad). The slide was then inserted into the TC20 instrument (Bio-Rad). The presence of the counting slide is automatically detected by the instrument. Cells were counted within 10 minutes of mixing trypan blue.

3.13. Zebrafish maintenance and egg collection

Danio rerio (zebrafish) was maintained and used according to EU Directive 2010/63/EU for animal use following protocols approved by the local committee (OPBA) and authorized by the Ministry of Health (Authorization Number 287/2018). Fish were maintained in 3 L of water at a controlled- temperature of 28.5 ℃ with alternate light-dark cycle, 14 h light and 10 h dark, and fed as described by Aleström and colleagues [138]. Mating was set up in organized tanks, upon fertilization the eggs were collected and placed in a Petri dish containing fish water and incubated at 28 °C. Tricaine (MS222; E10521, Sigma–Aldrich St. Louis, MO, USA) was added to the fish water for zebrafish embryos and larvae anesthesia at 0.02 % final concentration. The wild-type line used in this work included an AB strain (KIT Institute -Karlsruhe-Germany) and a transgenic line Tg(kdrl-EGFP) [139].

3.14. EVs uptake in zebrafish

Stock solutions of EVs were prepared for embryo exposure at 5, 10, and 15 µl in 2 mL fish water. Embryos were collected and selected to discard any dead embryos, while transferring all the remaining live embryos to new Petri dishes. At the gastrula stage (5 hours post-fertilization) were exposed to EV_{DMSO} or $EV_{sorafenib}$ at the selected dose by the classic immersion method [140,141] up to 96hpf. As a negative control, embryos were exposed to fish water plus 0.1% DMSO (expected mortality rate < 15 %). As a positive control for survival rate experiments, we used 3,4-dichloroaniline (DCS) (Sigma-Aldrich) dissolved in fish water at a concentration of 3.74 mg/L (expected mortality rate > 85-90%) [142]. For each treatment condition (EV_{DMSO} or $EV_{sorafenib}$), 30 embryos were used, and experiments were repeated three times. For all experiments only positive embryos (embryos labeled with marked EVs with DiI) were taken into consideration. The survival rate was recorded at 24, 48, 72, and 96 hours post-fertilization (hpf) respectively and a dose-response graph was plotted. The calculated percentages of dead embryos were below 15%, which is the expected mortality according to the OECD 2019 guidelines (Test Guideline No. 203, Fish Acute Toxicity Testing) [143] and a dose-response graph was plotted.

3.15. Induction of tumor xenografts

Tumor xenograft experiments were performed according to the protocol established by Basnet R.M. et al. in their paper [144] with minor modifications. To evaluate the effect of EVs on tumor growth, 48 hpf Tg (kdrl:EGFP) zebrafish embryos were dechorionated, anesthetized with tricaine at 0.02 % final concentration, followed by microinjection of the labeled MDA-MB-231 and MDA-MB-453 cells into the in the perivitelline space (PVS). Microinjections were performed with a FemtoJet electronic microinjector coupled with an InjectMan N12 manipulator (Eppendorf Italia, Milan, Italy). Approximately 250 cells/4 nL were injected into the in the perivitelline space (PVS) of each embryo (about 25 embryos/group); embryos were maintained in PTU/fish water in a 32 °C incubator to allow tumor cell growth. Pictures of injected embryos were acquired using Zeiss Axiozoom V13 (Zeiss, Jena, Germany) fluorescence microscope, equipped with Zen pro software, 2 h after cell injection (T0). 15 µl of $EV_{sorafenib}$ or EV_{DMSO} were directly added to the injected embryos in PTU/fish water at 2 hpi. At 1 day post-injection (T1) and at 3 days post-injection (T3), the effects of the EVs-based treatment on tumor xenografts growth were scored by representative pictures, to measure the tumor areas of each group at T0, T1 and T3 using Zen Blue software from ZEISS. Embryos with micrometastasis (indicated by the presence of at least one fluorescence dot outside the site of injection) and metastatic cells in the tails were counted. Representative xenografted embryos were fixed and embedded in low-melting agarose for image analysis.

3.16. Image analysis

Bright-field and fluorescence images of embryos at different development stages (anesthetized with tricaine 0.16 mg/mL embedded in 0.8% low melting agarose and mounted on a depression slide) were captured using a Zeiss Axio Zoom V16 equipped with Zeiss Axiocam 506 color digital camera and processed using Zen 3.5 (Blue Version) software from Zeiss (Oberkochen, Germany), magnification 32x and 40x. Embryos were also observed using AxioObserver.Z1/7 with Apotome 3, Objective EC Plan-Neofluar 20x/0.50 (Carl Zeiss S.p.A., Milan Italy). For Light Sheet analysis embryos were first anesthetized using tricaine (0.02% in fish water) and subsequently included in a low melting agarose matrix (Top Vision Low Melting Point Agarose, Thermo FisherScientific) (0.5% in fish water). Images were acquired using Zeiss LightSheet microscope V1 supported by ZenPro software using a 488–30 nm laser and 505–545 nm filter. Images from the same experiment were taken with the same laser intensity and exposure time to generate comparable images. After the acquisition, 3D images were generated and manipulated using Arivis Vision 4D (Zeiss

Oberkochen, Germany) 3D reconstructions of EGFP-positive cells were manipulated to obtain pictures comparable to each other in terms of fluorescence intensity. 3D reconstructions were exported as a single snap with the same compression setting.

3.17. Alkaline Phosphatase (AP) assay

AP assay was performed as described elsewhere, with minor modifications [145]. Briefly, embryos (n = 25) at one-day post-injection (72 hpf) were fixed in 4% PFA and then put in 100% (v/v) methanol-solution. The embryos were then equilibrated in Tris buffer (100 mM Tris HCl pH 9.5, 50 mM MgCl2, 100 mM NaCl, 0.1% Tween-20) and stained with nitro blue tetrazolium chloride (NBT) and 5-bromo-4-chloro-3'-indolyphosphate p-toluidine salt (BCIP) solution. The images were taken in a lateral and dorsal position at 32× magnification with a Zeiss AxiozoomV13 (Zeiss, Jena, Germany) microscope, equipped with a PlanNeoFluar Z 1×/0.25 FWD 56mm lens and Zen Pro software.

3.18. Statistics and Reproducibility

Statistical analysis was carried out using GraphPad Prism v8.0 (GraphPad Software, Inc., San Diego, CA, USA) software. Unpaired Student's t-test was used to determine the differences of ncRNAs levels in EVs between the sorafenib treated cells and their control (0.1% DMSO) and for cell proliferation after the EV-based treatment. Analysis of variance (ANOVA) followed by post-hoc Tukey's test was used to determine the significant differences in the ncRNAs levels after EV-based treatment as well as in the measurement of the tumor area, the assessment of micrometastases and angiogenesis in xenograft. All experiments conducted *in vitro* were performed two times, while *in vivo* experiments conducted in zebrafish, were performed three times and the number of embryos for each experimental point was n=30. Data was considered statistically significant when the *P*-value ≤ 0.05.

4. Results

4.1. Sorafenib treatment caused dysregulation of miR-23b-3p, miR-126-3p, and GAS5 in BC cells and in their cognate EVs.

To determine whether the treatment with this multikinase inhibitor can cause miR-23-3p, miR-126-3p and GAS5 dysregulation both intracellularly and in the released EVs, we analyzed 4 BC cell lines. HCC1937, MDA-MB-453, MCF-7, and MDA-MB-231 cells were treated for 24 h with 15 μM sorafenib or 0.1% dimethyl sulfoxide (DMSO) used as a dissolving compound. The conditioned media of serum-starved BC cells were collected and EVs were isolated throughout 3 different techniques. During this step, RNA was extracted from the cells for further analysis. Using droplet digital PCR (ddPCR) technology, we quantified the levels of miR-23b-3p, miR-126-3p and GAS5, measured as copies/μL, within EVs and cells. The vesicles isolated from cells subjected to sorafenib treatment were named "$EV_{sorafenib}$" while those originating from cells treated with DMSO were named "EV_{DMSO}". When the vesicles were analyzed, a general trend was observed represented by higher levels of the selected ncRNAs in $EV_{sorafenib}$ compared to EV_{DMSO}. Interestingly, when comparing the concentration of the selected ncRNAs in the EVs isolated using Exosome Isolation Reagent (precipitation) (Fig. 19A-B), ultracentrifugation (Fig. 20A-B) and immunoprecipitation (Fig. 21A-B), we noticed that those obtained by precipitation methods exhibited the highest levels of miR-23-3p, miR-126-3p and GAS5. Therefore, we decided to carry out the following experiments using this specific vesicle type.

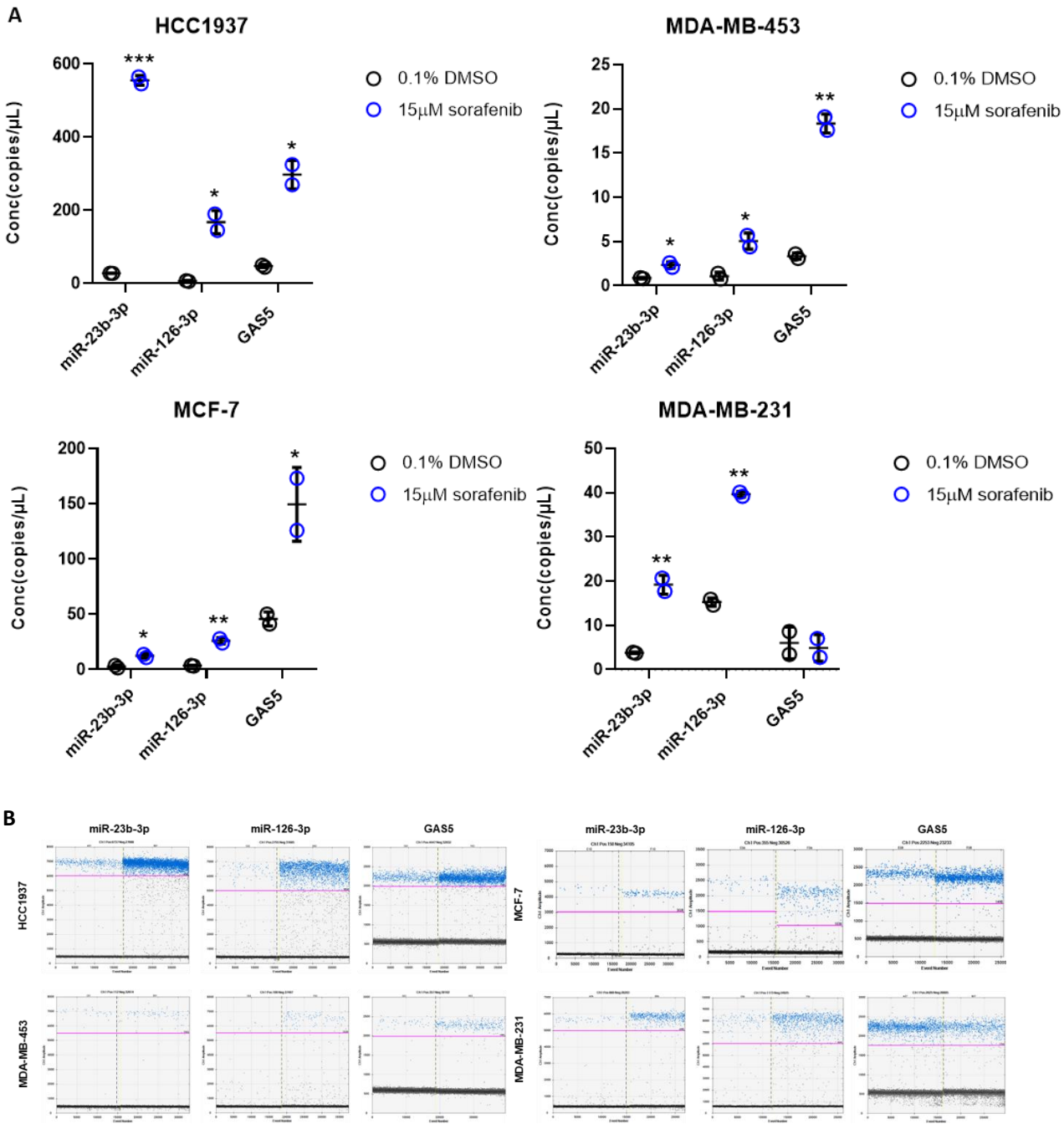

Figure 19. Levels of miR-23b-3p, miR-126-3p, and GAS5 in EVs isolated *via* precipitation. Levels of the 3 ncRNAs encapsulated in the EVs derived from HCC1937, MDA-MB-453, MCF-7, and MDA-MB-231 breast cancer cells after sorafenib treatment. **A** Concentration of each target is expressed as copies/µL. Treatment caused dysregulation of the level of the 3 selected ncRNAs. The graphics represent mean value; bars, SD. Unpaired t-test was used; *$p < 0.05$, **$p < 0.01$, ***$p < 0.001$. **B** 1D-plot of ddPCR reactions. Each lane represents EV_{DMSO} or $EV_{sorafenib}$. X-axis: droplet count; Y-axis: fluorescence intensity in the FAM-channel (blue dots, positive); pink line, threshold; grey dots, droplets with background fluorescence of non-incorporated probes (negative). Results are representative of two independent experiments.

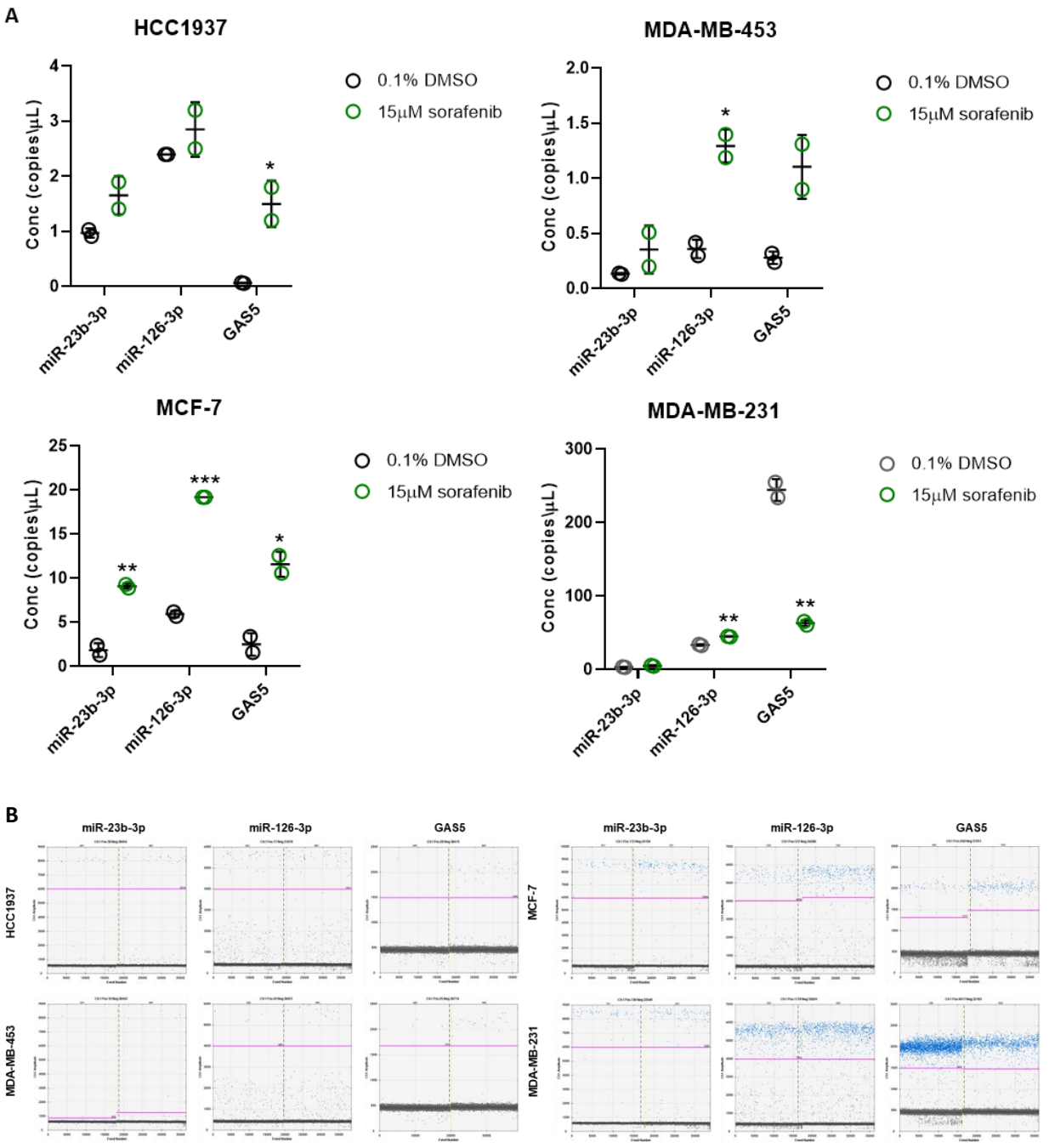

Figure 20. Levels of miR-23b-3p, miR-126-3p, and GAS5 in EVs isolated *via* ultracentrifugation. Levels of the 3 ncRNAs encapsulated in the EVs derived from HCC1937, MDA-MB-453, MCF-7, and MDA-MB-231 breast cancer cells after sorafenib treatment. **A** Concentration of each target is expressed as copies/µL. Treatment caused dysregulation of the level of the 3 selected ncRNAs. The graphics represent mean value; bars, SD. Unpaired t-test was used; *$p < 0.05$, **$p < 0.01$, ***$p < 0.001$. **B** 1D-plot of ddPCR reactions. Each lane represents EV_{DMSO} or $EV_{sorafenib}$. X-axis: droplet count; Y-axis: fluorescence intensity in the FAM-channel (blue dots, positive); pink line, threshold; grey dots, droplets with background fluorescence of non-incorporated probes (negative). Results are representative of two independent experiments.

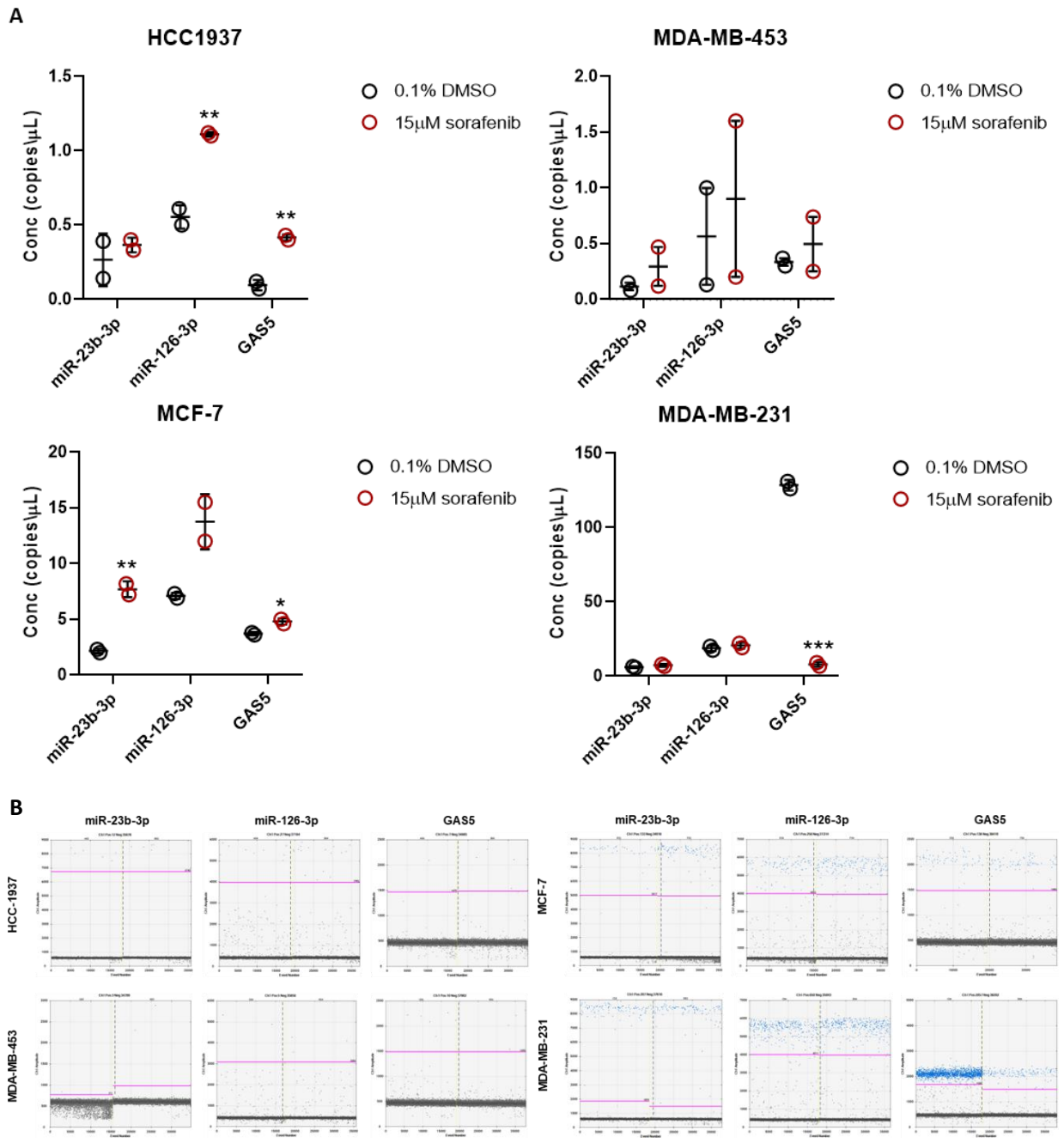

Figure 21. Levels of miR-23b-3p, miR-126-3p, and GAS5 in EVs isolated *via* immunoprecipitation. Levels of the 3 ncRNAs encapsulated in the EVs derived from HCC1937, MDA-MB-453, MCF-7, and MDA-MB-231 breast cancer cells after sorafenib treatment. **A** Concentration of each target is expressed as copies/µL. Treatment caused dysregulation of the level of the 3 selected ncRNAs. The graphics represent mean value; bars, SD. Unpaired t-test was used; *$p < 0.05$, **$p < 0.01$, ***$p < 0.001$. **B** 1D-plot of ddPCR reactions. Each lane represents EV_{DMSO} or $EV_{sorafenib}$. X-axis: droplet count; Y-axis: fluorescence intensity in the FAM-channel (blue dots, positive); pink line, threshold; grey dots, droplets with background fluorescence of non-incorporated probes (negative). Results are representative of two independent experiments.

The highest fold increases (F.I.) in vesicles obtained *via* precipitation, calculated as a *ratio* between (copies/µl) $EV_{sorafenib}$/ (copies/µl) EV_{DMSO}, were detected in $EV_{sorafenib}$ produced by HCC1937 cells (F.I. miR-23b-3p = 19.8; F.I. miR-126-3p = 24.4; F.I. GAS5 = 6.2). In $EV_{sorafenib}$ secreted by MDA-MB-453, MCF-7 and MDA-MB-231, the F.I. was comprised between 2.7 and 7.4 with just one exception represented by $EV_{sorafenib}$ from MDA-MB-231 where GAS5 displayed an opposite trend with a fold decrease (F.D), calculated as a *ratio* between (copies/µl) EV_{DMSO}/ (copies/µl) $EV_{sorafenib}$, expressed as negative value of -1.2 (Table 1). The fold increase/ decrease determined in EVs obtained by ultracentrifugation and immunoprecipitation are reported in Table 2 and Table 3.

Table 1. Factor increase/decrease was calculated as the ratio between (copies/µL) EVsorafenib / (copies/µL) EVDMSO derived from HCC1937, MDA-MB-453, MCF-7, and MDA-MB-231 breast cancer cells. EVs were obtained using Total Exosome Isolation Reagent (from cell culture media) (Thermo Fisher Scientific). The arrows in the table indicate the direction of regulation.

Cell line	miR-23b-3p	FI/ FD*	miR-126-3p	FI/ FD*	GAS5	FI/ FD*
HCC 1937	↑	19.8	↑	24.4	↑	6.2
MDA-MB-453	↑	2.7	↑	4.7	↑	5.5
MCF-7	↑	4.7	↑	7.4	↑	3.3
MDA-MB-231	↑	5	↑	2.6	↓	-1.2

Table 2. Factor increase/decrease was calculated as the ratio between (copies/µL) EVsorafenib / (copies/µL) EVDMSO derived from HCC1937, MDA-MB-453, MCF-7, and MDA-MB-231 breast cancer cells. EVs were obtained by ultracentrifugation. The arrows in the table indicate the direction of regulation.

Cell line	miR-23b-3p	FI/ FD*	miR-126-3p	FI/ FD*	GAS5	FI/ FD*
HCC 1937	↑	1.5	↑	1.2	↑	30
MDA-MB-453	↑	3.9	↑	4	↑	5.4
MCF-7	↑	3.7	↑	3.4	↑	3.7
MDA-MB-231	↑	1.5	↑	1.4	↓	-3.5

Table 3. Factor increase/decrease was calculated as the ratio between (copies/µL) EVsorafenib / (copies/µL) EVDMSO derived from HCC1937, MDA-MB-453, MCF-7, and MDA-MB-231 breast cancer cells. EVs were obtained by immunoprecipitation. The arrows in the table indicate the direction of regulation.

Cell line	miR-23b-3p	FI/ FD*	miR-126-3p	FI/ FD*	GAS5	FI/ FD*
HCC 1937	=	1	↑	1.8	↑	5.7
MDA-MB-453	↑	1.5	↑	1.5	↓	-1.5
MCF-7	↑	3.1	↑	1.6	↑	1.2
MDA-MB-231	=	1	↑	1.1	↓	-14.5

Furthermore, when the expression levels of the 3 selected ncRNAs were quantified intracellularly, we found that the treatment determined a dysregulation of their expression (Fig 22A-B). In HCC1937 and MDA-MB-453, sorafenib was able to determine an increased level of miR-23-3p, miR-126-3p and GAS5 in the cells and the same trend was observed in their cognate EVs. Conversely, in MDA-MB-231 the levels of the 2 miRNAs displayed an opposite trend being downregulated following sorafenib treatment, while GAS5 expression remained slightly unchanged. No changes of the 2 miRNAs expression levels were detected in MCF-7 cells, whereas GAS5 levels were higher compared to the control.

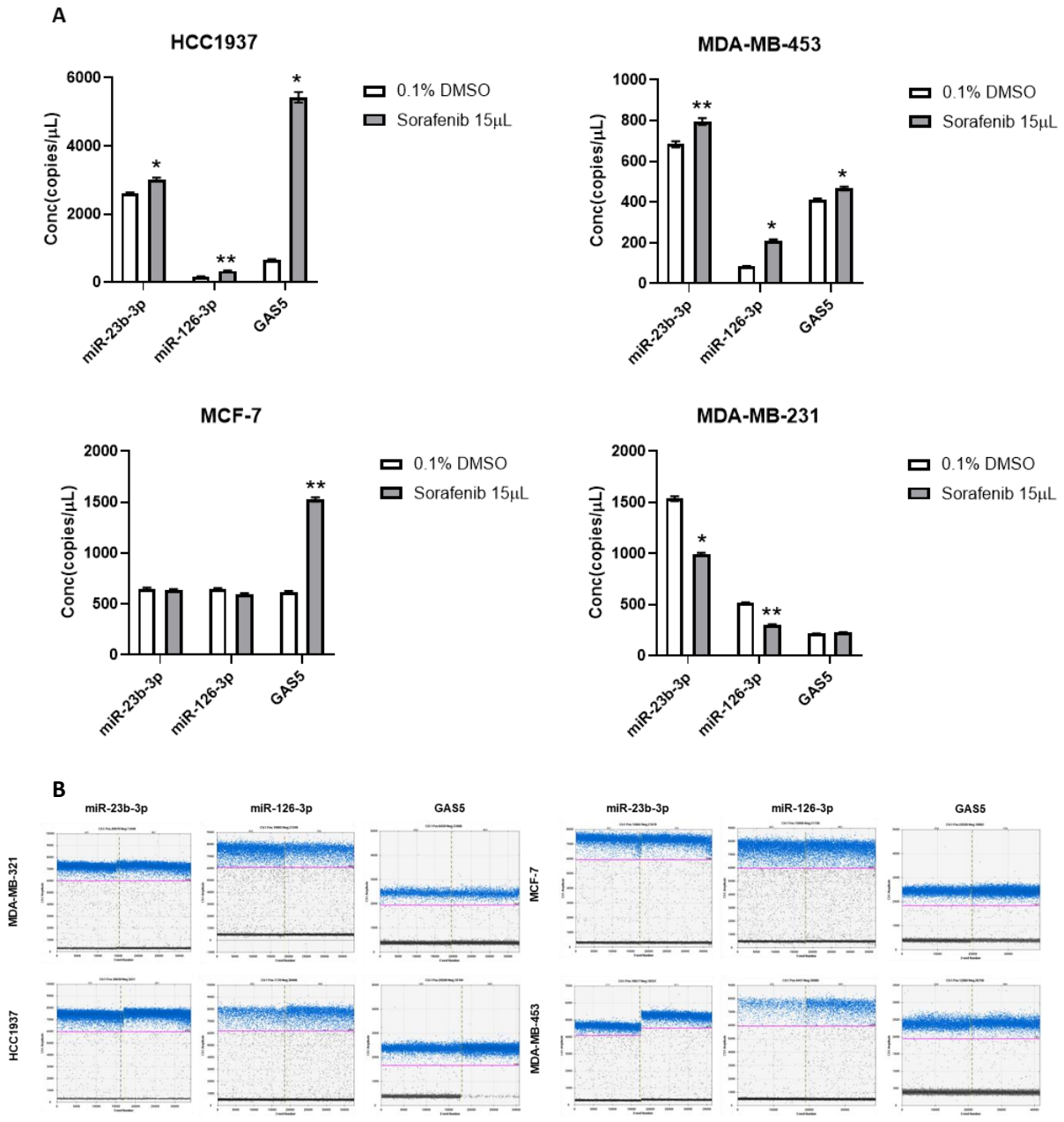

Figure 22. Expression levels of miR-23b-3p, miR-126-3p, and GAS5 in HCC1937, MDA-MB-453, MCF-7, and MDA-MB-231 breast cancer cells after sorafenib treatment. Levels of miR-23b-3p, miR-126-3p, and GAS5 were determined using ddPCR technology. **A** Concentration of each target is expressed as copies/µL. Treatment with sorafenib caused dysregulation of the level of the 3 selected ncRNAs. The graphics represent mean value; bars, SD. Unpaired t-test was used; *$p < 0.05$, **$p < 0.01$. **B** Fluorescent intensity of the droplets after amplification. The individual lanes correspond to EV_{DMSO} or $EV_{sorafenib}$. X axis, number of droplets with fluorescence; Y axis, fluorescence intensity detected in the FAM-channel (blue dots, positive); pink line, threshold; grey dots, droplets with background fluorescence of non-incorporated probes (negative). Results are representative of two independent experiments.

4.2. Characterization of the EVs.

The characterization of EVs is of great importance to determine their presence in the preparation and to measure their quality [106]. We chose to analyze EV_{DMSO} and $EV_{sorafenib}$ isolated through immunoprecipitation because this technique offers higher specificity. The isolated EVs were characterized *via* WB for specific EV markers, including the tetraspanins CD63, CD81, and CD9, as well as the MVB-related protein TSG101. The WB results showed the presence of distinct bands indicating that all four proteins were expressed on the EV membrane of interest (Fig.23A). Moreover, the presence of CD63 and TSG101 allowed us to hypothesize that the origin of these vesicles is endosomal. Due to heavy glycosylation, tetraspanin CD63 appears as a smear for both types of EVs released by MCF-7 cells (Fig. 23A, lanes 3-4). TEM analysis was performed on EVs obtained *via* ultracentrifugation, as the immunoprecipitation method was not suitable for this type of analysis. TEM images show specific round-shaped vesicles with characteristic size in the range of 50-150 nm in diameter (Fig. 23B).

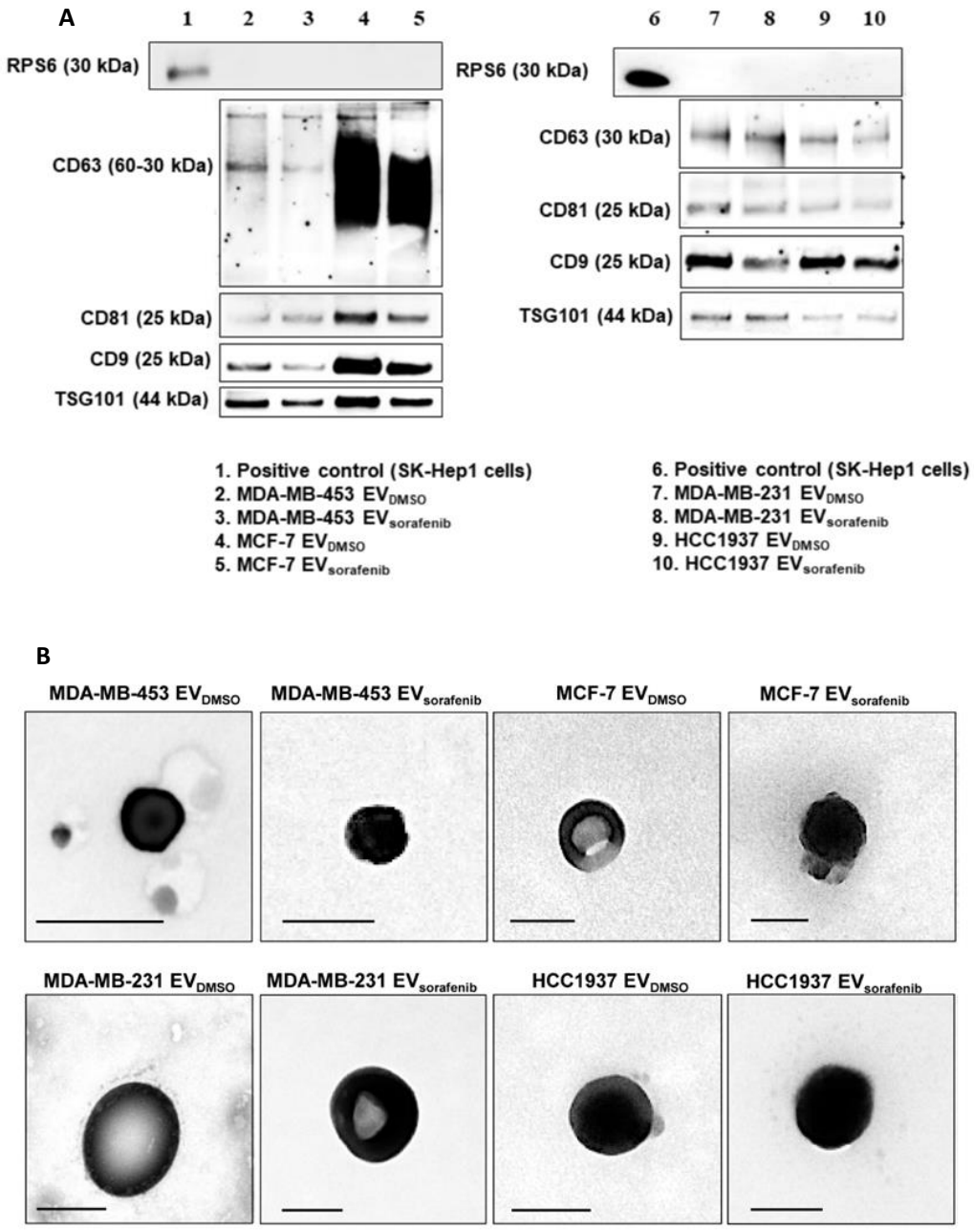

Figure 23. Characterization of EVs. **A** Western blot for tetraspanins (CD63, CD81, CD9), TSG101 and RPS6 was performed on EVs purified by immunoprecipitation and derived from MDA-MB-453, MCF-7, MDA-MB-231, and HCC1937 cells treated with sorafenib. **B** Transmission electron microscopy (TEM) on EVs obtained by ultracentrifugation showed vesicles with characteristic morphology and size, between 50 and 150 nm in diameter. Scale bar, 100 nm.

Furthermore, we decided to characterize just 2 types of EVs, by WB and TEM analysis, the ones employed for further experiments and isolated using precipitation methods; also, NTA was conducted but on all 4 types of EVs obtained by precipitation. According to MISEV 2023, to assess the presence of EVs and of non-EV co-isolated structure (NVEPs), at least one hallmark protein of categories 1, 2 and 3 should be tested [106]. In this study, precipitated EVs were tested by WB for RPS6, CD81, CD9 and TSG101. Therefore, in EV_{DMSO} and $EV_{sorafenib}$ released from MDA-MB-453 and MCF-7 cells, CD9 and CD81 tetraspanisn (protein of categories 1) and TSG101 (protein of categories 2) were present, while RPS6 (protein of categories 3), used as a negative control, was absent (Fig. 24A). In addition, TEM images demonstrated the presence of EVs with a typical round shape and an average size between 50 and 150 nm in diameter (Fig. 24B). NTA provided information regarding the concentration and dimension of the vesicles of our interest (Fig. 24C). EVs released from DMSO-treated BC cells are marked by heterogeneous size-distribution. EVs from MDA-MB-231 cells were characterized by a relevant subpopulation peak around 210 nm and similar mean and mode diameters (~220 nm *vs* ~210 nm, respectively), compared to those isolated from HCC1937 which presented high polydispersity with multiple subpopulation peaks and thus the largest difference between mean and mode diameters (312 nm *vs* ~175 nm, respectively) (Fig. 24D). EVs from MCF7 and MDA-MB-453 cells showed intermediate profiles (Fig. 24C and Table 4). In our culture conditions, the calculated EVs concentration was in the range of 10^8/ml, with MDA-MB-231 cells being the most efficient in particle release. In terms of size distribution, sorafenib treatment caused a shift for both subpopulations of smaller and larger EVs, and this effect was observed in all cell lines tested, regardless of the exclusion of particles >600 nm in dynamic light scattering (particularly relevant in the case of HCC1937 cells) and smaller particles, as demonstrated by the general increase in the mean/mode diameter ratio. Another effect caused by the treatment was in terms of concentration, where EVs derived from MCF-7 were characterized by a reduced concentration and an even more considerable one for MDA-MB-231 vesicles, while EVs from HCC1927 and MDA-MB-453 manifested an opposite trend (Table 4).

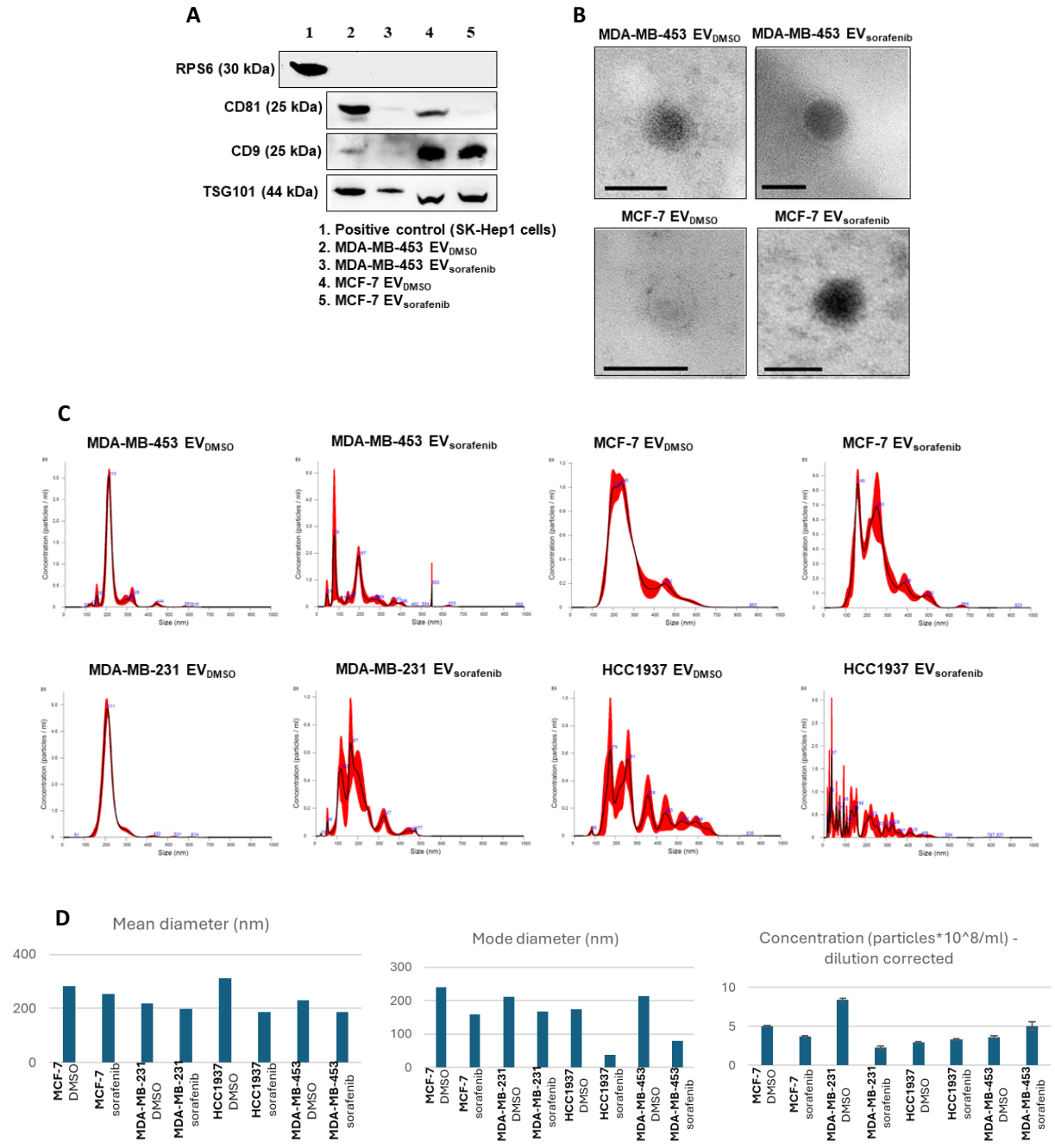

Figure 24. Characterization of EVs obtained with precipitation method. A Western blot for tetraspanins (CD81, CD9), TSG101 and RPS6 was performed on EVs purified with precipitation method and derived from MDA-MB-453 and MCF-7 cells treated with DMSO and Sorafenib. Lysate from SK-Hep1 cell was used as a positive control for RPS6. **B** Transmission electron microscopy (TEM) precipitated EVs showed vesicles with characteristic morphology and size of EVs. Scale bar, 100 nm. **C** Nanoparticle tracking analysis showed heterogeneous size-distribution profiles of the EVs derived from DMSO or sorafenib treated breast cancer cells. **D** EV_{DMSO} showed heterogeneous size-distribution profiles. Sorafenib treatment caused significant size shifts in favor of larger particle subpopulations, as demonstrated by the general increase in the mean/mode diameter ratio.

Table 4. Nanoparticle tracking analysis (NTA) of EVs derived from DMSO or sorafenib-treated MCF-7, MDA-MB-231, HCC1937 and MDA-MB-453 cancer cells showed heterogeneity in terms of size-distribution profiles and concentration.

Sample name (EVs)	Mean diameter (nm)	Mode diameter (nm)	Raw concentration (particles*10^ 8/ml)	SD (particles*10^ 8/ml)	Concentration (particles*10^ 8/ml) – dilution corrected	Mean/Mode diameter ratio
MCF-7$_{DMSO}$	283	239.7	1.69	0.0112	5.07	1.181
MCF-7$_{sorafenib}$	254.6	159.1	1.24	0.0798	3.72	1.600
MDA-MB-231$_{DMSO}$	219.8	210.1	2.8	0.23	8.4	1.046
MDA-MB-231$_{sorafenib}$	197	166.9	0.765	0.147	2.295	1.180
HCC1937$_{DMSO}$	312	174.7	0.983	0.065	2.949	1.786
HCC1937$_{sorafenib}$	185.9	36.7	1.12	0.0896	3.36	5.065
MDA-MB-453$_{DMSO}$	231.4	212.9	1.22	0.102	3.66	1.087
MDA-MB-453$_{sorafenib}$	185.6	78.5	1.69	0.51	5.07	2.364

4.3. Enriched EVs-based treatment impaired the proliferation ability of BC cells.

To verify treatment's ability to impair the proliferative capacity of BC cells, the 4 cell lines, HCC1937, MDA-MB-453, MCF7, and MDA-MB-231, were subjected to EV_{DMSO} and $EV_{sorafenib}$ in all possible combinations (Fig. 25A-D). After 24h, we assessed the MTT assay which resulted in a significant inhibition of the proliferation ability of MDA-MB-231 when receiving any of the 4 types of $EV_{sorafenib}$, in comparison to $EV_{DMSO.}$ The inhibition percentages were as follows: 19% ($p < 0.01$, MDA-MB-453 $EV_{sorafenib}$), 15% ($p<0.01$, MCF-7 $EV_{sorafenib}$), 10% ($p < 0.05$, MDA-MB-231 $EV_{sorafenib}$) and 10% ($p < 0.05$, HCC1937 $EV_{sorafenib)}$ (Fig. 25A). Using the same experimental conditions as obtaining the enriched EVs, in terms of dose and timing, BC cells were treated with 15 μM sorafenib for 24h and both cell proliferation and viability were assessed. The results showed the anti-proliferative effect of sorafenib in all cell lines with inhibition ranging from 12% (for HCC1937 cells) to 44% (for MCF7 cells) (Fig. 25E) and a reduction of cell viability between 11% (MCF7) and 38% (MDA-MB-231) (Fig. 25F).

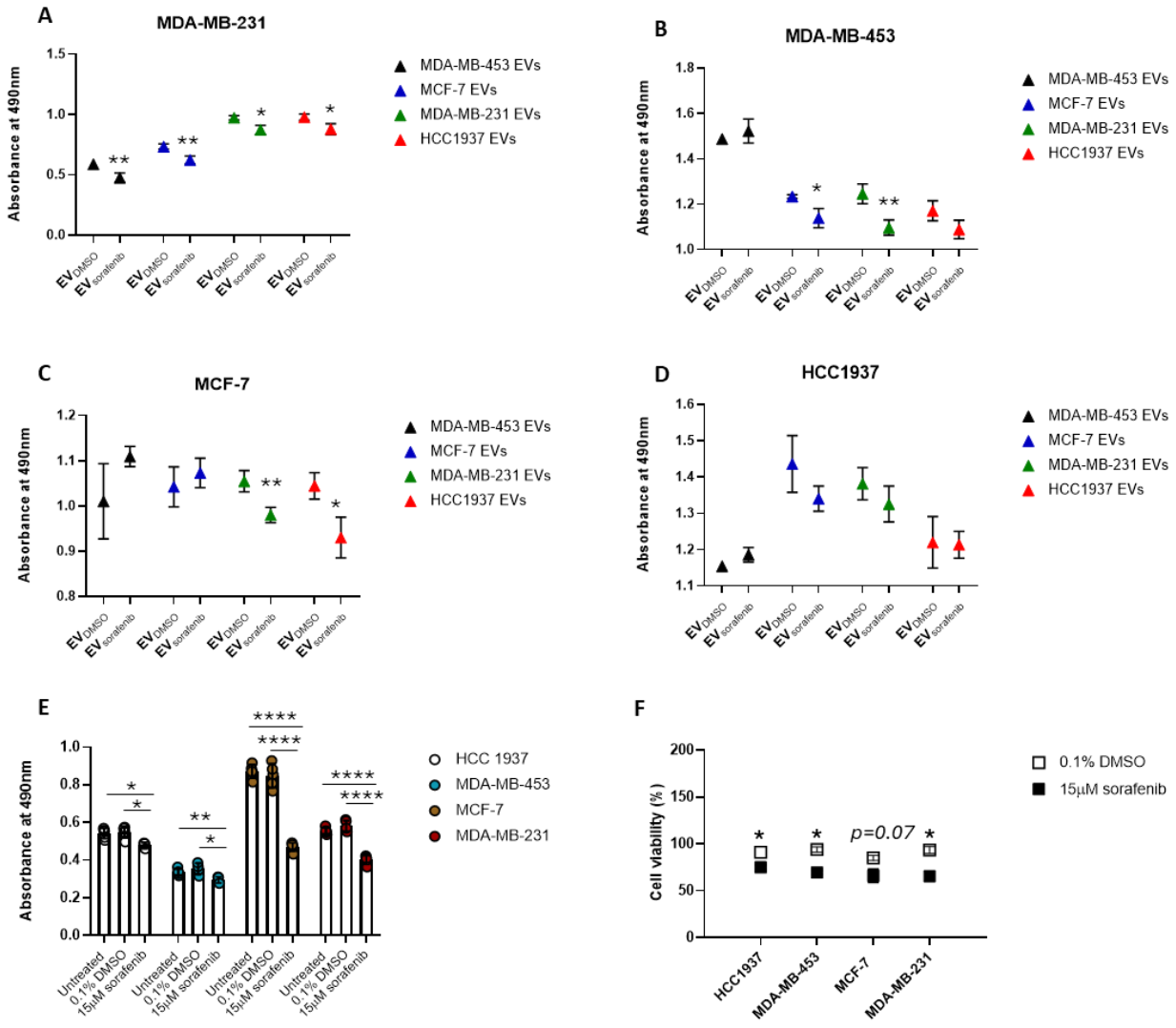

Figure 25. Cell proliferation is affected by both enriched EVs and sorafenib treatment. A MDA-MB-231, **B** MDA-MB-453, **C** MCF-7, and **D** HCC1937 cells were treated with different types of enriched EVs for 24h, and the effects on cell proliferation were assessed by MTT assay. **E** All four breast cancer cell lines followed a 24h treatment with either 0.1% DMSO or 15μM sorafenib, the effects on cell proliferation were assessed. **F** Cell viability was assessed 24h after treatment with 0.1% DMSO or 15μM sorafenib. Results are representative of one of two experiments. The graphics represent the average value of five replicates for each condition; the bars represent SD. Unpaired t-test was used; $*p < 0.05$, $**p < 0.01$, $****p < 0.0001$ ($n = 3$).

4.4. EVs as ncRNAs delivery vehicles to target BC cells.

To test whether EVs can be used as efficient carriers of selected ncRNAs, miR-23b-3p, miR-126-3p, and GAS5, we first wanted to verify their ability to enter the recipient cell. To do this, we introduced the fluorescent dye CM-DiI into the culture media of parental BC cells prior to the cell culture harvest and isolation step, thereby generating membrane-tagged EVs. The following experiments were conducted using 2 different cell lines and EVs derived from 2 distinct sources. The choice was based on the results obtained during proliferation assay; MDA-MB-231 cells treated with EVs derived from MDA-MB-453 cells were the combination that produced the highest percentage of cell proliferation inhibition, followed by MDA-MB-453 treated with EVs from MCF-7.

When treating MDA-MB-231 cells with MDA-MB-453-derived EVs (Fig. 26A) and MDA-MB-453 cells with MCF-7-derived EVs (Fig. 26B), we detected the presence of a distinct red, fluorescent signal of the labeled EVs in the cytoplasmatic compartment of the recipient cells, surrounding the nuclei tagged with DAPI. These results confirm the uptake of EVs by the targeted cancer cells. For a better understanding we used ddPCR technology to determine if besides their ability to enter the recipient cells, the vesicles can also release their cargo to modulate the cellular expression levels of the 3 selected ncRNAs. Therefore, MDA-MB-231 cells were treated with EV_{DMSO} and $EV_{sorafenib}$ produced by MDA-MB-453 cells (Fig. 26C) and MDA-MB-453 cells were treated with EV_{DMSO} and $EV_{sorafenib}$ released by MCF-7 cells (Fig. 26D). Indeed, at cellular level miR-23b-3p increased by 1.36 times in MDA-MB-231 cells and by 6.51 times in MDA-MB-453 cells. miR-126-3p increased by 1.29 times in MDA-MB-231 cells and by 6.85 times in MDA-MB-453 cells. GAS5 increased by 1.37 times in MDA-MB-231 cells and by 8.89 times in MDA-MB-453. All these results suggest that the EVs are successfully taken up by the recipient cells, managing to safely transport and release their cargo, leading to increased expression levels of miR-23b-3p, miR-126-3p, and GAS5.

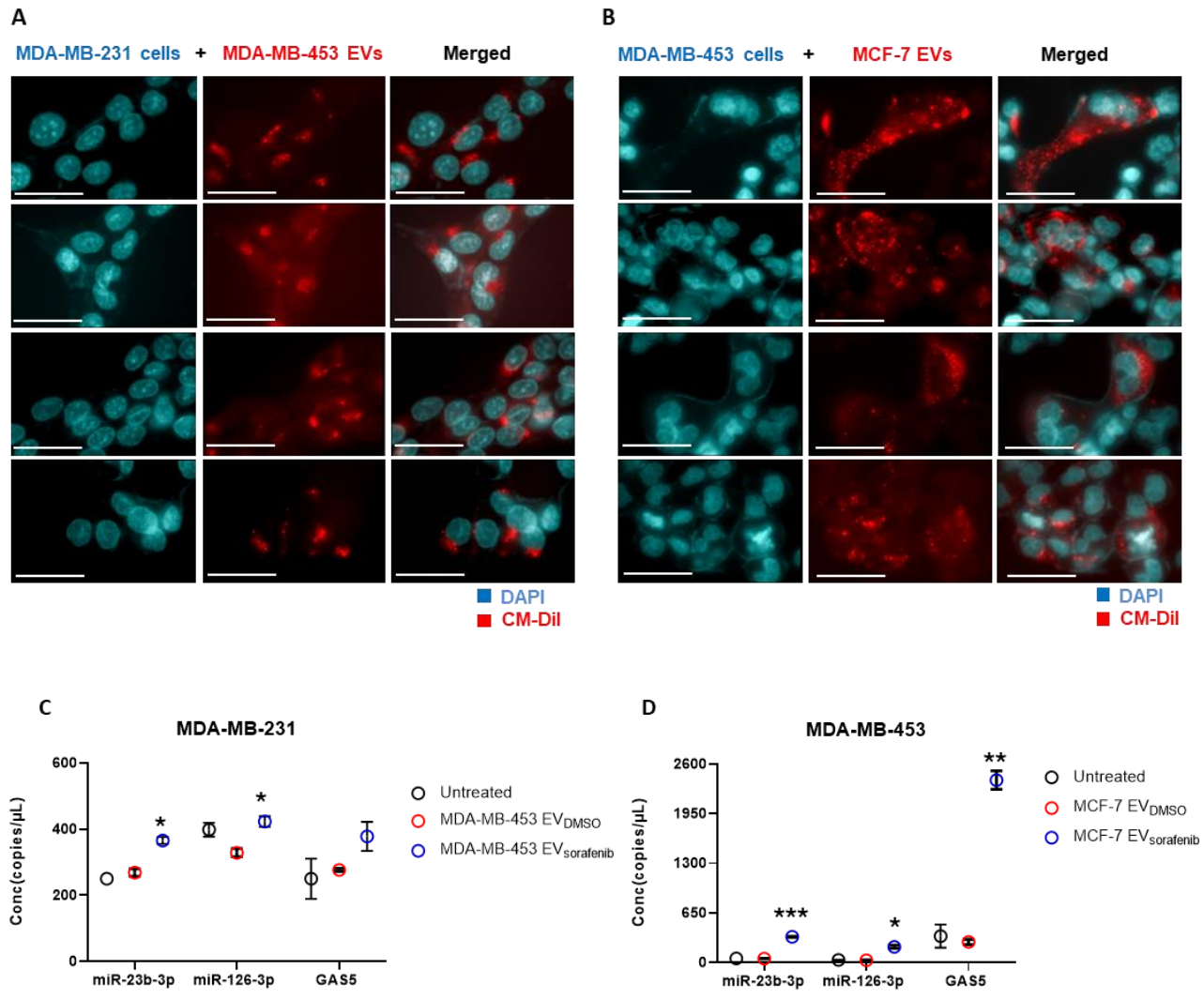

Figure 26. EVs-based ncRNAs delivery to target breast cancer cells. Representative fluorescent microscopy images showing the uptake of MDA-MB-453 and MCF-7 derived EVs labeled in red by **A** MDA-MB-231 and **B** MDA-MB-453 recipient BC cells at 24 hours post-treatment. Scale bars correspond to 30 µm for 63x magnification, and the fluorescent dyes used were DAPI (blue) for nuclei and CM-DiI (red) for EVs. The expression levels of cellular miR-23b-3p, miR-126-3p, and GAS5 were determined in terms of copies/µL using ddPCR technology. **C** Treatment with $EV_{sorafenib}$ derived from MDA-MB-453 resulted in an increased expression level of the three selected ncRNAs in MDA-MB-231 target cells. **D** Similarly, MDA-MB-453 target cells treated with $EV_{sorafenib}$ released by MCF-7 showed the same outcome. The graphics represent mean value; bars, SD. Unpaired t-test was used was used to compare $EV_{sorafenib}$ treatment *versus* EV_{DMSO}; $*p < 0.05$, $**p < 0.01$, $***p < 0.001$. Results are representative of two independent experiments.

4.5.Treatment and uptake of the EVs in the zebrafish model.

A dose-response curve experiment was performed to determine the toxicity of the EVs in zebrafish, as well as the appropriate dose. Zebrafish embryos were exposed to 5, 10, and 15 µL of EV_{DMSO} and $EV_{sorafenib}$, and the percentage of mortality was evaluated at three time points, 48 hpf, 72 hpf and 96 hpf, to determine the appropriate volume to use (Fig. 27A-B). The percentage of mortality was less than 15% in all the cases, therefore we decided to use the highest dose -15µL – to ensure the maximum concentration of EVs to be administered [142].

In this study transgenic zebrafish lines, Tg (*kdrl*:EGFP), were used which express green fluorescent protein (EGFP) specifically in endothelial cells, driven by the kdrl promoter [146]. To test the ability of zebrafish to take up the EVs, 15 µL of labeled EV_{DMSO} and $EV_{sorafenib}$ were added to the water of 48hpf zebrafish. At 72 hpf, the embryo mortality was determined (Fig. 27C-D) and fluorescence microscopy images of CM-DiI-labeled EVs were obtained. The presence of the red signal at the level of the tail of the fish indicated by the white arrows marks the successful uptake of the vesicles. The absence of the fluorescent signal in untreated fish was used as a negative control (Fig. 27E).

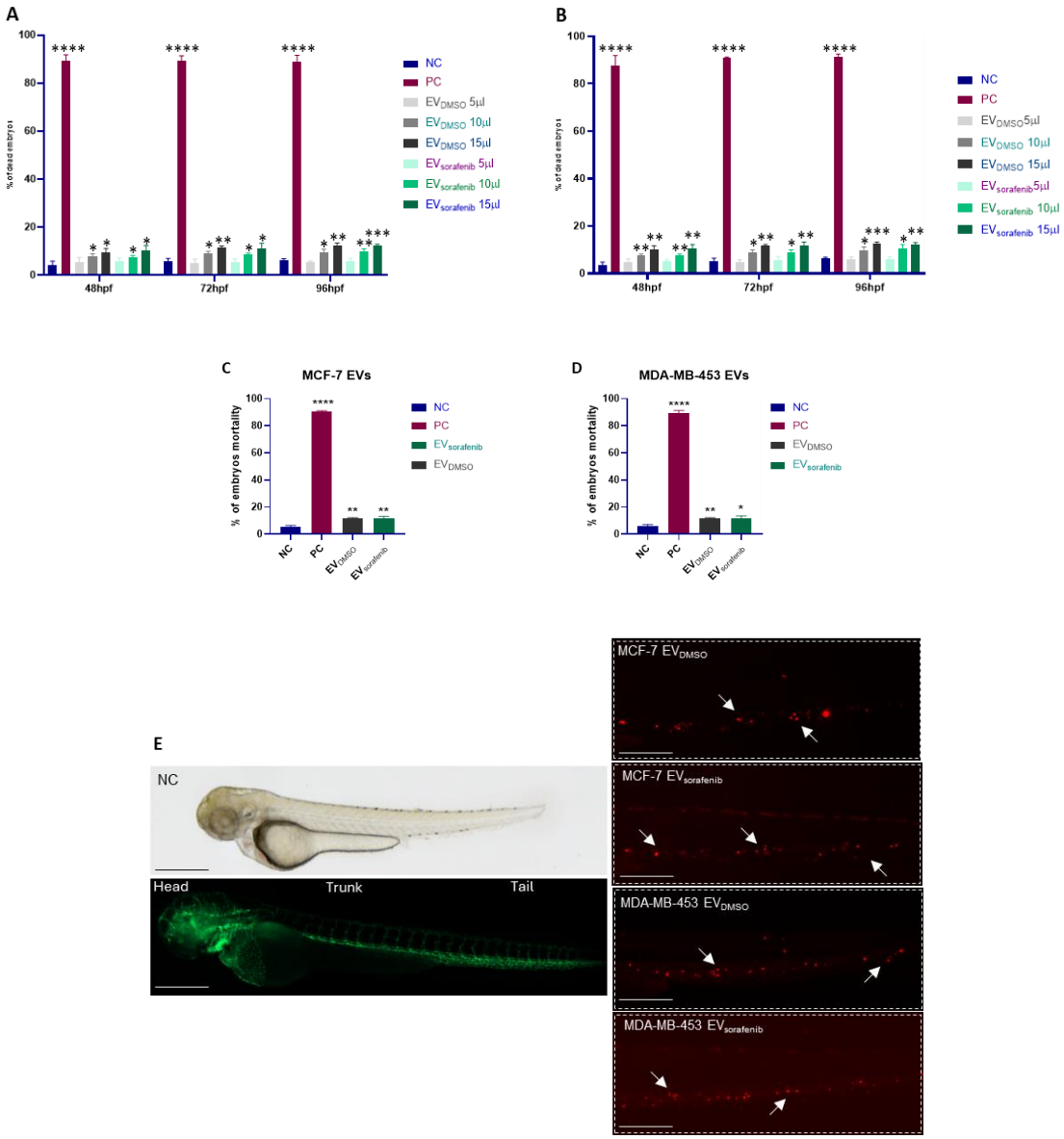

Figure 27. EVs uptake in zebrafish. The percentage of dead embryos treated with three different concentrations of **A** EV_{DMSO} or $EV_{sorafenib}$ derived from MDA-MB-453 and **B** EV_{DMSO} or $EV_{sorafenib}$ derived from MCF-7, was evaluated at 3 time-points (48hpf; 72hpf; 96hpf). Mortality analysis of the recipient transgenic zebrafish line Tg(kdrl:EGFP) treated with EVs derived from **C** MCF-7 and **D** MDA-MB-453 at 72 hpf. Data are representative of two replicates (n = 30 for each group) and are shown as the mean ± standard deviation; negative control embryos (NC) were exposed to 0.1% DMSO in fish water, while the positive control embryos (PC) were exposed to 3,4-DCA dissolved in fish water at a concentration of 3.74 mg/L; unpaired t-test was used; *p < 0.05, **p < 0.01, ***p < 0.001, ****p < 0.0001. **E** Fluorescent microscopy images of CM-DiI labeled EV_{DMSO} and $EV_{sorafenib}$ derived from MCF-7 and MDA-MB-453 cells can be observed at tail level. Green signal indicates fluorescent vasculature, while red signal indicates EVs. The absence of the luminescent signal marks the untreated fish used as negative control (NC). Magnification 20x and 32x. Scale bars correspond to 500 µm.

4.6. Enriched EV-based treatment inhibited the growth of tumor xenografts and micrometastasis formation in zebrafish

To test the efficacy of the EV-based treatment in limiting the aggressive properties of the selected BC cell lines, such as their high proliferation and migration abilities, we first performed xenotransplantation of BC cells into zebrafish, followed by treatment with enriched EVs. Briefly, cells were labelled in red using DiI dye and microinjected in the perivitelline space (PVS) of 48hpf zebrafish that were previously dechorionated. Afterwards, both types of vesicles, EV_{DMSO} or $EV_{sorafenib}$, released from MDA-MB-453 cells were added to the fish-water and effects were evaluated at different time-points. Pictures acquired at T_0 (2h post injection - hpi) using fluorescent microscopy reveal the presence of the red signal that marks the tumor mass formation at the trunk level of the fish and cells located halfway to the tail, indicating their aggressive migration feature. Not injected fish were used as negative control (NC) (Fig. 28A). Pictures at T_1 (24hpi) show no differences between injected/not treated fish and the EV_{DMSO} treated ones. Both groups manifested the same outcome, increased size of the tumor mass formation and micrometastases in the tails, while the fish treated with $EV_{sorafenib}$ had a significantly smaller tumor mass as well as fewer cells present in the tail (Fig. 28B). Precisely, we found an inhibition of 84% ($p < 0.0001$) of the tumor xenografts area (Fig. 28D) and a decrease of about 99% ($p < 0.0001$) of the tail micrometastases (Fig. 28E). Pictures acquired at T_3 (72hpi) revealed the presence of the micrometastases in the tail and cluster cell formation in EV_{DMSO}-treated fish while in $EV_{sorafenib}$-treated ones it did not (Fig. 28C), the size of the tumor mass deceased of about 88% ($p < 0.0001$; Fig. 28D) and the tail was free of cancer cells, with a percentage of diminished of 100% ($p < 0.0001$; Fig. 28E).

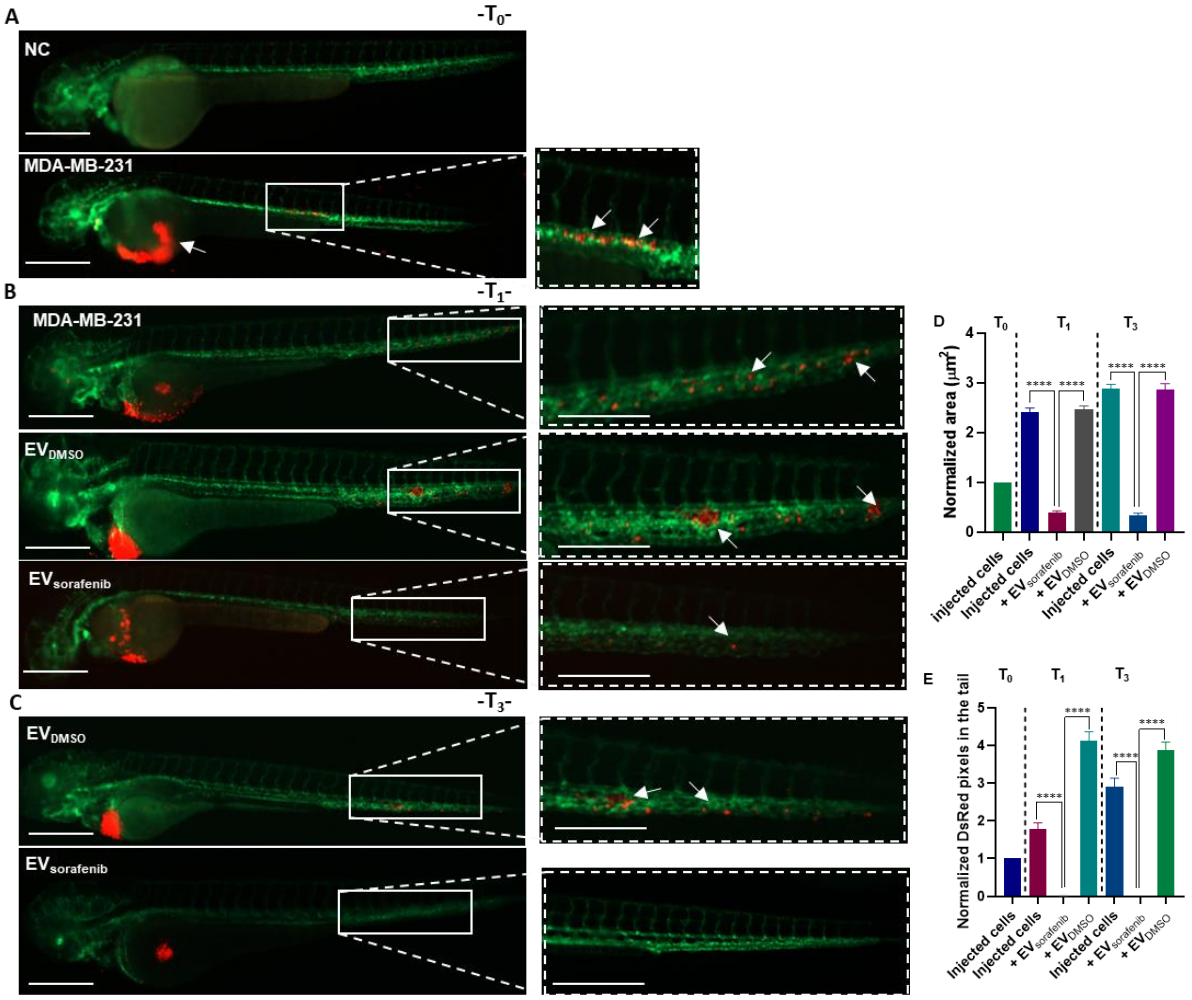

Figure 28. Effects of enriched EVs-based treatment on MDA-MB-231 xenografts at T0, T1, and T3. A Representative lateral view pictures of not injected Tg (kdrl:EGFP) fish were used as negative control (NC); CM-Dil labeled MDA-MB-231 breast cancer (BC) cells were injected into the perivitelline space of the 48 hpf zebrafish. Representative images of the zebrafish were acquired 2 hours post-injection (hpi) (T0); **B** at 24 hpi (T1) trunk and tail pictures were obtained, migrated cell number is regarded as an indicator of the aggressivity of MDA-MB-231 BC cells. **C** At 72 hpi (T3) illustrative pictures were acquired, and arrows indicate the cancer cell cluster formation at the tail level. The green signal indicates fluorescent vasculature, while the red signal indicates the cancer cells. Scale bars correspond to 500 µm for magnification of 20x and 32x. **D** The quantification of the tumor area in the xenografts and the assessment of the tumor cell number in the tail were conducted at T0, T1, and T3. Data was normalized to T0 and is representative of two replicates (n = 30 for each group). Results are shown as the mean ± standard deviation; ****$p < 0.0001$ in one-way ANOVA followed by Tukey's test.

To better prove the anti-tumor effect of enriched EVs, we tested a second cell line, MDA-MB-453 cells, and a different set of vesicles, EV_{DMSO} and $EV_{sorafenib}$ derived from MCF-7, the effect was measured at two time-points. At T_0 (2hpi) the red signal was present in the trunk of the fish and the tail as well as in the tail. Not injected fish were used as negative control (NC) (Fig. 29A). Fluorescent pictures acquired at T_1 (24hpi) present similar outcomes in both cases of untreated and EV_{DMSO}-treated fish, both presenting increased size of the tumor mass and significant number of migrating cancer cells towards the tail region (Fig. 29B). EV treatment demonstrated to be effective when evaluating the fish that received $EV_{sorafenib}$. In this case we observed a significant decrease in terms tumor xenograft size, the inhibition was of 85% ($p < 0.0001$) (Fig. 29C), and a decrease of about 99% ($p < 0.0001$) of the tail micrometastases (Fig. 29D). Acquiring results at T_3 was not possible due to severity of the phenotype and the presence of pericardial edema at 1 dpi (Fig. 29E).

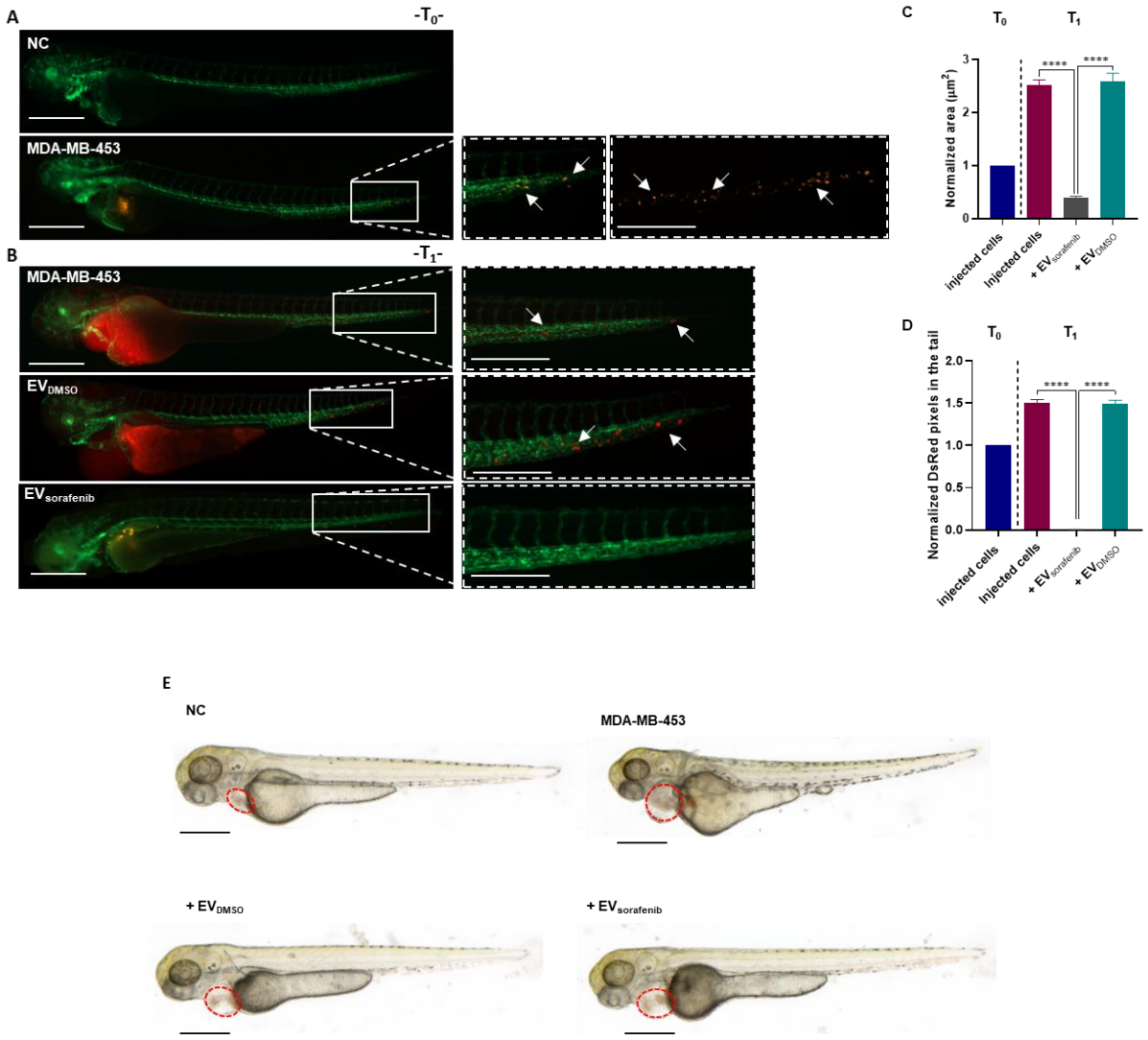

Figure 29. Effects of enriched EVs-based treatment on MDA-MB-453 xenografts at T0 and T1. A Lateral view images of not injected Tg (kdrl:EGFP) zebrafish were selected as the negative control (NC). CM-Dil labeled MDA-MB-453 breast cancer (BC) cells were injected into the perivitelline space of zebrafish at 48 hpf. Representative images of the zebrafish were captured at 2 hpi (T0). **B** At 24 hpi (T1), illustrative pictures of the trunk and tail were taken, with arrows indicating the presence of numerous cancer cells in the tail, reflecting the progression and aggressiveness of MDA-MB-453 BC cells. Green signal indicates fluorescent vasculature, while red signal indicates the cancer cells. Scale bars correspond to 500 µm for magnification of 20x and 32x. **C** Quantification of the tumor area of the xenografts as well as **D** quantification of tumor cells in the tail were determined at T0 and T1. Data was normalized to T0 and is representative of two replicates (n = 30 for each group). Results are shown as the mean ± standard deviation; ****$p <$ 0.0001 in one-way ANOVA followed by Tukey's test. **E** Within one day post-injection, a severe phenotype and pericardial edema, indicating toxicity caused by breast cancer cells microinjection, were observed in approximately 90-95% of the injected fish. The fish injected with MDA-MB-453 BC cells experienced mortality between days 2 and 3 post-injection. Scale bars represent 500 µm for magnification of 20x.

Light Sheet Microscopy was used to obtain pictures for a better visualization and appreciation of the treatment's efficacy in reducing tumor xenograft and micrometastases *in vivo*. We first induced the tumor mass by injecting CM-DiI labeled MDA-MB-231 in the PVS of zebrafish, followed by the treatment with MDA-MB-453 derived EVs and pictures were acquired at 24hpi and 72hpi (Fig. 30A). At both time-point, no major difference between untreated and EV_{DMSO}-treated fish were observed, the presence of the fluorescent signal specific for the tumor mass in the trunk, as well as a considerable number of cells in the tail that led to extravasation. On the contrary, in fish that received $EV_{sorafenib}$ as treatment, a noticeable decrease in tumor mass within the yolk sac, as well as a reduction in tail micrometastases, were observed. When evaluating the pictures acquired with the second cell line, MDA-MB-453, along with the treatment represented by EVs derived from MCF-7, we noticed that they displayed the same outcome. A considerable reduction in tumor mass and fewer micrometastases in the tail were observed in the fish treated with $EV_{sorafenib}$ compared to the ones treated with EV_{DMSO} (Fig. 30B). Taken together these results highlighted the effectiveness of the EVs rich in miR-23b-3p, miR-126-3p, and GAS5 in reducing the tumorigenicity in the zebrafish model.

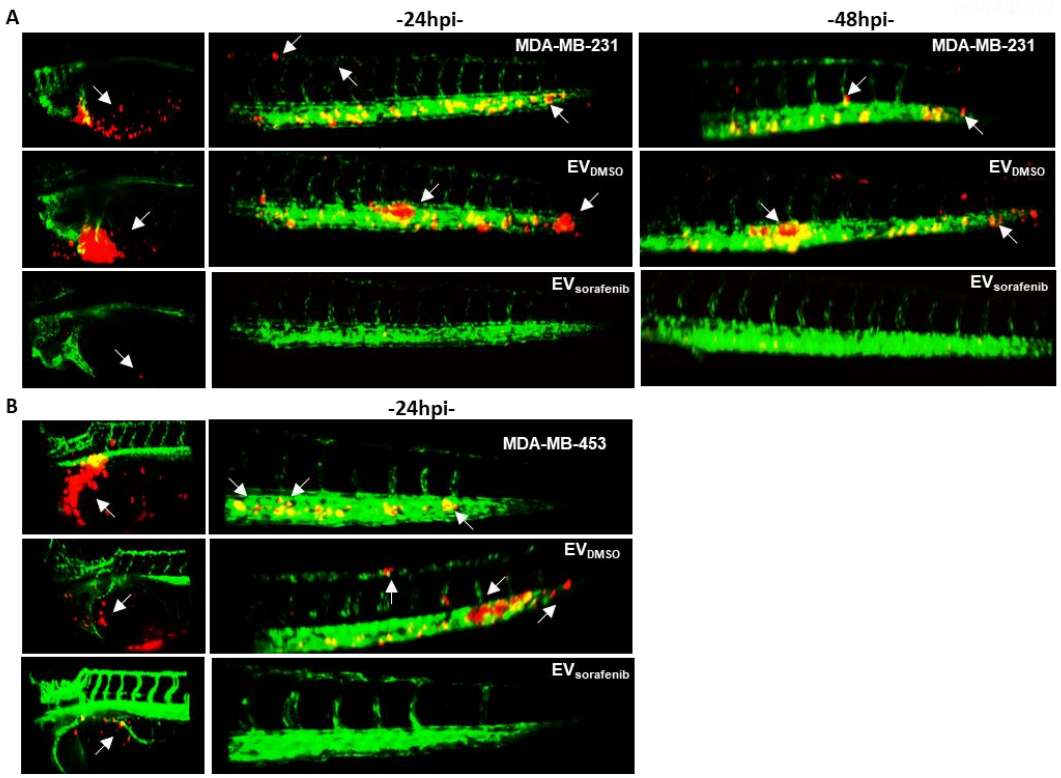

Figure 30. Images of cancer xenografts and micrometastases in zebrafish acquired by digital light sheet microscopy. A Representative image of the yolk sac and tail regions were captured at 24h and 48h after microinjection of MDA-MB-231 breast cancer (BC) cells labeled in red. **B** Additionally, images were taken at 24h after microinjection of MDA-MB-453 BC (red). Arrows were used to indicate the presence of tumor masses, micrometastases in the tail, as well as the formation of clusters of cancer cells (n = 30 for each group).

4.7. Levels of miR-23b-3p, miR-126-3p and GAS5 in zebrafish.

Given that a high percentage of the protein-coding human genes, about 70%, have a counterpart in zebrafish, we were able to analyze the expression levels of the three selected ncRNAs, previously analyzed in human BC cells, in zebrafish after xenotransplantation [147]. Using ddPCR technology we quantified the levels of miR-23b-3p, miR-126-3p and GAS5 in 4 groups of zebrafish embryos: (i) not injected, (ii) injected with MDA-MB-231 cells; (iii) injected with BC and treated with EV_{DMSO}, (iv) injected with BC cells and treated with $EV_{sorafenib}$. Because mature miR-23b-3p and miR-126-3p have the same sequence in human (hsa-miR-23b-3p) and in zebrafish (dre-miR-23b-3p), with one nucleotide (guanine) that differs in the case of miR-126-3p, it was difficult to distinguish the endogenous from the exogenous levels and it did not allowed the detection of any differences in expression levels of the 2 miRNAs (Fig. 31A-B). On the other hand, lncRNA GAS5 has a completely different sequence in human *vs.* zebrafish, which means that the quantified levels are exogenous and derived from the xenograft. In not-injected zebrafish, GAS5 was not expressed, as expected, while in the groups of fish that were either injected with BC cells or in the one treated with EV_{DMSO}, it displayed approximately the same level. Interestingly, injected fish that were treated with $EV_{sorafenib}$ shows a significant decrease of GAS5, of about 88.66% compared to EV_{DMSO}-treated fish, which could reflect the effect of the treatment in reducing the tumor mass and the micrometastases (Fig. 31C).

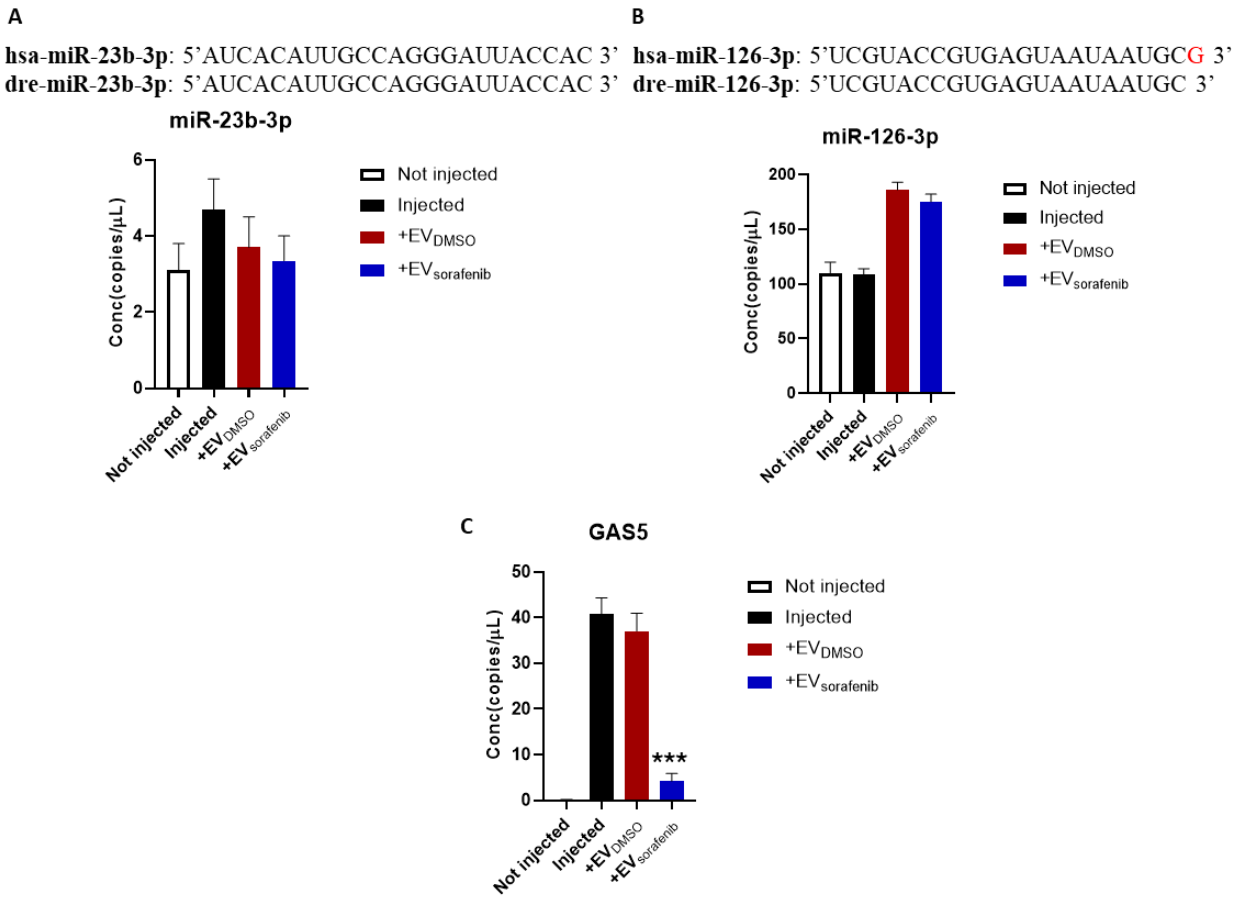

Figure 31. Expression levels of miR-23b-3p, miR-126-3p and GAS5 in zebrafish. Mature sequence of **A** miR-23b-3p and **B** miR-126-3p along with their expression levels were determined in zebrafish using ddPCR technology; **C** Expression level of GAS5 was also measured. Zebrafish embryos were not injected, injected with MDA-MB-231 cells, injected and treated with either EV_{DMSO} or $EV_{sorafenib}$ derived from MDA-MB-453 cells. Data are representative of two replicates (n = 30 for each group) and are shown as the mean ± standard deviation; One-way ANOVA test was used; ***$p < 0.001$.

4.8.The treatment with enriched EVs affected angiogenesis in vivo

To determine the effect of EVs rich in miR-23b-3p, miR-126-3p and GAS5 on the angiogenic process, MDA-MB-231 and MDA-MB-453 cells were injected into zebrafish at 48hpf and newly formed vessels of the subintestinal venous plexus (SIVP) in the anterior region of the yolk were used as an indicator of the ability of BC cells to induce angiogenesis. Following micro-injection, embryos were grown in fish water or treated with EVs until 72 hpf, then fixed in 4% (v/v) paraformaldehyde (PFA) and stained with alkaline phosphatase (AP) assay to visualize the ectopic sprouts [144]. In both cases of MDA-MB-231 and MDA-MB-453 xenografts, an important stimulation of the ectopic sprout originating from the SIVP basket was observed. However, upon the administration of $EV_{sorafenib}$, there was a significant decrease in sprout formation compared to the application of EV_{DMSO} (Fig. 32A-B). Using a scheme depicting angiogenesis-derived vessels, the percentage of angiogenesis inhibition was measured (Fig. 32C) and was 55% in both cases, indicating a significant reduction in sprout formation ($p < 0.0001$; Fig. 32D).

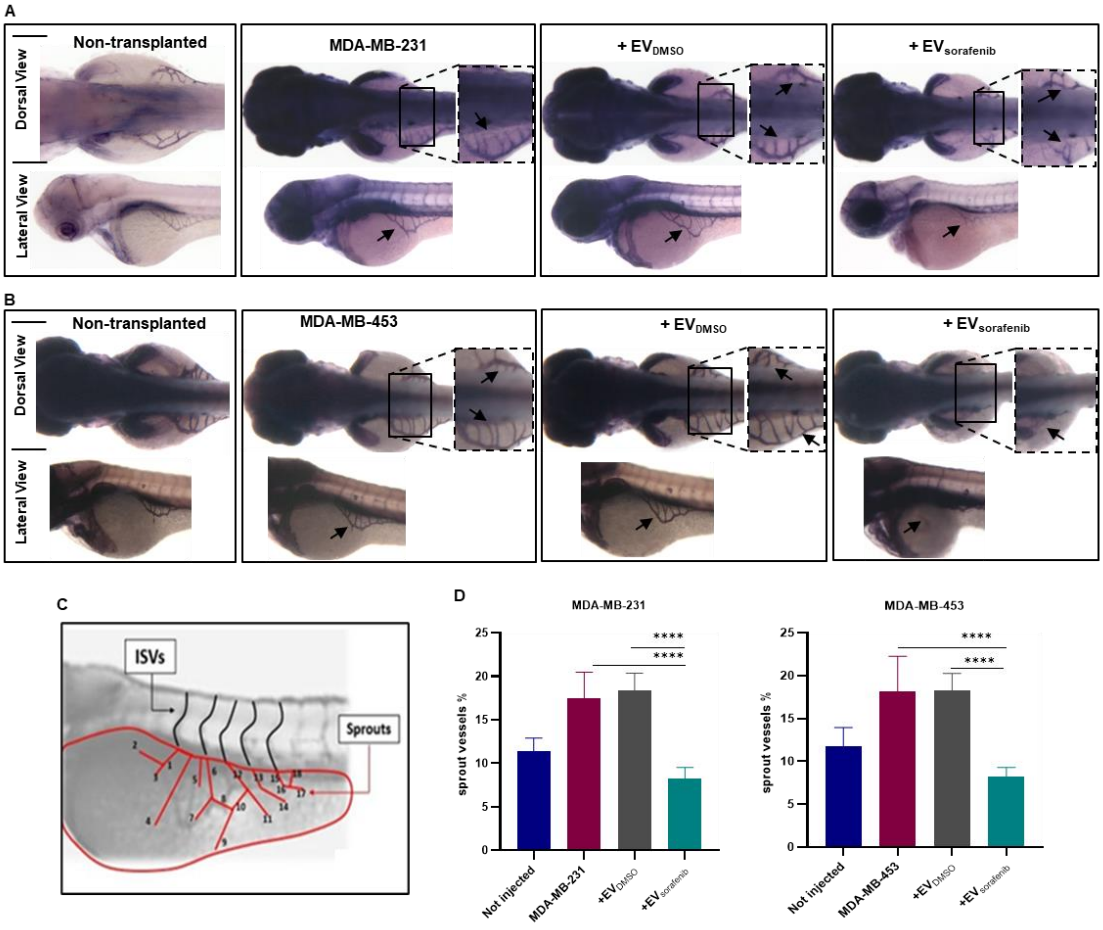

Figure 32. Xenotransplantation-induced angiogenesis in the zebrafish embryos. The alkaline phosphatase assay was performed to assess the angiogenic potential of two different cancer cell lines, **A** MDA-MB-231 and **B** MDA-MB-453, in embryos that were either untreated or treated, with enlargement of the sub-intestinal venous plexus (SIVP) region at 72 hpf (dorsal and lateral view). Magnification 32x. **C** The scheme depicts the counting of ectopic sprouts. **D** To present the results, a graph was generated showing the average number of SIVP branches at 72 hpf. Data are representative of two replicates (n = 30 for each group) and are shown as the mean ± standard deviation; ****$p < 0.0001$ in one-way ANOVA followed by Tukey's test.

4.9.Analysis of miRNome profiles in EVs released by breast cancer cells

In order to identify other miRNAs that may vary in EVs released by BC cells after sorafenib treatment, we performed a global analysis of the miRNome using RNA sequencing. A median number of 73 (min:22; max:143) miRNAs per sample were detected, and a total of 60 miRNAs were further analyzed. Principal component analysis revealed that the treatment has a global impact on the miRNA expression profile as well as the genetic background of the different cell lines analyzed. The analysis revealed also an outlier samples that do not cluster with the other (Fig. 33A). This sample was the one with the lower number of miRNAs detected (N = 22). Differential expression analysis identified 12 differentially expressed miRNAs: hsa-miR-7704, hsa-miR-663a-5p, hsa-miR-4492, hsa-miR-4454, hsa-miR-4488, hsa-miR-4497, hsa-miR-4516, hsa-miR-3648-3p, hsa-miR-9901, hsa-miR-25-3p, hsa-miR-342-3p and, hsa-let-7b-5p (Fig. 33B). The heatmap shows that most of these miRNAs were upregulated in $EV_{sorafenib}$ compared to EV_{DMSO} in all four types of EVs, with 2 exceptions: hsa-miR-25-3p and hsa-miR-4454, which showed a downregulation (Fig. 33C).

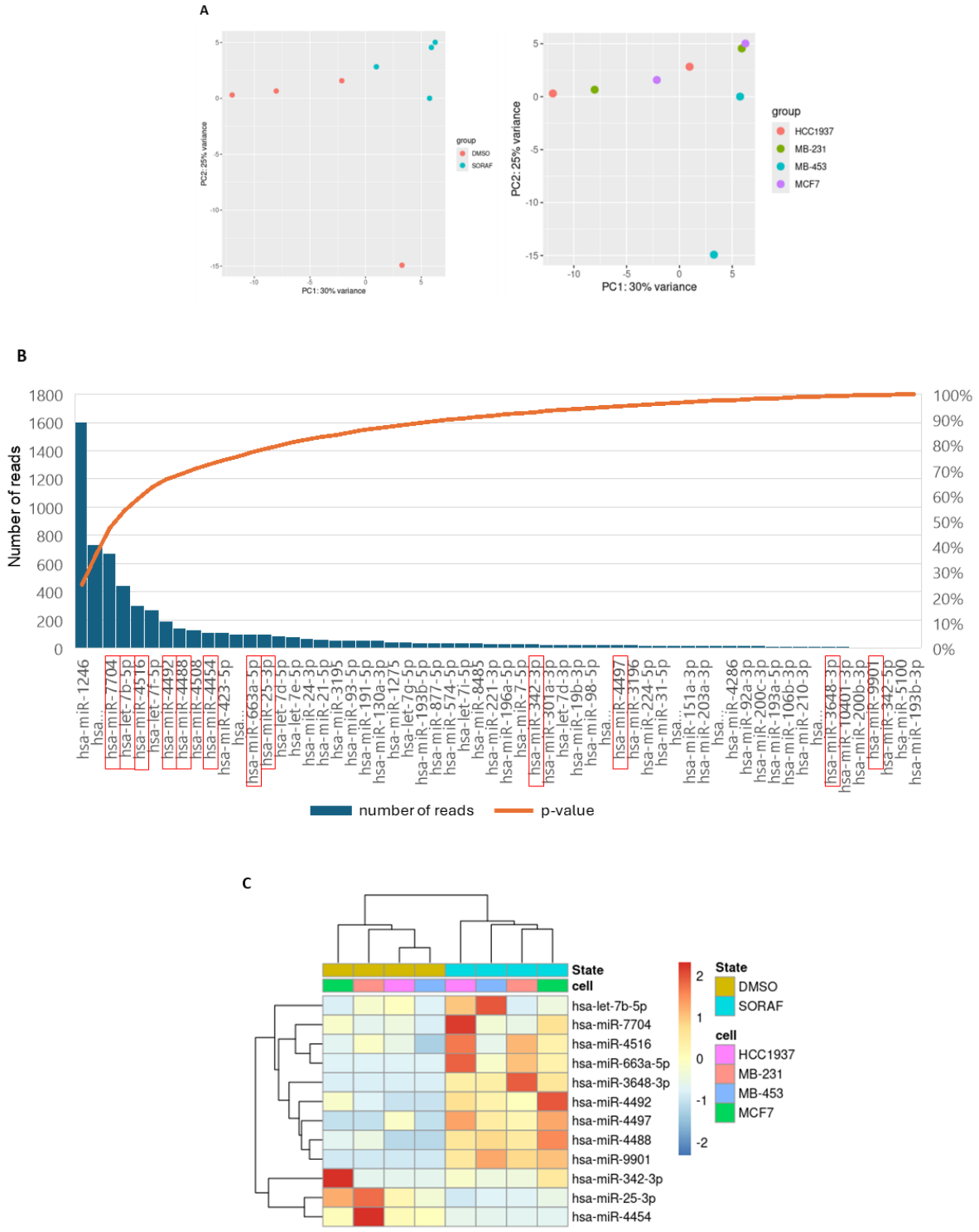

Figure 33. **Differential expression analysis of top 60 miRNAs in EVs**. **A** The Principal Component Analysis (PCA) of the two treatment groups and of each cellular group was conducted. **B** Chart of Pareto represents, on the primary axis, the mean number of reads (sorted from high to low) of each detected mature miRNA, while Pareto's line indicates the p-value of each miRNA. **C** Heatmap of top differentially expressed miRNAs ($p < 0.05$) between EV_{DMSO} and $EV_{sorafenib}$.

To further investigate the role of these miRNAs of interest, we searched the miRWalk database to predict the miRNAs targets and we found 10590 genes to be regulated by the 12 miRNAs. We then merged the list of potential targets with the full list of DEGs identified in tissues from 97 histologically confirmed breast cancer patients [148]. This analysis yielded a total of 1097 potential common target genes on which we performed functional enrichment analysis (Fig. 34A). According to KEGG analysis, the major pathways found to be deregulated include PPAR signaling pathway, which is known to have a role in promoting apoptosis in breast cancer cells, cell cycle, hepatitis B, cellular senescence, thyroid cancer, pathways in cancer, axon guidance, insulin resistance, Cushing syndrome and gastric cancer (Fig. 34B) [149].

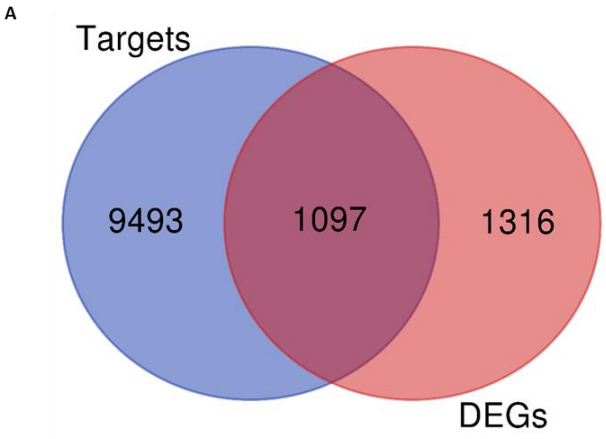

B

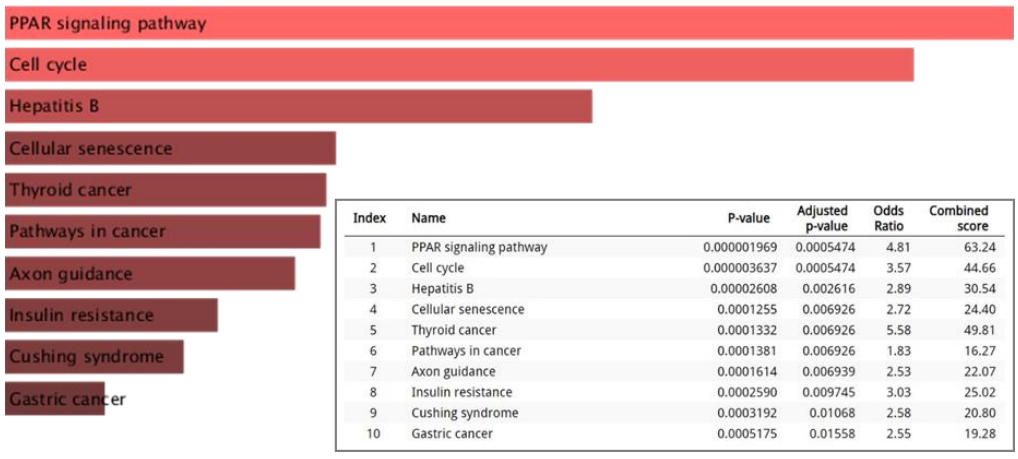

Index	Name	P-value	Adjusted p-value	Odds Ratio	Combined score
1	PPAR signaling pathway	0.000001969	0.0005474	4.81	63.24
2	Cell cycle	0.000003637	0.0005474	3.57	44.66
3	Hepatitis B	0.00002608	0.002616	2.89	30.54
4	Cellular senescence	0.0001255	0.006926	2.72	24.40
5	Thyroid cancer	0.0001332	0.006926	5.58	49.81
6	Pathways in cancer	0.0001381	0.006926	1.83	16.27
7	Axon guidance	0.0001614	0.006939	2.53	22.07
8	Insulin resistance	0.0002590	0.009745	3.03	25.02
9	Cushing syndrome	0.0003192	0.01068	2.58	20.80
10	Gastric cancer	0.0005175	0.01558	2.55	19.28

Figure 34. A Target predicted target for the selected miRNAs of our interest were compared with the 2413 DEGs found in breast tumor, identifying 1097 common targets (paper with Indian women). **B** Functional enrichment analysis of predicted targets was performed by querying the EnrichR web tool. The KEGG pathway analysis results are shown in the bottom panel.

To gain insight into the biological activities of the DEGs, we performed GO enrichment analysis. As shown, among the most perturbed biological processes include microtubule cytoskeleton organization involved in mitosis, cellular response to prostaglandin stimulus and negative regulation of apoptotic process. Collagen-containing extracellular matrix, cytoskeleton, actin cytoskeleton and focal adhesion were the most enriched cellular components GO terms. The most prevalent GO terms for molecular functions were metal ion binding, magnesium ion binding, adenyl ribonucleotide binding, and nuclear glucocorticoid receptor binding (Fig. 35).

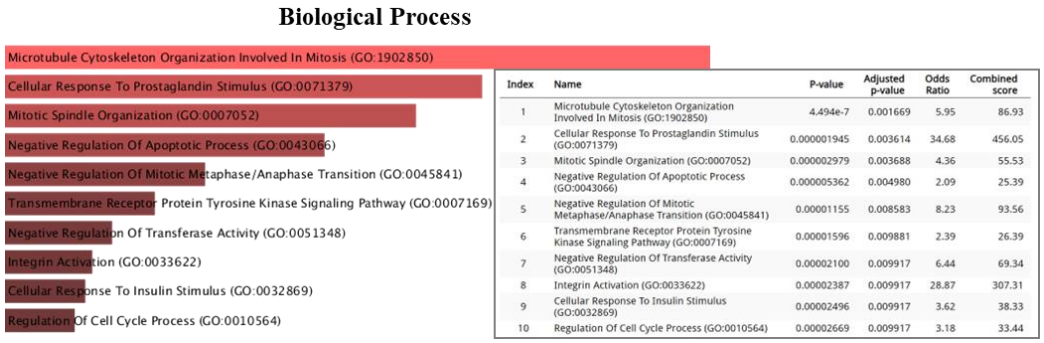

Index	Name	P-value	Adjusted p-value	Odds Ratio	Combined score
1	Microtubule Cytoskeleton Organization Involved In Mitosis (GO:1902850)	4.494e-7	0.001669	5.95	86.93
2	Cellular Response To Prostaglandin Stimulus (GO:0071379)	0.000001945	0.003614	34.68	456.05
3	Mitotic Spindle Organization (GO:0007052)	0.000002979	0.003688	4.36	55.53
4	Negative Regulation Of Apoptotic Process (GO:0043066)	0.000005362	0.004980	2.09	25.39
5	Negative Regulation Of Mitotic Metaphase/Anaphase Transition (GO:0045841)	0.00001155	0.008583	8.23	93.56
6	Transmembrane Receptor Protein Tyrosine Kinase Signaling Pathway (GO:0007169)	0.00001596	0.009881	2.39	26.39
7	Negative Regulation Of Transferase Activity (GO:0051348)	0.00002100	0.009917	6.44	69.34
8	Integrin Activation (GO:0033622)	0.00002387	0.009917	28.87	307.31
9	Cellular Response To Insulin Stimulus (GO:0032869)	0.00002496	0.009917	3.62	38.33
10	Regulation Of Cell Cycle Process (GO:0010564)	0.00002669	0.009917	3.18	33.44

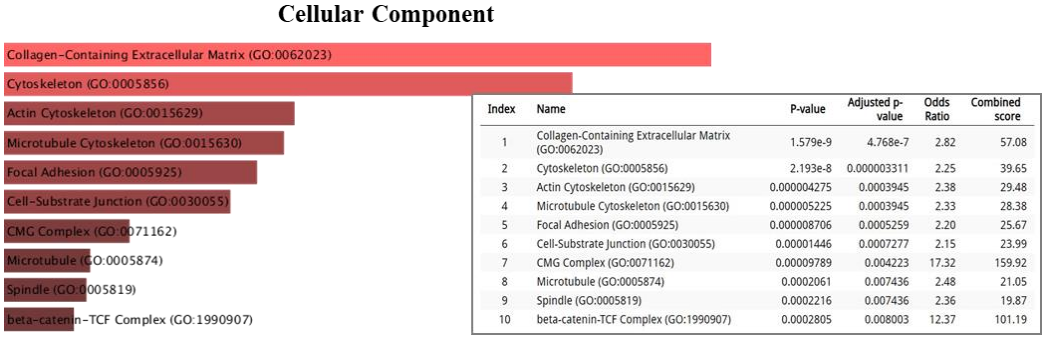

Index	Name	P-value	Adjusted p-value	Odds Ratio	Combined score
1	Collagen-Containing Extracellular Matrix (GO:0062023)	1.579e-9	4.768e-7	2.82	57.08
2	Cytoskeleton (GO:0005856)	2.193e-8	0.000003311	2.25	39.65
3	Actin Cytoskeleton (GO:0015629)	0.000004275	0.0003945	2.38	29.48
4	Microtubule Cytoskeleton (GO:0015630)	0.000005225	0.0003945	2.33	28.38
5	Focal Adhesion (GO:0005925)	0.000008706	0.0005259	2.20	25.67
6	Cell-Substrate Junction (GO:0030055)	0.00001446	0.0007277	2.15	23.99
7	CMG Complex (GO:0071162)	0.00009789	0.004223	17.32	159.92
8	Microtubule (GO:0005874)	0.0002061	0.007436	2.48	21.05
9	Spindle (GO:0005819)	0.0002216	0.007436	2.36	19.87
10	beta-catenin-TCF Complex (GO:1990907)	0.0002805	0.008003	12.37	101.19

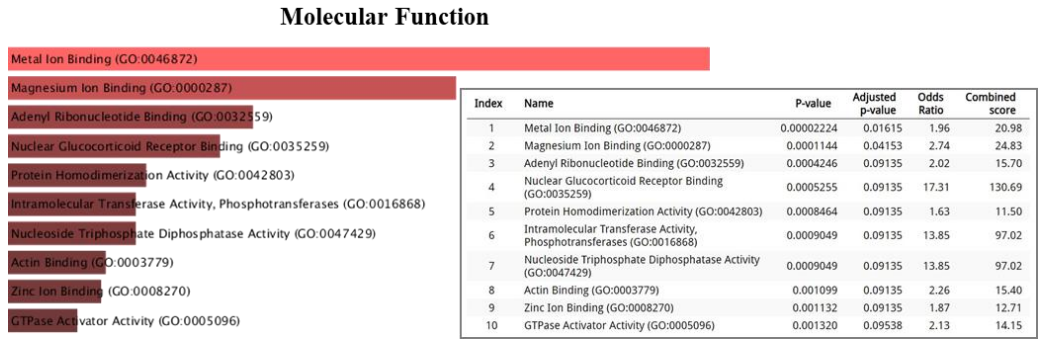

Index	Name	P-value	Adjusted p-value	Odds Ratio	Combined score
1	Metal Ion Binding (GO:0046872)	0.00002224	0.01615	1.96	20.98
2	Magnesium Ion Binding (GO:0000287)	0.0001144	0.04153	2.74	24.83
3	Adenyl Ribonucleotide Binding (GO:0032559)	0.0004246	0.09135	2.02	15.70
4	Nuclear Glucocorticoid Receptor Binding (GO:0035259)	0.0005255	0.09135	17.31	130.69
5	Protein Homodimerization Activity (GO:0042803)	0.0008464	0.09135	1.63	11.50
6	Intramolecular Transferase Activity, Phosphotransferases (GO:0016868)	0.0009049	0.09135	13.85	97.02
7	Nucleoside Triphosphate Diphosphatase Activity (GO:0047429)	0.0009049	0.09135	13.85	97.02
8	Actin Binding (GO:0003779)	0.001099	0.09135	2.26	15.40
9	Zinc Ion Binding (GO:0008270)	0.001132	0.09135	1.87	12.71
10	GTPase Activator Activity (GO:0005096)	0.001320	0.09538	2.13	14.15

Figure 35. Functional gene enrichment analysis on DEGs in BC. Analysis was performed by querying the EnrichR web tool. Top 10 enriched GO terms for "Biological Process", "Cellular Component" and "Molecular Function" categories.

5. Discussion

Breast cancer is still a global health challenge, being the most diagnosed cancer in the world [150]. When it comes to treatment strategies, chemotherapy, radiotherapy, and surgery are still the first line of treatment. Even though chemotherapy drugs became more advanced, cancer drug resistance phenomenon is widespread, a recent statistical analysis showed that approximatively 90% of cancer-related deaths are associated with drug resistance [151,152]. During past decades, the discovery of miRNA's emerging role in the prognosis, pathogenesis, diagnosis and treatment of cancer was groundbreaking and it led to their exploitation for miRNA-based anticancer therapies, alone or combined with existing target therapies, aimed to improve disease response and increasing cure rates [153,154]. Moreover, guided by the urge to find new therapeutic systems for the precise treatment of tumors, EVs offered numerous clinical application prospects in the diagnostic, prognosis and therapy of cancer [155]. In this light, the object of this research was to investigate the great potential of the EVs released by BC cells and enriched in miR-23b-3p, miR-126-3p and GAS5, to fight the aggressive characteristics of BC *in vitro* and *in vivo*. The focus on these specific ncRNAs was based on previous observation where they manifested dysregulation in different types of cancer after treatment with a multikinase inhibitor, named sorafenib [31,55]. This compact compound, sorafenib, was reported to inhibit various serine/threonine and tyrosine kinases, such as CRAF, BRAF, VEGFR-2 and -3, PDGFR-ß, FGFR-1, c-kit, and Fms-like tyrosine kinase 3 (Flt-3), involved in numerous cancer-causing signaling pathways [31].

miR-23b-3p as well as miR-126-3p tend to express low levels in different types of human malignant tumors such as prostate cancer, renal cell carcinoma, colorectal, liver and breast cancer [156,157]. Likewise, GAS5 has a tumor-suppressive role being downregulated in a variety of solid tumors and leading to tumor progression, tumor cell proliferation and therapy-related resistance across different types of cancers [158,159]. In our study, ddPCR analysis revealed that the expression levels of miR-23b-3p, miR-126-3p and GAS5 were dysregulated in tested BC cells and in their cognate EVs following 24 h sorafenib treatment. All these data support the idea that these ncRNAs hold a great potential as therapeutic target, in terms of restoring their tumor suppressor activity [156–158].

Most prokaryotic and eukaryotic cells rain EVs and since these vesicles reflect in real-time the status of the cells, analyzing their content is of high importance [160,161]. Over the years, their

emerging role in cancer development has been well demonstrated. For instance, it has been reported that the abnormal expression of a lncRNA involved in the X chromosome inactivation, named XIST, was observed in gastric cancer and EVs overexpressing XIST were found to promote breast cancer. The same data was reported regarding miRNAs, such as let-7a, miR29 family and miR-224, that are enclosed in the EVs and can participate in promoting the aggressive properties of different cancer cells, such as proliferation and migration by activating a variety of signaling pathways [162,163]. Only recently has the role of EVs in reducing the aggressive properties of cancer cells begun to be investigated. For example, it has been demonstrated that vesicles carrying overexpressed lncRNA-APC1 inhibited tumor growth in colorectal cancer [164]. In addition, EVs derived from mesenchymal stem cells and loaded with miR-206, miR-193a, miR-144-3p and miR-16-5p inhibited proliferation, migration, and invasion in different cancer cells, therefore exerting anti-cancer effects [165,166].

The aim of this study was to explore how enriched EVs containing certain ncRNAs released by BC cells influence the aggressive behavior of BC both *in vitro* and *in vivo*. To accomplish this, we generated and isolated EVs that had a high concentration of three ncRNAs known for their tumor-suppressive properties: miR-23b-3p, miR-126-3p, and GAS5. The choice of these specific ncRNAs was based on earlier findings related to their altered expression in various cancers following treatment with the multikinase inhibitor sorafenib [31,135]. This multiple-target tyrosine kinase inhibitor is well known for his ability to suppress angiogenesis by targeting PDGFR-β, VEGFR2, hepatocyte factor receptor (c-KIT) and to reduce cancer cell proliferation by inhibiting Raf-1, B-Raf, and kinase activity in the Ras/Raf/MEK/ERK signaling pathways [167]. For generating enriched EVs we opted for a cell-dependent, non-artificial and efficient approach. This method implies the incubation of BC cells for 24h with sorafenib followed by EVs isolation. Unlike the traditional transfection techniques typically employed to enhance the loading of specific ncRNAs into EVs, methods that can be labor - intensive and time - consuming, our approach effectively addresses these challenges [168,169]. To date, many techniques have been developed for EVs isolation, yet an optimal method has not been established [170]. Among the EV separation methods outlined in MISEV2023, the precipitation method offers the highest recovery rate, but the lowest specificity, resulting in the isolation of a mixture of extracellular particles (EPs). In contrast, immunoprecipitation generally provides the highest specificity but has the lowest recovery, while differential ultracentrifugation offers intermediate levels of both specificity and recovery [106].

Importantly, our findings showed a consistent trend in the levels of the three ncRNAs across all isolation methods, with very few exceptions. The variations in fold increase or decrease observed may be attributed to the differences in specificity and recovery among the methods. Overall, the results confirmed vesicle enrichment regardless of the isolation technique used; however, the highest yield of enrichment was achieved with the commercial kit.

It is well known that the cellular cargo may or may not reflect the one encapsulated in the EVs and it was very interesting to observe this behavior in our BC cells. For instance, in HCC1937 and MDA-MB-453, sorafenib treatment causes an increased level of the 3 ncRNAs in the cells and the same trend was observed in their cognate EVs. However, in MDA-MB-231 cells, the two miRNAs behave differently, being down-regulated within the cells but up-regulated in the EVs, while the expression of GAS5 remains relatively stable. This suggests that EVs may selectively package certain molecules, leading to divergent profiles between intracellular and vesicular content, depending on the cell type and the specific molecules involved. Thus, sorafenib appears to differentially affect the cellular and vesicular RNA content across various BC cell lines, indicating a complex and context-dependent regulatory mechanism.

To further confirm the presence of EVs in our preparation, we characterized the EVs, starting with the ones isolated using immunoprecipitation technique since it offers the highest specificity, by WB. This analysis confirmed the presence of classical EV markers, such as CD63, CD81, CD9 and TSG101, ensuring the specificity of our isolated vesicles. TEM pictured were acquired on ultracentrifugation-isolated EVs, given that this analysis is not suitable for the vesicles obtained using immunoprecipitation. This allowed us to visualize the characteristic cup-shaped morphology of the EVs, further confirming their identity. To fully characterize the EVs used in this study and because we selected the vesicles obtained *via* precipitation for further experiments, we performed WB, TEM, and NTA analyses on these EVs as well. WB results and TEM pictures of the EVs of our interest confirmed the presence of specific markers, while also verifying the absence of non-EV contaminants, and confirming again their classic round-shape. Additionally, NTA, conducted on all sets of EVs, revealed the size distribution and concentration of the EVs, showing that the majority of vesicles fell within the expected size range. These results provided robust evidence that our isolated vesicles were correctly identified, highly purified, and conformed to the size parameters defined for EVs [106].

Sorafenib's ability to inhibit proliferation and induce apoptosis in cancer cells has been well-documented, and our findings are consistent with these effects. However, the aim of our study is to demonstrate that EV-based treatment can achieve similar outcomes and reduce the aggressive characteristics of BC cells [171,172]. A key question in our study was whether these enriched EVs could induce biological changes in recipient cells. Notably, when we treated BC cells with these EVs for 24 hours, we observed a reduction in their proliferative capacity. This could be attributed to the influence of the three ncRNAs released into the recipient cells by the EVs. We are aware that the EVs carry more than just the three ncRNAs we evaluated, and other molecules within the EVs having tumor-suppressive functions might be disregulated. This finding is particularly important, as it suggests that EVs can mimic the anti-proliferative effects of conventional treatments, highlighting their potential as novel therapeutic agents in targeting aggressive cancer cell behavior.

Concerning the uptake of EVs by target BC cells, various tracking methods, including PKHs and DiD staining, and different methods have been employed [173,174]. In previous studies EVs were diluted and incubated with the dye of their choice, followed by a centrifugation step to discard the unbounded dye [175,176]. We opted for a different approach, and we used CM-DiI to stain the vesicle membranes by adding dye to the media of the parental cells then, the fate of two distinct types of EVs was tracked within two different types of recipient cells. While numerous studies have focused on finding the functional role of EV-mediated ncRNA transfer in various biological processes, only a few of them have determined the molecular effect [177,178]. Given the high interest in utilizing EVs as natural carriers for ncRNAs, in our study we subjected two distinct BC cell lines to two different types of enriched EVs and we evaluated their molecular effect [179]. ddPCR analysis revealed very interesting results, in both cases the treatment caused the increased expression levels of miR-23b-3p, miR-126-3p, and GAS5 in the recipient cells at 24h-post treatment. This supports the idea that enriched EVs can serve as efficient *in vitro* vehicles for delivering specific ncRNAs, as they have been shown to encapsulate, protect, transport, and release their cargo, inducing clear molecular changes in target cells.

To date, progress in selecting a model to study the *in vivo* uptake, fate, targets, and effects of enriched EVs has been challenged by their small size and the limited techniques suitable for their labeling [180]. Therefore, the first thing to be proved was that labeled EVs can be absorbed by the vertebrate animal model, zebrafish. When working with zebrafish, the compounds of interest can

be administrated through multiple ways such as microinjection, pretreatment of cancer cells prior implantation, or immersion and in this study, we went for the latter approach [181]. Dose-curve results along with fluorescent microscopy images allowed us to observe a successful uptake of these vesicles by the zebrafish, followed by rapid dispersion throughout the fish's body.

To our knowledge, no results have been reported on the use of EVs as a therapeutic tool to inhibit the progression of BC xenografts established in zebrafish. Therefore, our investigation of the therapeutic potential of enriched EVs represents a novel approach. This study primarily focuses on evaluating the effectiveness of vesicles enriched with miR-23b-3p, miR-126-3p, and GAS5 in the treatment of previously induced tumor xenografts [182,183].

Most researchers studied the dynamics of distribution, uptake and fate of EVs in zebrafish. There is one study in which was explored the potential of EVs isolated from melanoma to activate the innate immune system in zebrafish [184,185]. Additionally, a significant number of researchers have focused on the role of cancer-derived EVs in promoting tumor progression and inducing therapy resistance [182,183,186]. However, in our study, we have demonstrated, among other findings, that EVs derived from BC and enriched with the three specific tumor suppressor ncRNAs can effectively inhibit tumor growth *in vivo*. To demonstrate their benefits as well as their capacity to deliver their cargo with the aim of limiting the aggressiveness of BC, we conducted microinjections of two distinct cell lines, MDA-MB-231 and MDA-MB-453, into zebrafish, followed by the administration of enriched EVs as a treatment. Even though mouse xenotransplatation is often used, recent studies have shown that zebrafish is a good model to test patient breast tumors and is also a promising alternative to mice due to the experimental, economic, and visualization advantages they offer [187,188]. While the role of cancer-derived EVs in cell-to-cell communication to promote tumor metastasis is clear, our study is one of the fewer to reveal that they can also manifest an opposite effect, successfully reducing the aggressiveness of BC. Analysis of the data acquired up to 72 hours post-treatment reveals the significant therapeutic effect of the EV-enriched intervention, evidenced by a substantial reduction in tumor mass, with an approximate 80% decrease in tumor size. Furthermore, we meticulously considered another parameter, their metastatic behavior, which is indicative of the aggressive characteristics of these two BC cell lines. Results showed that by enriching the EVs in miR-23b-3p, miR-126-3p and GAS5, they can serve as a promising therapy to effectively reduce the formation of micrometastases [189,190]. Our pictures clearly show an almost complete eradication of micrometastases located in the tail of the xenograft-

induced zebrafish following treatment with $EV_{sorafenib}$. This result was validated in both BC cell lines with which we conducted our experiments and further consolidated through the light-sheet microscopy pictures. We opted for this microscope to enhance the visualization of the impact of this enriched EV-based treatment on the two most aggressive properties involved in tumor progression. Moreover, since the fact that GAS5 has a completely different sequence in humans compared to zebrafish provides a crucial indicator that the quantified levels of this lncRNA in our zebrafish model are exogenous, originating from the implanted human breast cancer xenograft rather than the host organism. This observation suggests that the low levels of GAS5 detected in the zebrafish post-treatment reflect the impact of EV-based treatment on the tumor mass. Therefore, the levels of GAS5 align with the observed inhibition of tumor progression, highlighting the treatment's role in reducing both tumor mass and micrometastatic potential in the zebrafish model. This result suggests that levels of GAS5 might represent a new way to monitor tumor growth.

Based on our findings regarding the significant therapeutic effects of EV-enriched treatment on tumor regression and micrometastasis, it is equally crucial to examine the role of angiogenesis in tumor progression, particularly as it relates to our objective of assessing how enriched-EVs can inhibit this critical process in both MDA-MB-231 and MDA-MB-453 BC cells. It is well-known that angiogenesis plays a crucial role in the development of tumors and the spread of metastases in various types of cancer, including BC [191]. To date, our study is the first to provide comprehensive evidence that microinjection of MDA-MB-231 and MDA-MB-453 BC cells into zebrafish induces a robust angiogenic response. Furthermore, we conducted a thorough assessment of the effectiveness of enriched EVs in inhibiting this angiogenesis. Our findings reveal that blocking the development of angiogenic processes resulted in a marked reduction of abnormal sprout formation from the SIVP basket, with both cell lines exhibiting an approximate 55% decrease in sprouting activity.

In this study, we emphasized the beneficial role of EVs rich in miR-23b-3p, miR-126-3p, and GAS5 in inhibiting the aggressive properties of BC, both *in vitro* and *in vivo*. As mentioned before, we are aware that other molecules present within these EVs may also be dysregulated and could possess tumor-suppressive functions. Thus, we conducted a miRNome analysis on EVs to identify other dysregulated miRNAs that might contribute to the observed effects. Results showed that a

total of 12 miRNAs were differentially expressed between EV_{DMSO} and $EV_{sorafenib}$. Of these, 10 were upregulated in $EV_{sorafenib}$, while 2 showed downregulation. MiR-23b-3p and miR-126-3p were not included among the 12 differentially expressed miRNAs, as both were excluded after applying the cut-off thresholds for statistical significance and fold-change. Notably, miR-3648-3p was upregulated in our EVs, consistent with previous studies that have linked its high expression to an increased recurrence score in BC [192]. Another study reported that high expression of miR-4488 enhances the migration and invasive potential of melanoma cells, supporting our findings that miR-4488 is upregulated in $EV_{sorafenib}$ compared to EV_{DMSO} [193]. Our analysis revealed that the expression of miR-25-3p was higher in EV_{DMSO} compared to $EV_{sorafenib}$, trend supported by other research showing that miR-25-3p was upregulated in BC tissues compared with corresponding non-tumor tissues [194]. Furthermore, after predicting the targets of these 12 differentially expressed miRNAs, we merged them with a list of DEGs identified in BC tissues from Indian women. This analysis revealed 1,097 common target genes involved in key pathways, including the PPAR pathway, which promotes apoptosis in BC cells, as well as other cancer-related pathways [148,149]. Our findings confirm that, in addition to miR-23b-3p and miR-126-3p, other miRNAs are significantly dysregulated following sorafenib treatment. These miRNAs, including miR-3648-3p and miR-4488, may play key roles in inhibiting BC, further expanding our understanding of EVs' potential therapeutic effects.

6. Conclusion and perspectives

EVs represent a promising frontier in the development of innovative therapeutic strategies, particularly as efficient delivery systems for ncRNAs. Due to their favorable characteristics, such as high biocompatibility, low toxicity, and enhanced stability within living organisms, EVs can act as highly effective carriers for a wide range of therapeutic agents, including nucleic acids like mRNA, siRNA, miRNA, and shRNer [195]. In our study, sorafenib-induced EVs were specifically enriched with miR-23b-3p, miR-126-3p, and GAS5, and we demonstrated their ability to significantly limit the aggressive properties of breast cancer both *in vitro* and *in vivo*, establishing a solid proof-of-concept for this approach.

Given that EVs can carry a diverse array of biomolecules - such as proteins, metabolites, mRNAs, and ncRNAs - the specific cargo they transport likely determines the effects on recipient cells. Thus, while we focused on the antitumoral effects of these three tumor-suppressor ncRNAs, it is possible that other dysregulated molecules within the EVs contributed to the observed therapeutic outcomes. This underscores the complexity of EV biology and highlights the need for further exploration of the molecular mechanisms behind their effects.

While our results in the zebrafish model are highly promising, offering insight into the therapeutic potential of EVs, additional research using other animal models is essential to fully understand the antitumor properties of these vesicles in BC. Only through continued research will EV-based therapies be able to advance towards clinical application and become reliable tools in precision medicine.

7. References

1. Fitzmaurice, C. *et al.* Global, Regional, and National Cancer Incidence, Mortality, Years of Life Lost, Years Lived With Disability, and Disability-Adjusted Life-Years for 29 Cancer Groups, 1990 to 2017: A Systematic Analysis for the Global Burden of Disease Study. *JAMA Oncol* **5**, 1749 (2019).

2. Chakraborty, S. & Rahman, T. The difficulties in cancer treatment. *Ecancermedicalscience* **6**, (2012).

3. Wu, M., Wang, M., Jia, H. & Wu, P. Extracellular vesicles: emerging anti-cancer drugs and advanced functionalization platforms for cancer therapy. *Drug Deliv* **2022**, 2513–2538 (2022).

4. Bray Bsc, F. *et al.* Global cancer statistics 2022: GLOBOCAN estimates of incidence and mortality worldwide for 36 cancers in 185 countries. (2024) doi:10.3322/caac.21834.

5. Winters, S., Martin, C., Murphy, D. & Shokar, N. K. Breast Cancer Epidemiology, Prevention, and Screening. *Prog Mol Biol Transl Sci* **151**, 1–32 (2017).

6. Al-thoubaity, F. K. Molecular classification of breast cancer: A retrospective cohort study. *Annals of Medicine and Surgery* **49**, 44–48 (2020).

7. Orrantia-Borunda, E., Anchondo-Nuñez, P., Acuña-Aguilar, L. E., Gómez-Valles, F. O. & Ramírez-Valdespino, C. A. Subtypes of Breast Cancer. *Breast Cancer* 31–42 (2022) doi:10.36255/EXON-PUBLICATIONS-BREAST-CANCER-SUBTYPES.

8. Tran B & Bedard PL. Luminal-B breast cancer and novel therapeutic targets. *Breast Cancer Research* **13**, (2011).

9. Mercogliano, M. F., Bruni, S., Mauro, F. L. & Schillaci, R. Emerging Targeted Therapies for HER2-Positive Breast Cancer. *Cancers* vol. 15 Preprint at https://doi.org/10.3390/cancers15071987 (2023).

10. Yildiz, B. *et al.* Clinicopathological characteristics of triple-negative breast cancers in the Northeast region of Turkey. *Balkan Med J* **31**, 126–131 (2014).

11. Lehmann, B. D. *et al.* Identification of human triple-negative breast cancer subtypes and preclinical models for selection of targeted therapies. *J Clin Invest* **121**, (2011).

12. Zerdan, M. B. *et al.* Triple Negative Breast Cancer: Updates on Classification and Treatment in 2021. *Cancers (Basel)* **2022**, 1253 (1253).

13. Rauf, F., Anderson, K. S. & Labaer, J. CEBP FOCUS Autoantibodies in Early Detection of Breast Cancer A C. *American Association for Cancer Research* 2475–2485 (2020) doi:10.1158/1055-9965.EPI-20-0331.

14. Barrios, C. H. Global challenges in breast cancer detection and treatment. *Breast* **62**, S3–S6 (2022).

15. Lv, X. *et al.* Induction chemotherapy with lobaplatin and fluorouracil versus cisplatin and fluorouracil followed by chemoradiotherapy in patients with stage III–IVB nasopharyngeal carcinoma: an open-label, non-inferiority, randomised, controlled, phase 3 trial. *Lancet Oncol* **22**, 716–726 (2021).

16. Obeagu, E. I. & Obeagu, G. U. Medicine ® Breast cancer A review of risk factors and diagnosis. (2024) doi:10.1097/MD.0000000000036905.

17. Bhushan, A., Gonsalves, A. & Menon, J. U. Current state of breast cancer diagnosis, treatment, and theranostics. *Pharmaceutics* vol. 13 Preprint at https://doi.org/10.3390/pharmaceutics13050723 (2021).

18. Cserni, G., Chmielik, E., Cserni, B. & Tot, T. The new TNM-based staging of breast cancer. *Virchows Archiv* vol. 472 697–703 Preprint at https://doi.org/10.1007/s00428-018-2301-9 (2018).

19. Teichgraeber, D. C., Guirguis, M. S. & Whitman, G. J. Breast cancer staging: Updates in the AJCC cancer staging manual, 8th edition, and current challenges for radiologists, from the AJR special series on cancer staging. *American Journal of Roentgenology* vol. 217 278–290 Preprint at https://doi.org/10.2214/AJR.20.25223 (2021).

20. Burguin, A., Diorio, C. & Durocher, F. Breast cancer treatments: Updates and new challenges. *J Pers Med* **11**, (2021).

21. Bastos, M. C. S., de Almeida, A. P., Bagnoli, F. & de Oliveira, V. M. Early breast cancer: concept and therapeutic review. *Rev Assoc Med Bras* **69**, (2023).

22. Gupta, N. & Ruiz, E. S. Current Perspectives in the Treatment of Locally Advanced Basal Cell Carcinoma. *Drug Des Devel Ther* **16**, 183–190 (2022).

23. Judith, D. N., Friederike, S., Anne, H., Thomas, F. & Landsberg, B. J. Clinical Management of Locally Advanced Basal-Cell Carcinomas and Future Therapeutic Directions. doi:10.6084/m9.figshare.12180051.

24. Margolese Richard G, Hortobagyi Gabriel N & Buchholz Thomas A. *Management of Metastatic Breast Cancer*. (2003).

25. Menon Gopal, Fadi Alkabban M & Ferguson Troy. *Breast Cancer Continuing Education Activity*. https://www.ncbi.nlm.nih.gov/books/NBK482286/.

26. Ye, S., Chen, S., Yang, X. & Lei, X. Drug resistance in breast cancer is based on the mechanism of exocrine non-coding RNA. *Discover Oncology* vol. 15 Preprint at https://doi.org/10.1007/s12672-024-00993-3 (2024).

27. Kinnel, B., Singh, S. K., Oprea-Ilies, G. & Singh, R. Targeted Therapy and Mechanisms of Drug Resistance in Breast Cancer. *Cancers* vol. 15 Preprint at https://doi.org/10.3390/cancers15041320 (2023).

28. Ji, X. *et al.* Chemoresistance mechanisms of breast cancer and their countermeasures. *Biomedicine & Pharmacotherapy* **114**, 108800 (2019).

29. Zafrakas, M., Papasozomenou, P. & Emmanouilides, C. Sorafenib in breast cancer treatment: A systematic review and overview of clinical trials. *World J Clin Oncol* **7**, 331–336 (2016).

30. Zhu, Y. J., Zheng, B., Wang, H. Y. & Chen, L. New knowledge of the mechanisms of sorafenib resistance in liver cancer. *Acta Pharmacologica Sinica* vol. 38 614–622 Preprint at https://doi.org/10.1038/aps.2017.5 (2017).

31. Faranda, T. *et al.* Differential expression profiling of long non-coding RNA GAS5 and miR-126-3p in human cancer cells in response to sorafenib. *Sci Rep* **9**, (2019).

32. Dattachoudhury, S., Sharma, R., Kumar, A. & Jaganathan, B. G. Sorafenib Inhibits Proliferation, Migration and Invasion of Breast Cancer Cells. *Oncology (Switzerland)* **98**, 478–486 (2020).

33. Bronte, G. *et al.* Sorafenib for the treatment of breast cancer. *Expert Opin Pharmacother* **18**, 621–630 (2017).

34. Toden, S., Zumwalt, T. J. & Goel, A. Non-coding RNAs and potential therapeutic targeting in cancer HHS Public Access. *Biochim Biophys Acta Rev Cancer* **1875**, 188491 (2021).

35. Yan, H. & Bu, P. Non-coding RNA in cancer. *Essays in Biochemistry* vol. 65 625–639 Preprint at https://doi.org/10.1042/EBC20200032 (2021).

36. Vishnoi, A. & Rani, S. miRNA Biogenesis and Regulation of Diseases: An Updated Overview. in *Methods in Molecular Biology* vol. 2595 1–12 (Humana Press Inc., 2023).

37. Lee, R. C., Feinbaum, R. L. & Ambrost, V. *The C. Elegans Heterochronic Gene Lin-4 Encodes Small RNAs with Antisense Complementarity to &II-14*. *Cell* vol. 75 (1993).

38. Wightman, B., Ha, L. & Ruvkun, G. *Posttranscriptional Regulation of the Heterochronic Gene Lin-14 by W-4 Mediates Temporal Pattern Formation in C. Elegans*. vol. 75 (1993).

39. O'Brien, J., Hayder, H., Zayed, Y. & Peng, C. Overview of microRNA biogenesis, mechanisms of actions, and circulation. *Frontiers in Endocrinology* vol. 9 Preprint at https://doi.org/10.3389/fendo.2018.00402 (2018).

40. Liu, J. *et al.* The Biogenesis of miRNAs and Their Role in the Development of Amyotrophic Lateral Sclerosis. *Cells* vol. 11 Preprint at https://doi.org/10.3390/cells11030572 (2022).

41. Annese, T., Tamma, R., De Giorgis, M. & Ribatti, D. microRNAs Biogenesis, Functions and Role in Tumor Angiogenesis. doi:10.3389/fonc.2020.581007.

42. Xie, M. *et al.* Mammalian 5'-capped microRNA precursors that generate a single microRNA. *Cell* **155**, 1568–1580 (2013).

43. Saliminejad, K., Khorram Khorshid, H. R., Soleymani Fard, S. & Ghaffari, S. H. An overview of microRNAs: Biology, functions, therapeutics, and analysis methods. *Journal of Cellular Physiology* vol. 234 5451–5465 Preprint at https://doi.org/10.1002/jcp.27486 (2019).

44. Wahid, F., Shehzad, A., Khan, T. & Kim, Y. Y. MicroRNAs: Synthesis, mechanism, function, and recent clinical trials. *Biochimica et Biophysica Acta - Molecular Cell Research* vol. 1803 1231–1243 Preprint at https://doi.org/10.1016/j.bbamcr.2010.06.013 (2010).

45. Naeli, P., Winter, T., Hackett, A. P., Alboushi, L. & Jafarnejad, S. M. The intricate balance between microRNA-induced mRNA decay and translational repression. *FEBS Journal* vol. 290 2508–2524 Preprint at https://doi.org/10.1111/febs.16422 (2023).

46. Wu, J., Yang, J., Cho, W. C. & Zheng, Y. Argonaute proteins: Structural features, functions and emerging roles. *Journal of Advanced Research* vol. 24 317–324 Preprint at https://doi.org/10.1016/j.jare.2020.04.017 (2020).

47. Xu, K., Lin, J., Zandi, R., Roth, J. A. & Ji, L. MicroRNA-mediated target mRNA cleavage and 3'-uridylation in human cells. *Sci Rep* **6**, (2016).

48. Toden, S., Zumwalt, T. J. & Goel, A. Non-coding RNAs and potential therapeutic targeting in cancer. *Biochimica et Biophysica Acta - Reviews on Cancer* vol. 1875 Preprint at https://doi.org/10.1016/j.bbcan.2020.188491 (2021).

49. Otmani, K., Rouas, R. & Lewalle, P. OncomiRs as noncoding RNAs having functions in cancer: Their role in immune suppression and clinical implications. *Frontiers in Immunology* vol. 13 Preprint at https://doi.org/10.3389/fimmu.2022.913951 (2022).

50. Yan, H. & Bu, P. Non-coding RNA in cancer. *Essays Biochem* 20200032 (2021) doi:10.1042/EBC20200032.

51. Chirshev, E., Oberg, K. C., Ioffe, Y. J. & Unternaehrer, J. J. Let - 7 as biomarker, prognostic indicator, and therapy for precision medicine in cancer . *Clin Transl Med* **8**, (2019).

52. Jiang, H. *et al.* miR-23b-3p rescues cognition in Alzheimer's disease by reducing tau phosphorylation and apoptosis via GSK-3β signaling pathways. *Molecular Therapy: Nucleic Acid* **28**, 539–557 (2022).

53. Guo, Y. X. *et al.* The role of miR-23b in cancer and autoimmune disease. *J Oncol* **2021**, (2021).

54. Grossi, I., Salvi, A., Baiocchi, G., Portolani, N. & De Petro, G. Functional Role of microRNA-23b-3p in Cancer Biology. *MicroRNA* **7**, 156–166 (2018).

55. Manganelli, M. *et al.* Longitudinal circulating levels of mir-23b-3p, mir-126-3p and lncrna gas5 in hcc patients treated with sorafenib. *Biomedicines* **9**, (2021).

56. Wang, W., Wang, Y., Liu, W. & van Wijnen, A. J. Regulation and biological roles of the multifaceted miRNA-23b (MIR23B). *Gene* vol. 642 103–109 Preprint at https://doi.org/10.1016/j.gene.2017.10.085 (2018).

57. Campos-Viguri, G. E. *et al.* MiR-23b-3p reduces the proliferation, migration and invasion of cervical cancer cell lines via the reduction of c-Met expression. *Sci Rep* **10**, (2020).

58. Klicka, K. *et al.* Decreased expression of miR-23b is associated with poor survival of endometrial cancer patients. *Sci Rep* **12**, (2022).

59. Majid, S., Dar, A. A., Saini, S., Deng, G. & Chang, I. MicroRNA-23b Functions as a Tumor Suppressor by Regulating Zeb1 in Bladder Cancer. *PLoS One* **8**, 67686 (2013).

60. Chen, Q., Chen, S., Zhao, J., Zhou, Y. & Xu, L. MicroRNA-126: A new and promising player in lung cancer (Review). *Oncology Letters* vol. 21 1–11 Preprint at https://doi.org/10.3892/ol.2020.12296 (2021).

61. Saito, Y. *et al.* Epigenetic therapy upregulates the tumor suppressor microRNA-126 and its host gene EGFL7 in human cancer cells. *Biochem Biophys Res Commun* **379**, 726–731 (2009).

62. Song, L. *et al.* MicroRNA-126 Targeting PIK3R2 Inhibits NSCLC A549 Cell Proliferation, Migration, and Invasion by Regulation of PTEN/PI3K/AKT Pathway. *Clin Lung Cancer* **17**, e65–e75 (2016).

63. Du, C. *et al.* MiR-126-3p suppresses tumor metastasis and angiogenesis of hepatocellular carcinoma by targeting LRP6 and PIK3R2. *J Transl Med* **12**, (2014).

64. Selven, H., Rasmussen Busund, L.-T., Andersen, S., Bremnes, R. M. & Kilvaer, T. K. High expression of microRNA-126 relates to favorable prognosis for colon cancer patients. doi:10.1038/s41598-021-87985-3.

65. Jalil, A. T. *et al.* The emerging role of microRNA-126 as a potential therapeutic target in cancer: a comprehensive review. *Pathology Research and Practice* vol. 248 Preprint at https://doi.org/10.1016/j.prp.2023.154631 (2023).

66. Han, I. B. *et al.* Down-regulation of MicroRNA-126 in glioblastoma and its correlation with patient prognosis: A pilot study. *Anticancer Res* **36**, 6691–6697 (2016).

67. Liu, R. *et al. MiR-126-3p Suppresses the Growth, Migration and Invasion of NSCLC via Targeting CCR1*.

68. Soofiyani, S. R. *et al.* Prognostic Value and Biological Role of miR-126 in Breast Cancer. *MicroRNA* **11**, 95–103 (2022).

69. Png, K. J., Halberg, N., Yoshida, M. & Tavazoie, S. F. A microRNA regulon that mediates endothelial recruitment and metastasis by cancer cells. *Nature* **481**, 190–196 (2012).

70. Zhang, X. *et al.* Molecular Sciences Mechanisms and Functions of Long Non-Coding RNAs at Multiple Regulatory Levels. doi:10.3390/ijms20225573.

71. Potemkin, N. & Clarkson, A. N. Non-coding RNAs in stroke pathology, diagnostics, and therapeutics. *Neurochem Int* **162**, (2023).

72. Zhang, X. *et al.* Molecular Sciences Mechanisms and Functions of Long Non-Coding RNAs at Multiple Regulatory Levels. doi:10.3390/ijms20225573.

73. Mattick, J. S. *et al.* nature reviews molecular cell biology Consensus statement Long non-coding RNAs: definitions, functions, challenges and recommendations. *Nat Rev Mol Cell Biol* **24**, 34 (2023).

74. Dykes, I. M. & Emanueli, C. Transcriptional and Post-transcriptional Gene Regulation by Long Non-coding RNA. *Chinese Academy of Sciences and Genetics Society of China. Genomics Proteomics Bioinformatics* **15**, 177–186 (2017).

75. Quinn, J. J. & Chang, H. Y. Unique features of long non-coding RNA biogenesis and function. *Nature Reviews Genetics* vol. 17 47–62 Preprint at https://doi.org/10.1038/nrg.2015.10 (2016).

76. Liu, Y. *et al.* Long non-coding RNAs: Biogenesis, functions, and clinical significance in gastric cancer. *Molecular Therapy Oncolytics* vol. 23 458–476 Preprint at https://doi.org/10.1016/j.omto.2021.11.005 (2021).

77. Bhat, S. A. *et al.* Long non-coding RNAs: Mechanism of action and functional utility. *Non-coding RNA Research* vol. 1 43–50 Preprint at https://doi.org/10.1016/j.ncrna.2016.11.002 (2016).

78. Tüncel, Ö., Kara, M., Yaylak, B., Erdoğan, İ. & Akgül, B. Noncoding RNAs in apoptosis: identification and function. *Turkish Journal of Biology* vol. 46 1–40 Preprint at https://doi.org/10.3906/biy-2109-35 (2022).

79. Mattick, J. S. *et al.* nature reviews molecular cell biology Consensus statement Long non-coding RNAs: definitions, functions, challenges and recommendations. *Nat Rev Mol Cell Biol* **24**, 34 (2023).

80. Dahariya, S. *et al.* Long non-coding RNA: Classification, biogenesis and functions in blood cells. *Molecular Immunology* vol. 112 82–92 Preprint at https://doi.org/10.1016/j.molimm.2019.04.011 (2019).

81. Wang, W. *et al.* Biological Function of Long Non-coding RNA (LncRNA) Xist. *Frontiers in Cell and Developmental Biology* vol. 9 Preprint at https://doi.org/10.3389/fcell.2021.645647 (2021).

82. Chen, G. *et al.* Long Non-coding RNAs in Cancer: Implications for Diagnosis, Prognosis, and Therapy. *Frontiers in Medicine | www.frontiersin.org* **7**, 612393 (2020).

83. Huarte, M. The emerging role of lncRNAs in cancer. (2015) doi:10.1038/nm.3981.

84. Chen, G. *et al.* Long Non-coding RNAs in Cancer: Implications for Diagnosis, Prognosis, and Therapy. *Frontiers in Medicine | www.frontiersin.org* **7**, 612393 (2020).

85. Jiang, M.-C., Ni, J.-J., Cui, W.-Y., Wang, B.-Y. & Zhuo, W. Emerging roles of lncRNA in cancer and therapeutic opportunities. *Am J Cancer Res* **9**, 1354–1366 (2019).

86. Li, S. *et al.* LncRNA LENGA acts as a tumor suppressor in gastric cancer through BRD7/TP53 signaling. *Cellular and Molecular Life Sciences* **80**, (2023).

87. Xu, J., Wang, X., Zhu, C. & Wang, K. A review of current evidence about lncRNA MEG3: A tumor suppressor in multiple cancers. *Frontiers in Cell and Developmental Biology* vol. 10 Preprint at https://doi.org/10.3389/fcell.2022.997633 (2022).

88. Guzel, E. *et al.* Tumor suppressor and oncogenic role of long non-coding RNAs in cancer REVIEW BIOCHEMISTRY. *North Clin Istanb* **7**, 81–86 (2020).

89. Goustin, A. S., Thepsuwan, P., Kosir, M. A. & Lipovich, L. The growth-arrest-specific (GAS)-5 long non-coding RNA: A fascinating lncrnawidely expressed in cancers. *Non-coding RNA* vol. 5 Preprint at https://doi.org/10.3390/ncrna5030046 (2019).

90. Xue, Y. *et al.* Functional Network of the Long Non-coding RNA Growth Arrest-Specific Transcript 5 and Its Interacting Proteins in Senescence. (2021) doi:10.3389/fgene.2021.615340.

91. Ji, J., Dai, X., Yeung, S. C. J. & He, X. The role of long non-coding RNA GAS5 in cancers. *Cancer Management and Research* vol. 11 2729–2737 Preprint at https://doi.org/10.2147/CMAR.S189052 (2019).

92. Frank, F. *et al.* The lncRNA Growth Arrest Specific 5 Regulates Cell Survival via Distinct Structural Modules with Independent Functions. *Cell Rep* **32**, (2020).

93. Smith, C. M. & Steitz, J. A. Classification of gas5 as a Multi-Small-Nucleolar-RNA (snoRNA) Host Gene and a Member of the 5′-Terminal Oligopyrimidine Gene Family Reveals Common Features of snoRNA Host Genes. *Mol Cell Biol* **18**, 6897–6909 (1998).

94. Dsouza, V. L. *et al.* Small nucleolar RNA and its potential role in breast cancer – A comprehensive review. *Biochimica et Biophysica Acta - Reviews on Cancer* vol. 1875 Preprint at https://doi.org/10.1016/j.bbcan.2020.188501 (2021).

95. Pickard, M. R. & Williams, G. T. Molecular and cellular mechanisms of action of tumour suppressor GAS5 LncRNA. *Genes* vol. 6 484–499 Preprint at https://doi.org/10.3390/genes6030484 (2015).

96. Yang, X., Xie, Z., Lei, X. & Gan, R. Long non-coding RNA GAS5 in human cancer (Review). *Oncol Lett* **20**, 2587–2594 (2020).

97. Grossi, I., Marchina, E., De Petro, G. & Salvi, A. The Biological Role and Translational Implications of the Long Non-Coding RNA GAS5 in Breast Cancer. *Cancers* vol. 15 Preprint at https://doi.org/10.3390/cancers15133318 (2023).

98. Lin, G., Wu, T., Gao, X., He, Z. & Nong, W. Research Progress of Long Non-Coding RNA GAS5 in Malignant Tumors. *Frontiers in Oncology* vol. 12 Preprint at https://doi.org/10.3389/fonc.2022.846497 (2022).

99. Doyle, L. M. & Wang, M. Z. cells Overview of Extracellular Vesicles, Their Origin, Composition, Purpose, and Methods for Exosome Isolation and Analysis. doi:10.3390/cells8070727.

100. Palazzolo, S., Canzonieri, V. & Rizzolio, F. The history of small extracellular vesicles and their implication in cancer drug resistance. *Frontiers in Oncology* vol. 12 Preprint at https://doi.org/10.3389/fonc.2022.948843 (2022).

101. Nunez, E. A., Wallis, J. & Gershon, M. D. *Secretory Processes in Follicular Cells of the Bat Thyroid 111. THE OCCURRENCE OF EXTRACELLULAR VESICLES AND COLLOID DROPLETS DURING AROUSAL FROM HIBERNATION*. *Am. J. ANAT* vol. 141 (1974).

102. Couch, Y. *et al.* A brief history of nearly EV-erything – The rise and rise of extracellular vesicles. *J Extracell Vesicles* **10**, (2021).

103. Sheta, M., Taha, E. A., Lu, Y. & Eguchi, T. Extracellular Vesicles: New Classification and Tumor Immunosuppression. *Biology* vol. 12 Preprint at https://doi.org/10.3390/biology12010110 (2023).

104. Di Bella, M. A. Overview and Update on Extracellular Vesicles: Considerations on Exosomes and Their Application in Modern Medicine. *Biology (Basel)* **2022**, 804 (2022).

105. Skotland, T., Sagini, K., Sandvig, K. & Llorente, A. An emerging focus on lipids in extracellular vesicles. *Advanced Drug Delivery Reviews* vol. 159 308–321 Preprint at https://doi.org/10.1016/j.addr.2020.03.002 (2020).

106. Welsh, J. A. *et al.* Minimal information for studies of extracellular vesicles (MISEV□□□): From basic to advanced approaches. (2024) doi:10.1002/jev2.12404.

107. Tricarico, C., Clancy, J., D'souza-Schorey, C. & Francis©, T. &. Small GTPases Biology and biogenesis of shed microvesicles. (2017) doi:10.1080/21541248.2016.1215283.

108. Akers, J. C., Gonda, D., Kim, R., Carter, B. S. & Chen, C. C. Biogenesis of extracellular vesicles (EV): exosomes, microvesicles, retrovirus-like vesicles, and apoptotic bodies. doi:10.1007/s11060-013-1084-8.

109. Meldolesi, J. Exosomes and Ectosomes in Intercellular Communication. *Current Biology* vol. 28 R435–R444 Preprint at https://doi.org/10.1016/j.cub.2018.01.059 (2018).

110. Doyle, L. M. & Wang, M. Z. Overview of extracellular vesicles, their origin, composition, purpose, and methods for exosome isolation and analysis. *Cells* vol. 8 Preprint at https://doi.org/10.3390/cells8070727 (2019).

111. Kakarla, R., Hur, J., Kim, Y. J., Kim, J. & Chwae, Y.-J. Apoptotic cell-derived exosomes: messages from dying cells. *Exp Mol Med* **52**, 1–6 (2020).

112. Battistelli, M. & Falcieri, E. Apoptotic Bodies: Particular Extracellular Vesicles Involved in Intercellular Communication. doi:10.3390/biology9010021.

113. Théry, C. *et al.* Minimal information for studies of extracellular vesicles 2018 (MISEV2018): a position statement of the International Society for Extracellular Vesicles and update of the MISEV2014 guidelines. *J Extracell Vesicles* **7**, (2018).

114. Zhao, Z., Wijerathne, H., Godwin, A. K. & Soper, S. A. Extracellular Vesicles and Circulating Nucleic Acids Isolation and analysis methods of extracellular vesicles (EVs). *Extracell Vesicles Circ Nucleic Acids* **2**, 80–103 (2021).

115. De Sousa, K. P. *et al.* Isolation and characterization of extracellular vesicles and future directions in diagnosis and therapy. (2022) doi:10.1002/wnan.1835.

116. Kalluri, R. & Mcandrews, K. M. The Role of Extracellular Vesicles in Cancer. doi:10.1016/j.cell.2023.03.010.

117. Zhang, X. *et al.* The Biology and Function of Extracellular Vesicles in Cancer Development. *Frontiers in Cell and Developmental Biology* vol. 9 Preprint at https://doi.org/10.3389/fcell.2021.777441 (2021).

118. Xu, R. *et al.* Extracellular vesicles in cancer — implications for future improvements in cancer care. *Nature Reviews Clinical Oncology* vol. 15 617–638 Preprint at https://doi.org/10.1038/s41571-018-0036-9 (2018).

119. Chang, W. H., Cerione, R. A. & Antonyak, M. A. Extracellular Vesicles and Their Roles in Cancer Progression. in *Methods in Molecular Biology* vol. 2174 143–170 (Humana Press Inc., 2021).

120. Wu, M., Wang, M., Jia, H. & Wu, P. Extracellular vesicles: emerging anti-cancer drugs and advanced functionalization platforms for cancer therapy. *Drug Deliv* **29**, 2513–2538 (2022).

121. Han, Y. *et al.* processes Overview and Update on Methods for Cargo Loading into Extracellular Vesicles. (2021) doi:10.3390/pr9020356.

122. Peruzzi, J. A. *et al.* Enhancing extracellular vesicle cargo loading and functional delivery by engineering protein-lipid interactions. *& Neha P. Kamat* **11**, 12.

123. Samuels, M. *et al.* The role of non-coding RNAs in extracellular vesicles in breast cancer and their diagnostic implications. *Oncogene* vol. 42 3017–3034 Preprint at https://doi.org/10.1038/s41388-023-02827-y (2023).

124. Robinson, H. *et al.* Caveolin-1-driven membrane remodelling regulates hnRNPK-mediated exosomal microRNA sorting in cancer. *Clin. Transl. Med* 11 (2021) doi:10.1002/ctm2.381.

125. Wozniak, A. L. *et al.* The RNA binding protein FMR1 controls selective exosomal miRNA cargo loading during inflammation. *Journal of Cell Biology* **219**, (2020).

126. Rahman Khan, F. & Sulaiman Alhewairini, S. Zebrafish (Danio rerio) as a Model Organism . in *Current Trends in Cancer Management* (IntechOpen, 2019). doi:10.5772/intechopen.81517.

127. Tavakoli, S., Rothschild, H. & Zon, L. I. Zebrafish as a Model for Human Diseases. in *Encyclopedia of Life Sciences* 1–8 (Wiley, 2017). doi:10.1002/9780470015902.a0005580.pub2.

128. Dooley Kimberly & Zon I Leonard. Zebrafish: a model system for the study of human disease. *Current Opinion in Genetics & Developmen* **10**, 252–256 (2000).

129. Teame, T. *et al.* The use of zebrafish (Danio rerio) as biomedical models. **9**, (2019).

130. Adhish, M. & Manjubala, I. Effectiveness of zebrafish models in understanding human diseases—A review of models. *Heliyon* vol. 9 Preprint at https://doi.org/10.1016/j.heliyon.2023.e14557 (2023).

131. Astell, K. R. & Sieger, D. Zebrafish In Vivo Models of Cancer and Metastasis. (2020) doi:10.1101/cshperspect.a037077.

132. Fontana, C. M. & Van Doan, H. Zebrafish xenograft as a tool for the study of colorectal cancer: a review. *Cell death & disease* vol. 15 23 Preprint at https://doi.org/10.1038/s41419-023-06291-0 (2024).

133. Gamble, J. T., Elson, D. J., Greenwood, J. A., Tanguay, R. L. & Kolluri, S. K. biology The Zebrafish Xenograft Models for Investigating Cancer and Cancer Therapeutics. (2021) doi:10.3390/biology10040252.

134. Russo, I. *et al.* The Zebrafish model in dermatology: an update for clinicians. *Discover Oncology* vol. 13 Preprint at https://doi.org/10.1007/s12672-022-00511-3 (2022).

135. Guerra, F. *et al.* Modulation of RAB7A Protein Expression Determines Resistance to Cisplatin through Late Endocytic Pathway Impairment and Extracellular Vesicular Secretion. doi:10.3390/cancers11010052.

136. Kreger, B. T., Johansen, E. R., Cerione, R. A. & Antonyak, M. A. The enrichment of survivin in exosomes from breast cancer cells treated with paclitaxel promotes cell survival and chemoresistance. *Cancers (Basel)* **8**, (2016).

137. Nagy, A. *et al.* Evaluation of TaqMan qPCR System Integrating Two Identically Labelled Hydrolysis Probes in Single Assay OPEN. (2017) doi:10.1038/srep41392.

138. Aleström, P. *et al.* Zebrafish: Housing and husbandry recommendations. *Lab Anim* **54**, 213 (2020).

139. Ruggiero, C. *et al.* FSCN1 as a new druggable target in adrenocortical carcinoma. *Int J Cancer* (2023) doi:10.1002/IJC.34526.

140. Gao, C. *et al.* A user-friendly herbicide derived from photo-responsive supramolecular vesicles. *Nat Commun* **9**, (2018).

141. Matinha-Cardoso, J. *et al.* Novel protein carrier system based on cyanobacterial nano-sized extracellular vesicles for application in fish. *Microb Biotechnol* **15**, 2191–2207 (2022).

142. von Hellfeld, R., Brotzmann, K., Baumann, L., Strecker, R. & Braunbeck, T. Adverse effects in the fish embryo acute toxicity (FET) test: a catalogue of unspecific morphological changes versus more specific effects in zebrafish (Danio rerio) embryos. *Environ Sci Eur* **32**, 1–18 (2020).

143. *Test No. 203: Fish, Acute Toxicity Test*. (OECD, 2019). doi:10.1787/9789264069961-en.

144. Basnet, R. M. *et al.* Caffeine Inhibits Direct and Indirect Angiogenesis in Zebrafish Embryos. *Int. J. Mol. Sci* **22**, 4856 (2021).

145. Serbedzija, G. N., Flynn, E. & Willett, C. E. Zebrafish angiogenesis: A new model for drug screening. *Angiogenesis* **3**, 353–359 (1999).

146. Jin, S. W., Beis, D., Mitchell, T., Chen, J. N. & Stainier, D. Y. R. Cellular and molecular analyses of vascular tube and lumen formation in zebrafish. *Development* **132**, 5199–5209 (2005).

147. Renaud, L., Da Silveira, W. A., Glen, W. B., Hazard, E. S. & Hardiman, G. Send Orders for Reprints to reprints@benthamscience.ae Interplay Between MicroRNAs and Targeted Genes in Cellular Homeosta-sis of Adult Zebrafish (Danio rerio). *Curr Genomics* **19**, 615–629 (2018).

148. Malvia, shreshtha *et al.* Study of Gene Expression Profiles of Breast Cancers in Indian Women. doi:10.1038/s41598-019-46261-1.

149. Qian, Z., Chen, L., Liu, J., Jiang, Y. & Zhang, Y. The emerging role of PPAR-alpha in breast cancer. *Biomedicine and Pharmacotherapy* vol. 161 Preprint at https://doi.org/10.1016/j.biopha.2023.114420 (2023).

150. Wilkinson, L. & Gathani, T. Understanding breast cancer as a global health concern 1. *Br J Radiol* **95**, 20211033 (2021).

151. Si, W., Shen, J., Zheng, H. & Fan, W. The role and mechanisms of action of microRNAs in cancer drug resistance. *Clinical Epigenetics* vol. 11 Preprint at https://doi.org/10.1186/s13148-018-0587-8 (2019).

152. Pavan Kumar, D. Drug resistance mechanisms in cancers: Execution of pro-survival strategies. (2024) doi:10.7555/JBR.37.20230248.

153. Menon, A., Abd-Aziz, N., Khalid, K., Poh, C. L. & Naidu, R. miRNA: A Promising Therapeutic Target in Cancer. *International Journal of Molecular Sciences* vol. 23 Preprint at https://doi.org/10.3390/ijms231911502 (2022).

154. Iorio, M. V. & Croce, C. M. microRNA involvement in human cancer. *Carcinogenesis* **33**, 1126–1133 (2012).

155. Wu, M., Wang, M., Jia, H. & Wu, P. Extracellular vesicles: emerging anti-cancer drugs and advanced functionalization platforms for cancer therapy. *Drug Deliv* **29**, 2513–2538 (2022).

156. He, R. Q. *et al.* Downregulated miR-23b-3p expression acts as a predictor of hepatocellular carcinoma progression: A study based on public data and RT-qPCR verification. *Int J Mol Med* **41**, 2813–2831 (2018).

157. Di Paolo, D. *et al.* Cotargeting of miR-126-3p and miR-221-3p inhibits PIK3R2 and PTEN, reducing lung cancer growth and metastasis by blocking AKT and CXCR4 signalling. *Mol Oncol* **15**, 2969–2988 (2021).

158. Kaur, J. *et al.* Tumor Suppressive Effects of GAS5 in Cancer Cells. *Non-coding RNA* vol. 8 Preprint at https://doi.org/10.3390/ncrna8030039 (2022).

159. Lambrou, G. I., Hatziagapiou, K. & Zaravinos, A. Molecular Sciences The Non-Coding RNA GAS5 and Its Role in Tumor Therapy-Induced Resistance. doi:10.3390/ijms21207633.

160. Xu, D. *et al.* MicroRNAs in extracellular vesicles: Sorting mechanisms, diagnostic value, isolation, and detection technology. *Frontiers in Bioengineering and Biotechnology* vol. 10 Preprint at https://doi.org/10.3389/fbioe.2022.948959 (2022).

161. Llorens-Revull, M. *et al.* Comparison of Extracellular Vesicle Isolation Methods for miRNA Sequencing. *Int J Mol Sci* **24**, (2023).

162. Xu, D. *et al.* MicroRNAs in extracellular vesicles: Sorting mechanisms, diagnostic value, isolation, and detection technology. *Frontiers in Bioengineering and Biotechnology* vol. 10 Preprint at https://doi.org/10.3389/fbioe.2022.948959 (2022).

163. Zhang, X. *et al.* The Biology and Function of Extracellular Vesicles in Cancer Development. *Frontiers in Cell and Developmental Biology* vol. 9 Preprint at https://doi.org/10.3389/fcell.2021.777441 (2021).

164. Wang, F. W. *et al.* APC-activated long noncoding RNA inhibits colorectal carcinoma pathogenesis through reduction of exosome production. *Journal of Clinical Investigation* **129**, 727–743 (2019).

165. Zhang, H. *et al.* Bone marrow mesenchymal stem cell-derived exosomal miR-206 inhibits osteosarcoma progression by targeting TRA2B. *Cancer Lett* **490**, 54–65 (2020).

166. Tominaga, N. Anti-cancer role and therapeutic potential of extracellular vesicles. *Cancers* vol. 13 Preprint at https://doi.org/10.3390/cancers13246303 (2021).

167. Tang, W. *et al.* The mechanisms of sorafenib resistance in hepatocellular carcinoma: theoretical basis and therapeutic aspects. *Signal Transduction and Targeted Therapy* vol. 5 Preprint at https://doi.org/10.1038/s41392-020-0187-x (2020).

168. Ohno, S. I. *et al.* Systemically injected exosomes targeted to EGFR deliver antitumor microrna to breast cancer cells. *Molecular Therapy* **21**, 185–191 (2013).

169. Chen, Z., Wang, H., Xia, Y., Yan, F. & Lu, Y. Therapeutic Potential of Mesenchymal Cell–Derived miRNA-150-5p–Expressing Exosomes in Rheumatoid Arthritis Mediated by the Modulation of MMP14 and VEGF. *The Journal of Immunology* **201**, 2472–2482 (2018).

170. Sanz-Ros, J. *et al.* Extracellular Vesicles as Therapeutic Resources in the Clinical Environment. *International Journal of Molecular Sciences* vol. 24 Preprint at https://doi.org/10.3390/ijms24032344 (2023).

171. Yang, Q. *et al.* Sorafenib prevents the proliferation and induces the apoptosis of liver cancer cells by regulating autophagy and hypoxia-inducible factor-1. *Exp Ther Med* **22**, (2021).

172. Wei, J. C. *et al.* Sorafenib inhibits proliferation and invasion of human hepatocellular carcinoma cells via up-regulation of p53 and suppressing FoxM1. *Acta Pharmacol Sin* **36**, 241–251 (2015).

173. Reclusa, P. *et al.* improving extracellular vesicles visualization: from static to motion. doi:10.1038/s41598-020-62920-0.

174. Lerner, N., Avissar, S. & Beit-Yannai, E. Extracellular vesicles mediate signaling between the aqueous humor producing and draining cells in the ocular system. *PLoS One* **12**, (2017).

175. Koponen, A. *et al.* Label-free characterization and real-time monitoring of cell uptake of extracellular vesicles. *Biosens Bioelectron* **168**, (2020).

176. Gupta, R., Luo, X., Lin, Z., Tian, Y. & Ajit, S. K. Uptake of Fluorescent Labeled Small Extracellular Vesicles In Vitro and in Spinal Cord. doi:10.3791/62537.

177. Kenneweg, F. *et al.* Long Noncoding RNA-Enriched Vesicles Secreted by Hypoxic Cardiomyocytes Drive Cardiac Fibrosis. doi:10.1016/j.omtn.2019.09.003.

178. Chen, F. *et al.* Extracellular vesicle-packaged HIF-1α-stabilizing lncRNA from tumour-associated macrophages regulates aerobic glycolysis of breast cancer cells. *Nat Cell Biol* **21**, 498–510 (2019).

179. Born, L. J., Harmon, J. W. & Jay, S. M. Therapeutic potential of extracellular vesicle-associated long noncoding RNA. *Bioengineering and Translational Medicine* vol. 5 Preprint at https://doi.org/10.1002/btm2.10172 (2020).

180. Verweij, F. J., Hyenne, V., Van Niel, G. & Goetz, J. G. Extracellular Vesicles: Catching the Light in Zebrafish. (2019) doi:10.1016/j.tcb.2019.07.007.

181. Metsäniitty, M. *et al.* Zebrafish larvae as a model for studying the impact of oral bacterial vesicles on tumor cell growth and metastasis. *Hum Cell* (123AD) doi:10.1007/s13577-024-01114-6.

182. Chang, W. H., Cerione, R. A. & Antonyak, M. A. Extracellular Vesicles and Their Roles in Cancer Progression. in *Methods in Molecular Biology* vol. 2174 143–170 (Humana Press Inc., 2021).

183. Bao, Q. *et al.* Tumor-Derived Extracellular Vesicles Regulate Cancer Progression in the Tumor Microenvironment. *Frontiers in Molecular Biosciences* vol. 8 Preprint at https://doi.org/10.3389/fmolb.2021.796385 (2022).

184. Verdi, V., Bécot, A., van Niel, G. & Verweij, F. J. In vivo imaging of EVs in zebrafish: New perspectives from "the waterside". *FASEB BioAdvances* vol. 3 918–929 Preprint at https://doi.org/10.1096/fba.2021-00081 (2021).

185. Biagini, V. *et al.* Zebrafish Melanoma-Derived Interstitial EVs Are Carriers of ncRNAs That Induce Inflammation. *Int J Mol Sci* **23**, (2022).

186. Kalluri, R. & McAndrews, K. M. The role of extracellular vesicles in cancer. *Cell* vol. 186 1610–1626 Preprint at https://doi.org/10.1016/j.cell.2023.03.010 (2023).

187. Wawruszak, A., Okoń, E. & Dudziak, K. Advancements in Zebrafish Models for Breast Cancer Research: Unveiling Biomarkers, Targeted Therapies, and Personalized Medicine. *Medical Science Monitor* vol. 29 Preprint at https://doi.org/10.12659/MSM.940550 (2023).

188. Zampedri, C., Martínez-Flores, W. A. & Melendez-Zajgla, J. The Use of Zebrafish Xenotransplant Assays to Analyze the Role of lncRNAs in Breast Cancer. *Frontiers in Oncology* vol. 11 Preprint at https://doi.org/10.3389/fonc.2021.687594 (2021).

189. Suetsugu, A. *et al.* Imaging exosome transfer from breast cancer cells to stroma at metastatic sites in orthotopic nude-mouse models. *Advanced Drug Delivery Reviews* vol. 65 383–390 Preprint at https://doi.org/10.1016/j.addr.2012.08.007 (2013).

190. Hyenne, V. *et al.* Studying the Fate of Tumor Extracellular Vesicles at High Spatiotemporal Resolution Using the Zebrafish Embryo. *Dev Cell* **48**, 554-572.e7 (2019).

191. Madu, C. O., Wang, S., Madu, C. O. & Lu, Y. Angiogenesis in Breast Cancer Progression, Diagnosis, and Treatment. *J Cancer* **11**, 4474–4494 (2020).

192. Kudela, E. *et al.* Mirna expression profiles in luminal a breast cancer—implications in biology, prognosis, and prediction of response to hormonal treatment. *International Journal of Molecular Sciences* vol. 21 1–20 Preprint at https://doi.org/10.3390/ijms21207691 (2020).

193. Castaldo, V. *et al.* Upregulated expression of miR-4443 and miR-4488 in drug resistant melanomas promotes migratory and invasive phenotypes through downregulation of intermediate filament nestin. *Journal of Experimental and Clinical Cancer Research* **42**, (2023).

194. Zhao, T. *et al.* Identification of miR-25-3p as a tumor biomarker: Regulation of cellular functions via TOB1 in breast cancer. *Mol Med Rep* **23**, (2021).

195. Androuin, A., Verweij, F. J. & Van Niel, G. Zebrafish as a preclinical model for Extracellular Vesicle-based therapeutic development q. (2021) doi:10.1016/j.addr.2021.05.025.

8. Acknowledgements

Words cannot express the appreciation and acknowledgement I have for the people who support me throughout this journey.

My sincere appreciation to Prof. Giuseppina De Petro, who welcomed me and gave me the invaluable opportunity to conduct my PhD program in her lab and be part of her excellent research team, as well as for all the constructive advice she has given me over the years.

I would like to express my deep and sincere gratitude to Prof. Alessandro Salvi, a person with a brilliant mind and a big heart. He has been my mentor throughout these three years, teaching me with patience and passion everything I know today. I will always be grateful for his support and the knowledge he has shared with me. Thanks to him, I have grown both professionally and personally.

A special person with whom I shared many beautiful moments is Dr. Ilaria Grossi. I would like to thank her for her constant willingness to offer help whenever I was in need and for being not only a colleague but also a friend to me.

Last but not least, I would like to thank my mother and sister for their unconditional love and support every step of the way, my partner who stood by me all these years and with whom I had the pleasure of sharing this beautiful experience, and all my wonderful friends, both old and new.

9. List of publications

- **In extenso**

- M. Dobre, A. Salvi, I.A. Pelisenco, F. Vasilescu, G. De Petro, V. Herlea, E. Milanesi.

"Crosstalk Between DNA Methylation and Gene Mutations in Colorectal Cancer." Front Oncol **2021**, 11, doi:10.3389/fonc.2021.697409.

- I. Grossi, C. Assoni, L. Lorini, D. Smussi, C. Gurizzan, S. Grisanti, A. Paderno, D. Mattavelli, C. Piazza, I.A. Pelisenco, G. De Petro, A. Salvi, P. Bossi.

"Evaluation of DNA methylation levels of SEPT9 and SHOX2 in plasma of patients with head and neck squamous cell carcinoma using droplet digital PCR." Oncology Reports, **2024,** 51, 52. https://doi.org/10.3892/or.2024.8711

- Giulia Girolimetti, Iulia Andreea Pelisenco, Leonardo Henry Eusebi, Claudio Ricci, Beatrice Cavina, Ivana Kurelac, Tiziano Verri, Matteo Calcagnile, Pietro Alifano, Alessandro Salvi, Cecilia Bucci, and Flora Guerra.

"Dysregulation of a Subset of Circulating and Vesicle-Associated miRNA in Pancreatic Cancer". Non-Coding RNA **2024**, 10, 29. https://doi.org/10.3390/ ncrna10030029.

- C.A. Donofrio, A. Fioravanti, L. Riccio, M.Cominetti, M.R. Cappelletti, D. Generali, F. Servadei, I. Grossi, I.A. Pelisenco, A. Salvi, G. De Petro.

"Determination of longitudinal circulating levels of miR-21-5p, miR-23b-3p and miR-34a-5p in plasma of patients with glioblastoma using droplet digital PCR." Biomedicines 2024, under revision.

- I.A. Pelisenco, D. Zizioli, F. Guerra, I. Grossi, C. Bucci, L. Mignani, G. Girolimetti, R. Di Corato, V.G. D'Agostino, E. Marchina, G. De Petrp, A. Salvi.

"*miR-23b-3p, miR-126-3p and GAS5 delivered by extracellular vesicles inhibit breast cancer xenografts in zebrafish".* Cell Commun Signal. **2024** Nov 18;22(1):552. doi: 10.1186/s12964-024-01936-9.

- **Abstracts**

1. *I.A. Pelisenco, D. Zizioli, F. Guerra, I. Grossi, C. Bucci, L. Mignani, G. Bramato, E. Marchina, G. De Petro, A. Salvi.* **The enrichment of miR-23b-3p, miR-126-3p and GAS5 in extracellular vesicles from breast cancer cells treated with sorafenib inhibited the tumor growth of xenografts in zebrafish model.** EMBO Workshop "Non-coding RNA medicine". Poznan, Poland, 15/05/2023 - 18/05/2023.
2. *E. Milanesi, A. Salvi, G. De Petro, T. Manuc, I. A. Pelisenco, M. Manuc, C. Tieranu, G. Becheanu, M. Dobre.* **Endocannabinoid system in inflammatory bowel diseases: mucosal gene expression preliminary data.** UEG Week. Copenhagen, Denmark, 14/10/2023 - 17/10/2023.
3. *I.A. Pelisenco, I. Grossi, D. Zizioli, F. Guerra, C. Bucci, L. Mignani, G. Girolimetti, R. Di Corato, E. Marchina, G. De Petro, A. Salvi.* **miR-23b-3p, miR-126-3p and GAS5 encapsulated in extracellular vesicles from breast cancer cells treated with sorafenib inhibited the growth of tumor xenografts in zebrafish model.** National Ph.D. Meeting. Bologna, Italy, 25/03/2024 - 27/03/2024
4. *Grossi, C. Assoni, L. Lorini, D. Smussi, C. Gurizzan, S. Grisanti, A. Paderno, D. Mattavelli, C. Piazza, I.A. Pelisenco, G. De Petro, A. Salvi, P. Bossi.* **Droplet digital PCR Development to quantify the DNA methylation levels of SEPT9 and SHOX2 in plasma from patients with Head and Neck Squamous Cell Carcinoma**. NO-CANCER 2024 Congress. Novara, Italy, 27/05/2024 - 28/05/2024
5. *I.A. Pelisenco, I. Grossi, D. Zizioli, F. Guerra, C. Bucci, L. Mignani, G. Girolimetti, R. Di Corato, V.G. D'Agostino, E. Marchina, G. De Petro, A. Salvi.* **Extracellular vesicles derived from breast cancer cells rich in miR-23b-3p, miR-126-3p, and GAS5 inhibited the tumor growth of zebrafish xenograft model.** EACR 2024 Congress. Rotterdam, Netherlands, 10/06/2024 - 13/06/2024
6. *A. Pelisenco, I. Grossi, D. Zizioli, F. Guerra, C. Bucci, L. Mignani, G. Girolimetti, R. Di Corato, E. Marchina, G. De Petro, A. Salvi.* **The delivery of miR-23b-3p, miR-126-3p, and GAS5 by extracellular vesicles inhibited the tumor growth of zebrafish breast cancer xenografts.** CIB Meeting 2024. Milan, Italy, 02/07/2024
7. *I.A. Pelisenco, I. Grossi, F. Guerra, D. Zizioli, C. Bucci, L. Mignani, G. Girolimetti, R. Di Corato, V.G. D'Agostino, E. Marchina, G. De Petro, A. Salvi.* **Effects of miR-23b-3p,**

miR-126-3p, and GAS5 delivered by EVs on breast cancer xenografts developed in zebrafish. XXII Congresso Nazionale A.I.B.G. Salerno, Italy, 19/09/2024 – 21/09/2024.

- **Posters**

8. *E. Milanesi, A. Salvi, G. De Petro, T. Manuc, I. A. Pelisenco, M. Manuc, C. Tieranu, G. Becheanu, M. Dobre.* **Endocannabinoid system in inflammatory bowel diseases: mucosal gene expression preliminary data. UEG Week.** Copenhagen, Denmark, 14/10/2023 - 17/10/2023.
9. *I.A. Pelisenco, I. Grossi, D. Zizioli, F. Guerra, C. Bucci, L. Mignani, G. Girolimetti, R. Di Corato, E. Marchina, G. De Petro, A. Salvi.* **miR-23b-3p, miR-126-3p and GAS5 encapsulated in extracellular vesicles from breast cancer cells treated with sorafenib inhibited the growth of tumor xenografts in zebrafish model.** National Ph.D. Meeting. Bologna, Italy, 25/03/2024 - 27/03/2024
10. *I.A. Pelisenco, I. Grossi, D. Zizioli, F. Guerra, C. Bucci, L. Mignani, G. Girolimetti, R. Di Corato, V.G. D'Agostino, E. Marchina, G. De Petro, A. Salvi.* **Extracellular vesicles derived from breast cancer cells rich in miR-23b-3p, miR-126-3p, and GAS5 inhibited the tumor growth of zebrafish xenograft model.** EACR 2024 Congress. Rotterdam, Netherlands, 10/06/2024 - 13/06/2024
11. *A. Pelisenco, I. Grossi, D. Zizioli, F. Guerra, C. Bucci, L. Mignani, G. Girolimetti, R. Di Corato, E. Marchina, G. De Petro, A. Salvi.* **The delivery of miR-23b-3p, miR-126-3p, and GAS5 by extracellular vesicles inhibited the tumor growth of zebrafish breast cancer xenografts.** CIB Meeting 2024. Milan, Italy, 02/07/2024
12. *I.A. Pelisenco, I. Grossi, F. Guerra, D. Zizioli, C. Bucci, L. Mignani, G. Girolimetti, R. Di Corato, V.G. D'Agostino, E. Marchina, G. De Petro, A. Salvi.* **Effects of miR-23b-3p, miR-126-3p, and GAS5 delivered by EVs on breast cancer xenografts developed in zebrafish.** XXII Congresso Nazionale A.I.B.G. Salerno, Italy, 19/09/2024 – 21/09/2024.

- **Oral communications to conferences:**

- 15/05/2023 - 18/05/2023, EMBO Workshop "Non-coding RNA medicine". Poznan, Poland.
- 16/05/2024, My 3-min PhD thesis. Brescia, Italy.